Distribution of I_h Channels and their Function in the Stomatogastric Ganglion.

vorgelegt von

Marie-Luise Göritz

aus Marburg

(Köln 2008)

2

Zusammenfassung:

Stereotype Bewegungsmuster wie Fortbewegung, Verdauung und Atmung werden durch repetitive Entladungen von Motoneuronen in relativ autonomen neuronalen Netzwerken, sogenannten zentralen Rhythmusgeneratoren oder Central Pattern Generators (CPGs) generiert. Innerhalb eines solchen Netzwerkes erzeugt das Zusammenspiel einzelner Neurone rhythmische Aktivitaetsmuster, die typischerweise unabhaengig von synaptischen Eingaengen uebergeordneter Zentren generiert werden koennen. In der vorliegenden Studie wurde die Bedeutung der hyperpolarisations-aktivierten I_h Kationenkanaele im pylorischen Netzwerk des stomatogastrischen Ganglions untersucht. Dieses rhythmisch aktive Netzwerk steuert Bewegungen des Hummermagens. Von besonderem Interesse waren die Rolle von I_h bei der Aufrechterhaltung regelmaessiger Aktivitaetsmuster, die Lokalisation von I_h Kanaelen innerhalb des Ganglions, und die Regulation synaptischer Uebertragung durch Aktivierung von I_h.

Ich beschreibe eine kompensatorische Interaktion zwischen I_h und dem transienten Kaliumstrom I_A in verschiedenen Motoneuronen, bei der die Ueber-Expression des I_A Gens *shal* durch RNA-Injektion zu einer Zunahme von I_h fuehrte. Zusaetzlich zu I_h habe ich eine weitere Komponente des hyperpolarisations-aktivierten Einwaerts-Stromes gefunden, die im Vergleich zu unbehandelten Neuronen mit hoeherer Wahrscheinlichkeit nach Injektion von *shal*-RNA and *gfp*-RNA auftrat. Weiterhin zeige ich, dass der Mechanismus der kompensatorische Zunahme von I_h richtungsabhaengig ist; die Ueberexpression des I_h Gens *PIIH* fuehrte zu keiner messbaren Veraenderung des A-Stromes.

In einer immunocytochemischen Untersuchung charakterisiere ich die Verteilung von I_h Protein innerhalb des stomatogastrischen Ganglions. I_h Protein wurde in stomatogastrischen Neuronen vor allem in der synapsenreichen Region des feinen Neuropils gefunden.

Schliesslich demonstriere ich, dass I_h moeglicherweise an der Regulierung synaptischer Uebertragung beteiligt ist. In einer elektrophysiologischen Studie war

die Amplitude postsynaptischer Potentiale vom Aktivierungzustand der I_h-Kanaele abhaengig und wurde mit zunehmender Aktivierung von I_h verringert.

Abstract:

Generation of rhythmic patterns in the absence of descending commands is an essential and powerful trait of many motor networks. Cyclic rhythmic discharges of motoneurons in repeated motor activities like locomotion, mastication and respiration require underlying circuits of neurons, which are called central pattern generators (CPG). This study examined the possible roles of I_h cation channels in the pyloric network of the stomatogastric nervous system, a rhythmically active network of motoneurons that controls movements of the lobster foregut. Of specific interest were the H-current's involvement in maintaining firing properties, the distribution of I_h channels within the stomatogastric ganglion, and a potential role for I_h in regulation of synaptic strength. I was able to confirm a homeostatic interaction of I_h with A-type potassium channels, where the over-expression of the I_A *shal* gene after RNA injection evoked a compensatory increase of I_h in different motoneuron types. I observed an additional, non-I_h component of the hyperpolarization activated current, which was more likely to occur in *shal*-RNA and *gfp*-RNA injected neurons, compared to untreated neurons. Further, I showed that the homeostatic response of I_h increase is unidirectional; overexpression of the I_h protein PIIH did not lead to an increase of I_A. In an immunocytochemical study, I found high concentrations of I_h protein localized in the fine neuropil of the stomatogastric ganglion, an area which is rich in synaptic contacts. Finally, I demonstrate a potential role for I_h in regulating synaptic transmission, for which I found evidence in electrophysiological experiments, where the amplitude of inhibitory postsynaptic potentials decreased with increasing activation of I_h.

1 Introduction

This study examined the possible roles of I_h cation channels in a rhythmically active motor network of the lobster foregut. Of specific interest were the role of I_h in maintaining firing properties, the localization of I_h protein PIIH in neurons of this network, and its potential role in regulation of synaptic strength.

1.1 Rhythmically Active Networks

Generation of rhythmic patterns in the absence of descending commands is an essential and powerful trait of many motor networks. Cyclic rhythmic discharges of motoneurons in repeated motor activities like locomotion, mastication and respiration require underlying circuits of neurons, which are called central pattern generators (CPG), and can be as small as one single cell. Membrane oscillations or repetitive bursting in the absence of phasic sensory input are distinguishing features of such a network (Hooper, DiCaprio 2004, Kiehn 2006a, Lund, Kolta 2006, Selverston, Moulins 1985, Stein 2007a, Wyman 1976, Yamaguchi 2004). The smallest CPG can be a single neuron, but it more often consists of a network of cells. Rhythm generating networks integrate multiple processes including the appropriately timed activation of ion channels and synaptically driven transmitter receptors within motor networks (Nistri et al. 2006a). A number of ionic currents contribute to the integrated function of motoneurons and CPG interneurons (Butt, Harris-Warrick and Kiehn 2002, Harris-Warrick 1993, Harris-Warrick 2002, Kiehn et al. 2000). Rhythm-generating networks exist to drive behaviors of different levels of complexity. In the spinal cord, CPG networks underlie neuronal activity of variable and complex behaviors like walking, crawling or swimming (Hooper, DiCaprio 2004, Kiehn 2006b, Kiehn, Kjaerulff 1998, Stein 2007b). CPGs in the brainstem control rhythmic breathing (Ramirez, Richter 1996, Wyman

8

1976). Rhythmicity is also an important feature of non motor networks, where learning and recalling of memory involve synchronous activity within cortical and hippocampal networks (McCormick, Contreras 2001), and studies of CPG networks may provide insights into how these other rhythmic patterns are generated and controlled. Output from CPGs needs to be robust to prevent interruptions of essential motor behavior, but must also be modifiable in a context dependent way. Flexibility of rhythmic patterns produced by CPGs is provided by neuromodulation and sensory input (Dickinson 2006, Harris-Warrick 1993, Marder and Bucher 2007, McLarnon 1995, Nistri et al. 2006b, Pinsker 1982, von Euler 1981).

The net output of a rhythm-generating network therefore depends on:

1. The hardwiring of the network, which is set by the pattern of synaptic connectivity. Connections can be inhibitory or excitatory and can be realized through chemical or electrical synapses, or a combination of both. 2. Sub-cellular properties of individual cells, which are reflected in the diversity and distribution of ion channels, receptor proteins and secondary messenger pathways. 3. Neuromodulation of these properties, which can shape the strength and direction of synapses, change the binding characteristics of receptors, as well as modifying the intrinsic firing properties of the component neurons by influencing gating of ion channels and controlling second messenger pathways. Sensory input can trigger neuromodulatory effects by acting through modulatory neurons and can affect the timing and phasing of rhythmic output. Current questions regarding rhythmic pattern generation focus on the underlying principles of these features: What mechanisms control the balance between robust stereotypic network activity and flexibility? How is the hardwired system adjusted for different behavioral tasks or developmental states? What homeostatic mechanisms exist to achieve consistent motor output? How is synaptic input of different origin weighted during different behavioral states or under varying external conditions?

Sub-threshold or subliminal currents appear to play important roles in generating rhythmic activity in a number of systems. These are currents that activate at or

below the firing threshold and shape the cell's firing properties. Among the best known are the persistent sodium current I_{NaP}, the T-type calcium current I_{CA-T}, subtreshold A-type potassium currents and the hyperpolarization activated inward current I_h (Hammond, 2001, Jerng et al., 2004, Harris-Warrick, 2002, Johnston et al., 2000, Magee 1999). Cell specific differences in channel expression help to create a neuron's unique function within a network. Based on these differences, neuromodulation of sub-threshold channels changes the input-output properties of individual neurons and can alter the resulting network output. Here, I studied cellular and synaptic aspects of I_h function and I_h channel distribution in the pyloric motor network, which controls movements of the lobster stomach. I found a potential role for I_h in balancing network output and in regulation of synaptic strength.

1.2 *The Crustacean Stomatogastric Nervous System*

Invertebrate motor networks are model systems for rhythmic pattern generation. The organization of cyclic motor activity has been well studied in the crustacean stomatogastric nervous system (STNS), in crayfish swimmeret movement, in the locust flight system, and in cockroach and stick insect walking behavior, among many others (Harris-Warrick and Marder, 1991, Hooper and DiCaprio, 2004, Duysens et al., 2000, Bueschges and ElManira, 1998, Clarac and Cattaert, 1996, Clarac et al., 2000, Wiersma and Hughes, 1960, Delcomyn, 1980, Selverston et al., 1976). One advantage of these networks compared to vertebrate preparations is the smaller degree of centralization and fusion of the nervous system, leading to relatively small circuits of functionally connected neurons. Further, these neurons are often large and repeatedly identifiable, which allows the use of intracellular recording techniques like two-electrode voltage clamp, facilitates molecular manipulation of protein levels through RNA injection, and allows evaluation of gene expression levels within single cells through RT-PCR. Many of these preparations can be isolated and studied in vitro.

10

Organization

This study of I_h distribution and function was performed in pyloric neurons of the stomatogastic ganglion (STG) in the California Spiny Lobster *Panulirus interruptus* (Figure 1.1A). The stomatogastric nervous system (STNS) has been extensively studied as a model system for rhythm generation and neuromodulatory control of motor output (Maynard, 1972, Harris-Warrick and Marder, 1991, Hooper and DiCaprio, 2004, Marder and Bucher, 2006). It controls movement of the foregut (Figure 1.1 B, Figure 1.2 A and B) through repetitive activation of several groups of muscles, which attach externally to the stomach wall. The STNS consists of the connected paired commissural ganglia (CoGs), the esophageal ganglion (OG) and the stomatogastric ganglion.
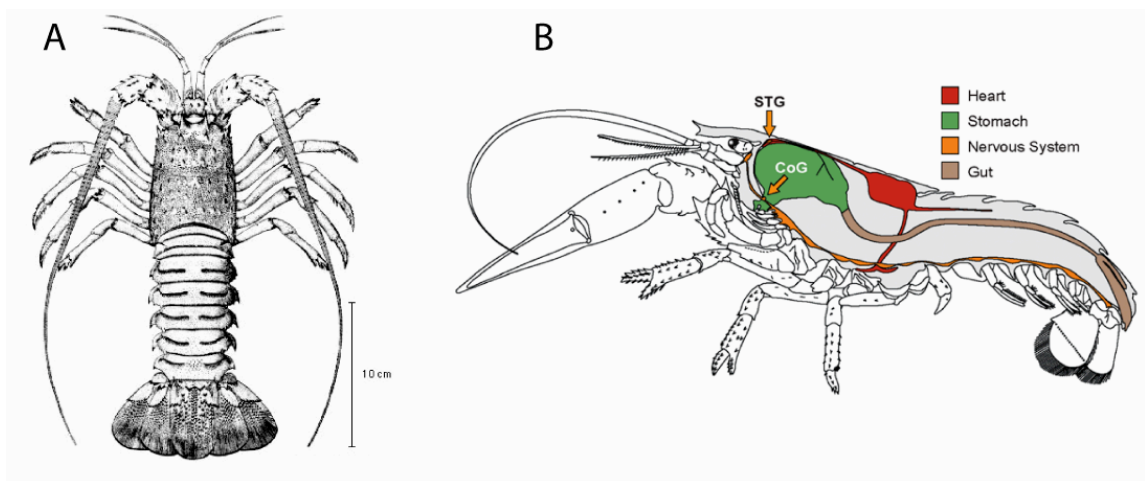
Figure 1.1 A. Dorsal drawing of a California Spiny Lobster *Panulirus interruptus* (L.B. Holthuis, Rathbun, 1884) B. Location of the foregut or stomach and parts of the nervous system in a stylized lateral view of the Maine Lobster *Hommarus americanus* (from Marder and Bucher, 2006)

The STG contains about 30 cells of 20 different cell types. With the exception of two identified interneurons (AB and INT1), most of these neurons are bi-functional: they are both members of CPGs that drive rhythmic foregut movements and motor neurons that innervate pyloric and gastric mill muscles and drive the movements evoked by CPG activity. The crustacean STNS can stay alive and

produce spontaneous rhythmic firing up to 5 days in culture. The pyloric network (Figure 1.2C,D) is one of three spontaneously active networks in the STG (Harris-Warrick et al., 1998, 1992) and controls rhythmic peristaltic and filtering movements of the posteror foregut to move food particles into the midgut at a frequency of 1-2 Hz. This network contains six different types of neurons, five of them motoneurons, which all have been well characterized (Hille, 2001, Turrigiano,1994, 1999, Harris-Warrick et al., 1992. Selverston and Moulins, 1986, Marder and Thirumalai, 1996, Marder and Calabrese, 2002). The pyloric network produces a stereotyped triphasic output with characteristic phases for each neuron (Figure 1.2D). Order of firing is determined both by synaptic interactions and by differences in intrinsic properties of the neurons, including rhythmic oscillatory bursting, bistability, post-inhibitory rebound and spike adaptation; these depend on the coordinated activity of different currents in the different neurons. In the presence of modulatory input from the CoGs, endogenous bursting of the AB interneuron plays the most important role to set the frequency of the pyloric rhythm. The two PD neurons are electrically coupled to the AB cell. This pacemaker group bursts together and inhibits all other pyloric neurons. Within the pyloric network, all known chemical synapses are inhibitory and mediated by glutamate, with the exception of the PD and VD neurons, which use acetylcholine in their inhibitory synapses onto other cells (Cleland and Selverston 1998, Eisen and Marder 1982, King 1976a, King 1976b, Marder and Eisen 1984, Marder and Paupardin-Tritsch 1978, Wyman 1976). Rectifying and non-rectifying electrical synapses also exist within the network.

12
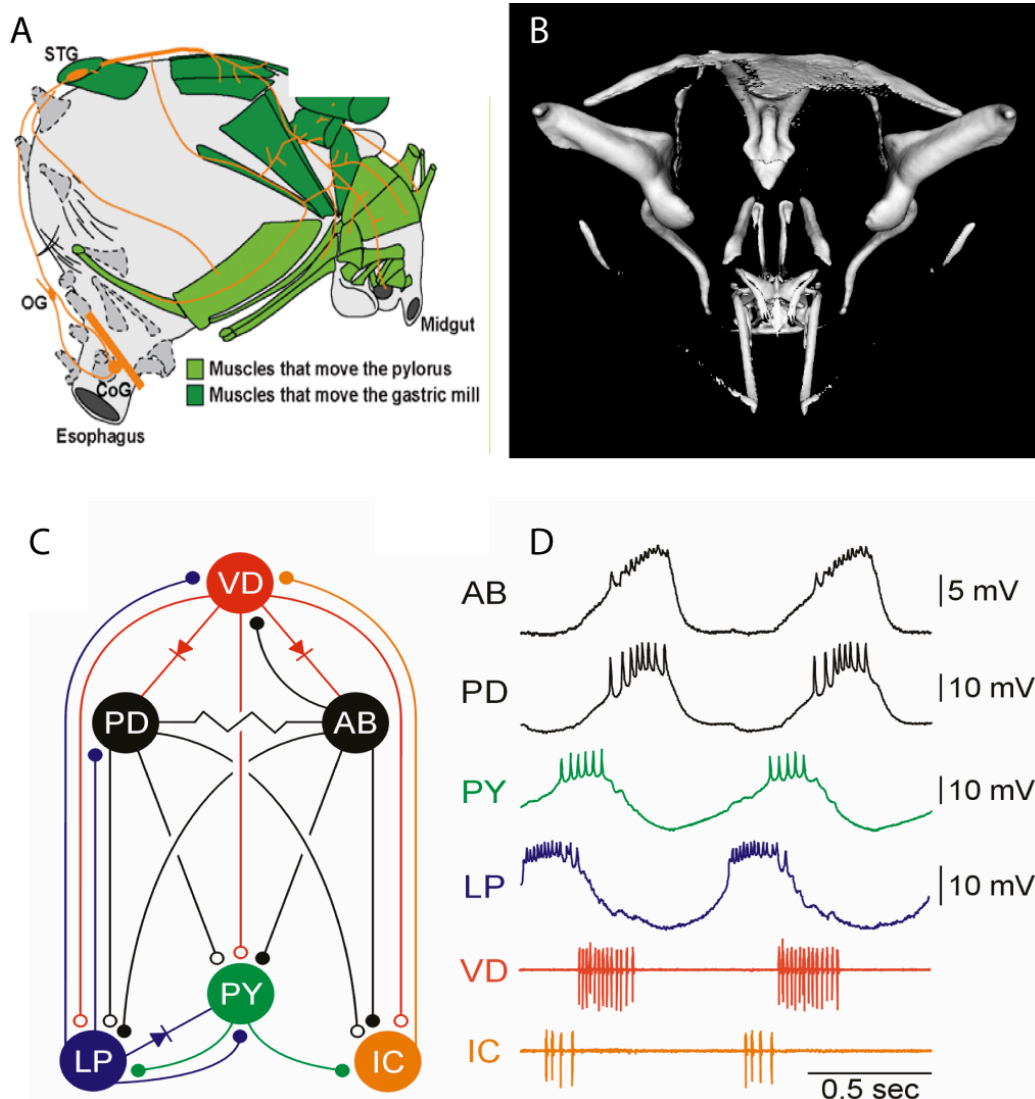
Figure 1.2 Schematics of the crustacean stomach and nervous system. A. In situ position of the stomatogastric nervous system (orange) and its target muscles (green) in a lateral view of the stomach. B. Reconstruction of the oscicles which span the foregut. C. Neuron types of the pyloric network: anterior burster interneuron (AB), lateral pyloric (LP), inferior cardiac (IC), ventral dilator (VD), two pyloric dilator (PD) and up to 8 pyloric (PY) neurons. D. Rhythmic activity of pyloric neurons in intracellular (top four) and extracellular (bottom two) recordings. (A from Marder and Bucher, 2007; B from K. H. Hobbs and S. L. Hooper, 2007,unpublished; C and D from Weaver, 2002)

The other neurons in the STG belong to the gastric-mill and the cardiac-sac networks. Chewing movements of the median and lateral teeth are caused by the slower and more variable gastric mill rhythm, which usually shows periods of 8-20 s (Clemens et al., 1998, Marder, Bucher 2007). Occasionally, a third monophasic rhythm can be observed in the STG that drives contraction of the cardiac sac. This slow rhythm with a period from 15-20sup to several minutes recruits the pyloric VD and PD neurons to elicit long bursts with characteristically large amplitudes of underlying depolarization in phase with the cardiac dilator neuron (CD2). Other cardiac-sac neurons are located in the commissural ganglia (CoGs) and in ivn fibers (Ayali, Harris-Warrick 1998, Dickinson 2006). Behavioral studies have confirmed the existence of similar nerve and muscle activity patterns in vivo in resting and feeding animals (Heinzel, Weimann and Marder 1993).

Modulation

Motor output from STG neurons can be altered through application of neuromodulators. Their effects on network activity can be slow or rapid and last from seconds to hours (Marder 1976, Marder and Eisen, 1984, Katz et al., 1990, Marder and Bucher, 2001, Nusbaum, 2001, Harris-Warrick et al., 1998, Dickinson 2006, Marder and Bucher 2006). *In vivo*, the CoGs and the OG provide over 100 axons which generate descending modulatory input to the STG, the loss of which temporarily abolishes spontaneous bursting of STG neurons (Marder and Bucher, 2006, Thoby-Brisson et al., 2002, Turrigiano 1995, Harris-Warrick et al., 1995, Golowasch et al. 1992). Sensory feedback from serotonin-containing mechanoreceptors provides another source of modulation is (Katz and Harris-Warrick 1989a,b,c, 1990, 1991, Beenhakker et al., 2004, Beenhakker et al., 2005, Beenhakker and Nussbaum, 2004, Blitz et al., 2004). Neuromodulators target both the intrinsic firing properties of pyloric network neurons and their chemical and electrical synapses. All synapses of the STG can be modulated, and the sensitivity to a large number of different neuromodulators has been shown (Ayali, Harris-Warrick 1998, Ayali, Harris-Warrick 1999, Johnson, Kloppenburg and

14

Harris-Warrick 2003, Kiehn, Harris-Warrick 1992, Marder, Bucher 2007, Marder, Eisen 1984, Peck et al. 2001a, Turrigiano, Marder 1993). Often, application of the same modulator causes opposite effects in different cells or even different synapses of the same neuron. For example, dopamine differently affects the mixed electrical-chemical synapse between pyloric (PY) and lateral pyloric (LP) neurons. It reduces the excitatory electrical component of the synapse and strengthens the chemical inhibition, functionally inverting the sign of the synaptic interaction (Ayali, Johnson and Harris-Warrick 1998, Johnson, Harris-Warrick 1997, Johnson, Peck and Harris-Warrick 1995).

Cell-type specific modulation of intrinsic cellular firing properties can arise due to expression of modulatory receptor types with different second messenger mechanisms or the differential expression of ion channels which could be modulated. Recent data show that ion channel expression in pyloric neurons seems to follow a cell type-specific pattern. Differences in the expression of potassium currents like I_A, I_{KV}, and I_h, calcium activated I_{KCA}, as well as L-type calcium and persistent sodium current have been characterized (Baro et al. 2000, French, Lanning and Harris-Warrick 2002, Gruhn et al. 2005, Harris-Warrick et al. 1995a, Ouyang, Goeritz and Harris-Warrick 2007b, Peck et al. 2001a, Schneider et al. 2000, Zhang, Wootton and Harris-Warrick 1995). For several channels, expression levels have been estimated based on the number of mRNA transcripts, which can been determined in individual cell types with the help of single cell RT-PCR (Baro et al., 1996, 1997, (Schulz, Goaillard and Marder 2006, Schulz, Goaillard and Marder 2007). Depending on the neuron type, these currents can respond oppositely to the same neurotransmitter. Dopamine for example increases the transient I_A in PD neurons, while it reduces the same current in LP, AB, IC and PY neurons (Kloppenburg et al, 1999, Peck et al., 1995).

Of these currents, I_h is of special interest because of its involvement in homeostatic mechanisms and its interaction with the fast potassium outward current I_A (MacLean et al. 2003, Zhang et al. 2003b). Its susceptibility to neuromodulation

is well known, but its functional role in the STG is still poorly understood (Peck et al. 2006).

1.3 *The Hyperpolarization-Activated Inward Current I$_h$*

I$_h$ is a hyperpolarization-activated, small inward current of mixed cations, mostly carried by Na$^+$ and K$^+$ ions. It reacts very sensitively to changes of the external K$^+$ concentration. The hyperpolarization-induced activation of I$_h$ channels usually follows a very slow time course with time constants (τ) on the order of seconds. Because of its slow kinetics and its extremely hyperpolarized V$_{1/2act}$ of -70mV and below, it is likely that in many neurons I$_h$ channels mainly function as a leak conductance within the neuron's physiological range of membrane potentials. The channel is a tetramer, of which each subunit contains six trans-membrane domains. All I$_h$ subunits show an intracellular cyclic nucleotide (CN)-binding site close to the C-terminus.

Modulation and Pharmacological Interactions of I$_h$

I$_h$ is found in the central and peripheral nervous system and in cardiac pacemaker tissue (Pape 1996, Kaupp and Seifert 2002, Robinson and Siegelbaum 2003). It is best known for contributing to the resting membrane potential and for being involved in rhythm generation. I$_h$ helps set the resting potential as a leak current, plays a role in the generation of plateau potentials (Kiehn and Harris-Warrick, 1992, Robinson and Siegelbaum, 2003, Beaumont and Zucker, 2000,) and functions as a depolarizing pacemaker current in the heart (Baruscotti and Difrancesco 2004, DiFrancesco 2006, DiFrancesco and Ojeda 1980). I$_h$ contributes to postinhibitory rebound by generating depolarizing sag potentials upon hyperpolarization, which deactivate only slowly upon repolarization (Harris-Warrick et al. 1995a, Pape 1996, Robinson and Siegelbaum 2003). It is also involved in regulation of synaptic transmission, long term facilitation and integration of synaptic events through shaping temporal summation as well as

16

spatial normalization of distant synaptic events (Beaumont and Zucker 2000, Genlain, Godaux and Ris 2007, Harris-Warrick et al. 1995b, Magee, 1998, 1999, Williams and Stuart, 2000, Berger et al. 2003, Migliore et al., 2004). In layer V pyramidal cells of the somatosensory cortex, I_h channel activation at hyperpolarized membrane potentials disconnects somatic and dendritic spike innitiation zones and thus may prevent initiation of dendritic calcium action potentials in the absence of proximal input (Berger et al., 2003). In the STG and at the neuromuscular junction, I_h could be partially responsible for enhancement of synaptic strength during aminergic modulation (Beaumont and Zucker, 2000) (Harris-Warrick 2002, Johnson and Harris-Warrick 1997).

Neurotransmitters can facilitate I_h activation by increasing the cAMP level (Rateau and Ropert 2006, Robinson and Siegelbaum 2003, Rosenkranz and Johnston 2006, Santoro and Baram 2003, Svoboda and Lupica 1998). Binding of cAMP at the CN-binding site shifts the voltage dependence of activation to more depolarized potentials and enhances the amplitude of maximal conductance. This site also binds cGMP with a lower affinity (Robinson and Siegelbaum 2003). During prolonged whole cell recordings, a dramatic run-down of I_h occurs, which can shift the voltage dependence of activation by 40-50 mV in the hyperpolarizing direction. Reductions in cAMP levels account for less than half of the run-down effect, and it is still unknown what regulatory factor causes the largest part of this shift (Chen 2004, DiFrancesco 1986, Robinson and Siegelbaum 2003). Of the vertebrate isoforms of I_h, HCN2 - 4 are most sensitive to up-regulation by cAMP (Pape 1996, Robinson and Siegelbaum 2003). I_h has been found in all six pyloric neuron types in the STG, where it is subject to differential monoaminergic modulation (Harris-Warrick et al. 1995a; Peck et al. 2006; Thirumalai et al. 2006). For example, dopamine enhances I_h in the lateral pyloric (LP) neuron by shifting the voltage dependence of activation to more depolarized values and by accelerating its rate of activation. In motor-neurons of the feeding circuit of the snail *Lymnaea*, modulation by serotonin increases I_h, causing prolonged depolarization of the membrane potential, triggering conditional endogenous bursting properties, and

enhancing postinhibitory rebound (PIR) properties (Straub and Benjamin, 2001). In higher brain regions like the hypothalamus, hippocampus and medulla oblongata, serotonin diminishes I_h by reducing the maximal conductance and causing a negative shift of the voltage dependence of activation. This effect is mediated by 5-HT2 receptors, which activate protein kinase C (Liu et al., 2003). Pharmacologically, I_h can be blocked by bath application of 5-10 mM CsCl, 50-200 µM ZD7288 or, in the case of HCN1 channels, by the drug zatebradine and the VR1 receptor antagonist capsazepine (Gill et al. 2006, Kiehn, Harris-Warrick 1992, Ouyang, Goeritz and Harris-Warrick 2007). Forskolin increases I_h by upregulation of cAMP. The anticonvulsant drug lamotrogine enhances I_h in the dendrites of pyramidal neurons by shifting the voltage dependence of activation (Poolos et al., 2002). Gabapentin enhances I_h in pyramidal CA1 neurons by increasing the conductance without influencing the properties of activation (Surges et al., 2003).

Soma recordings of I_h in pyloric neurons show that the activation and deactivation of this current is most likely too slow to directly impact firing properties by changing its conductance on a cycle-by-cycle basis in the pyloric network. The large degree of I_h modulation in many rhythmically active systems suggests a functional role of I_h, which may vary in a state-dependent way. I_h could be simply help set the membrane resting potential, but it could also participate in more complicated mechanisms that affect regulation of the strength of synaptic transmission or temporal integration of synaptic events. Knowledge of I_h channel distribution in the STG might imply a functional role more clearly.

1.4 Homeostatic Relationship of I_h and I_A

A compensatory homeostatic relationship between I_h and the fast transient outward current I_A has been previously described (MacLean et al. 2003, MacLean et al. 2005, Zhang et al. 2003a). IA is a transient depolarization-activated potassium current which rapidly inactivates during maintained depolarization but shows a fast

recovery from inactivation at hyperpolarized levels. I_A is involved in several aspects of neuronal excitability, including the timing of action potentials after hyperpolarization, the time course of postinhibitory rebound during bursting, spike adaptation and control of the interspike interval (Graubard and Hartline, 1991, Golowasch and Marder, 1992, Tierney and Harris-Warrick, 1992, Harris-Warrick et al., 1995a,b, 1998, Kloppenburg et al., 1999, Peck et al., 2001, Hille, 2001).

Enhancing I_A in the PD neuron during bath application of dopamine dampens its bursting properties. Increased I_A reduces the rate of rebound after the post-burst hyperpolarization, increasing the first spike-latency and length of first inter-spike interval, and reducing the number of spikes per burst (Harris-Warrick et al. 1995a, Kloppenburg, Levini and Harris-Warrick 1999, Peck et al. 2001b, Tierney, Harris-Warrick 1992). Therefore, over-expression of I_A by RNA injection of its gene, *shal*, would be expected to cause dramatic changes of firing properties. Instead, previous work from our lab found that the firing patterns after I_A over-expression to be unchanged, due to a compensatory up-regulation of I_h (MacLean et al., 2003; 2005). The homeostatic interaction of these two currents appeared to be independent of activity changes, as over-expression of a mutated, non-functional form of I_A still caused an increase of the measured I_h. Therefore, a novel molecular mechanism was proposed to exist, which could recognize the presence of additional I_A mRNA or protein, and trigger a compensatory increase of I_h.

This homeostatic response could be unique for PD neurons or might be a more general mechanism of maintaining stable levels of rhythmically active networks. Knowledge of its presence in other STG neurons might indicate whether or not similar I_A-I_h interactions could be expected to be found in other systems. Similarly, a reverse interaction where overexpression of I_h leads to increased I_A would point to this response as a more general homeostatic mechanism. Ectopic expression of I_h by injection of RNA from a closely related species, *Panulirus*

argus, did not affect the expression of I_A, but this could be an artifact of inter-species differences in the I_h sequence (Zhang et al. 2003).

1.5 Aim of this Study

In order to better understand the role of I_h in the pyloric network, I examined three aspects of I_h. First, homeostatic interactions of I_A and I_h in pyloric neurons were examined in more detail, to determine whether this could be a general mechanism to regulate network activity. The directionality of the homeostatic response was studied by overexpressing I_h splice variants of *P. interruptu*s in oocytes and PD neurons, to see if a species-specific form of I_h could lead to an up-regulation of I_A. Second, the distribution of endogenous I_h protein in STG neurons was determined by immunocytochenistry and confocal imaging and compared to the expression pattern of a synaptic marker and of I_A protein. Finally, a potential role of I_h in regulating graded synaptic transmission was examined by studying the effects of I_h activation at the graded glutamatergic LP to PD synapse.

20

2 Methods

2.1 STG dissection and PD cell identification

Adult California spiny lobsters, *P. interruptus*, were obtained from Don Tomlinson Commercial Fishing (San Diego, CA) and maintained in artificial sea water at 16°C until use. Lobsters were anesthetized by keeping them on ice for 30 min before dissection. The STG, along with its motor nerves and associated commissural and esophageal ganglia, was dissected and pinned in a silicone elastomer (Sylgard)- coated dish containing saline, as described by Mulloney and Selverston (1974). The physiological saline solution consisted of (in mM): 479 NaCl, 12.8 KCl, 13.7 CaCl$_2$, 3.9 Na$_2$SO$_4$, 10.0 MgSO$_4$, 2 glucose, and 11.1 Tris base, pH 7.4 (Mulloney and Selverston 1974). The PD, VD and LP neurons were identified during intracellular recordings (3 M KCl, 10–25 MΩ) by their typical membrane potential oscillation shapes and synaptic inputs (Kloppenburg et al. 1999), and IC neurons and gastric neurons were identified by extracellular recordings with suctions or pin electrodes of the respective nerves.

2.2 RNA microinjection into neurons

Pyloric neurons

Capped RNA was transcribed from linearized DNA clones with a T3 (*shal, shal*-GFP, *mshal)* or SP6 (*PIIH,* G*FP*) mMessage mMachine kit (Ambion), using T3 or SP6 RNA polymerase. The capped transcripts were cleaned using the RNeasy mini kit (Qiagen).

The RNA solution contained 0.25– 0.5 μg/μl *PIIH* or *GFP*(control) cRNA and 0.08% Fast Green to monitor the injection and was centrifuged at 3600 rpm for 10

minutes prior to injection. After identification, pyloric neurons were injected with RNA using pressure pulses (40 psi; 0.2 Hz, 30- to 70-ms duration) driven by a homemade pressure injector and a pulse generator (Master-8; AMPI, Jerusalem, Israel). After injection, the whole preparation was incubated in sterilized recording saline without Tris base, but containing 5 mM HEPES, pH7.4, 2 g/l glucose, 100,000 unit/l penicillin, and 100 mg/l streptomycin at 16°C for 4–5 days to allow protein expression.

Xenopus oocytes

Stage V to VI oocytes were surgically removed from female frogs during anesthesia in 0.15% MS222 (3-aminobenzoic acid ethyl ester). The eggs were then treated with 1 mg/ml collagenase type IA in solution containing (in mM): 82.5 NaCl, 2 KCl, 1 MgCl$_2$, and 5 HEPES (pH 7.5) for 60 min. The oocytes were defolliculated, but the vitelline membrane was not removed. Isolated oocytes were injected with 40 nl of *shal* or *PIIH* cRNAs (250–500 ng/µl) and cultured in ND96 solution containing (in mM): 96 NaCl, 2 KCl, 1.8 CaCl$_2$(_2H$_2$O), 1 MgCl$_2$, and 5 HEPES (PH7.6) supplemented with 50 mg/l gentamicin, 2.5 mM Na pyruvate, and 5% horse serum for 3–4 days until recording.

Oocytes were injected with a Sutter Instrument microinjector (model NA-1)(San Rafael, CA). This was used to inject ~ 100nl of cRNA (concentration ~50 ng/µl) into *Xenopus* oocytes, which were isolated and maintained according to Quick et al. (1992). Recordings were made by two electrode voltage clamp 3 days later.

2.3 Electrophysiology

Voltage clamp

Immediately after identification or after 4–5 days in organ culture, PD neurons were voltage clamped using an Axoclamp 2A amplifier and pClamp8 software (Axon Instruments, Foster City, CA). Microelectrodes were filled with 3 M KCl and had a tip resistance of 8–10 MΩ for voltage recording and <8 MΩ for current

injection. To isolate neurons from most synaptic input and to isolate I_h and I_A from most other currents, we superfused the ganglion with saline containing 10^{-7} TTX, 5 x 10^{-6} M picrotoxin and 20 mM tetraethylammonium chloride (TEA). For some experiments, 5 and 10 mM CsCl or 50 and 100 µM ZD7288 were added to block I_h. To measure I_h, the cells were held at -40 mV, and the voltage dependence of activation was measured with a series of 8-s hyperpolarizing voltage steps in 5-mV increments from -45 to -120 mV at 20-s intervals. Because the time constant of activation is slow, no leak subtraction was used, so any instantaneous leak current is detectable at the beginning of the step; this value was subtracted from the amplitude of I_h. The reversal potential of I_h was measured from the tail currents after a pre-activating pulse to -100 mV for 8 s with a series of 4-s pulses from -70 to $+30$ mV in 10-mV increments.

To measure I_A, the cells were held at -50mV and the voltage dependence of activation was measured following a deinactivating prepulse to -120 mV for 400 ms and then a series of 400-ms voltage steps from -50 mV to $+40$ mV in 10-mV increments. A control protocol for activation of non-I_A currents was the same as the activation but without the deinactivating step to -120 mV. Traces were leak subtracted using a P/6 protocol with steps opposite to the sign of activation. The control protocol currents were digitally subtracted from the activation protocol currents to isolate I_A.

Synaptic transmission measurements

The PD and LP cells were impaled with two electrodes each to allow independent current injection and voltage recording in each cell. Synaptic measurements were recorded during current clamp with constant amplitude depolarizations of the pre-synaptic LP neuron to evoke IPSPs in the PD cell. Action potentials and transient potassium currents were blocked with 0.1 µM TTX, and 4 mM 4-AP. LP-evoked IPSPs were recorded in the PD during current injection to evoke a range of

hyperpolarizing steps in PD neurons that activated I_h to differing extents. The amplitudes of IPSPs were measured with and without I_h activation by taking advantage of the very slow activation rate of I_h channels. At the beginning of PD hyperpolarization I_h channels have only just begun to open, so I_h activation is low. IPSP amplitudes at this point were compared to those recorded after 8 s of PD hyperpolarization, when I_h channels were more completely activated. Current injection protocols were generated by Clampex software (Molecular Devices, CA). The PD membrane potential was changed by a series of 8-sec current injecting steps in 0.5 - 2 nA increments, at one minute intervals to allow recovery of I_h. If necessary, a bias current was injected into the PD cell to hold the membrane potential at -58mV, which was approximately the average PD membrane potential after blocker application. This is a relatively hyperpolarized potential compared to typical cycling PD neurons, which have a trough around -55 mV. It was chosen to include a maximal number of earlier recordings, when bias current injection was not applied. IPSPs were elicited by 200 ms depolarizing steps to -30 mV into the LP cell at the beginning or at the end (after7.8 sec) of the PD polarization. The LP cell was held at -58 to -60mV between steps. To avoid Cl^- loading during the current steps, which would alter the V_{rev} of the IPSP, we used electrodes filled with 0.6M KSO4 + 20mM KCl. and relatively high resistance (20 MΩ or higher) electrodes were used for the voltage recording. IPSP amplitudes were measured and plotted against the membrane potential prior to the IPSP.

Xenopus oocytes

A standard two-microelectrode voltage clamp was used to measure the current properties of the PIIH splicing variants. The oocytes were voltage clamped using a Geneclamp amplifier driven by Clampex 8.0 software (Molecular Devices, CA). All recording were made in standard ND96 solutions without gentamicin, Na pyruvate, and horse serum. For some experiments, 5-10 mM CsCl or 50-100 µM ZD7288 were included. Microelectrodes were filled with 3 M KCl and had a tip

24

resistance of 1–5 MΩ. We measured I_h from a holding potential of –40 mV with steps from -50 to -120 mV, as described above. These protocols were used in all of the PIIH splice variants except PIIH-I. For PIIH-I, the voltage activation curve was measured with hyperpolarizing voltage steps from −70 to −140 mV, and the preactivating pulse for measuring the reversal potential was to −120 mV. The effect of cAMP was tested by recording the basic parameters before and after switching to a bath solution containing the membrane- permeable cAMP analog, 8-Br-cAMP. Perhaps due to the presence of the vitelline membrane on the oocytes, bath application of 1 mM 8-Br-cAMP caused only a subtle modulation of the activation kinetics and voltage-dependent activation of PIIH channels after 1.5 h. To accelerate the rate of increase in intracellular cAMP in the large oocytes surrounded by a vitelline membrane, we increased the concentration of 8-Br-cAMP to 10 mM; responses to this larger dose were seen within 30 min.

Current analysis

To compare data with earlier work, I_h amplitudes were measured from single exponential fits of the data performed in Clampfit, version 9.0 (Molecular Devices), extrapolated back to the beginning of the hyperpolarizing step (at the point of the leak current) and forward to approximate the steady state at 10 s. Currents were converted to conductances, using a reversal potential (Vrev) of -30 mV for STG neurons and -40 mV for oocytes. (Zhang et al. 2003). The conductance-voltage data were fit to a first order Boltzmann equation (1):

$$\frac{g}{g_{max}} = \frac{1}{(1 + e^{\frac{-(V_m - V_{1/2})}{s}})^n}$$

where g is the conductance, g_{max} is the maximal conductance, $V_{1/2}$ is the voltage of half-activation, s is the slope factor and n = 1 for I_h. The voltage dependence of activation of I_A was determined by converting the peak current to a peak conductance, g, assuming V_{rev} = –86 mV (Hartline and Graubard, 1992). The resulting g/V curve was fitted to a Boltzmann relation (Eq. 1) but with n = 3.

Analysis of rhythmic activity

We analyzed rhythmic activity in PD neurons using Spike2 (Cambridge Electronic Design, Cambridge, UK). The minimal membrane potential (V_{min}) was measured at the most hyperpolarized potential in the trough of the oscillation. The oscillation amplitude was the difference between V_{min} and the most depolarized potential of the slow wave oscillation (at the base of the action potentials, V_{max}). The time to the first spike was the time from V_{min} to the top of the first spike. The cycle duration was the time between the V_{min} of two adjacent oscillations, and the duty cycle was the burst duration divided by the cycle duration. All measures were based on average measures of 40 cycles.

Statistics

All values are given as the mean ± SD. Statistical significances were determined using ANOVA and Student's t-test. Regression lines were plotted, and R values determined using SigmaPlot and SigmaStat 10.0 (Systat Software).

Modeling of IPSP amplitudes.

The ratio of IPSP amplitudes at different membrane potentials was predicted by a simplified model, that takes into account the internal and external chloride and potassium activities and reflects the changing driving force for the IPSP at different membrane potentials (Hille, 2001, Hammond, 2001). In this model, IPSP amplitudes were considered proportional only to the changing driving force of the synaptic chloride currents through the inhibitory glutamate receptors (GluR), while

26

all other voltage-dependent changes of the membrane conductance were either blocked or insignificant. Ohm's law (1) describes the amplitude of IPSPs recorded from the soma. The driving force for the synaptic chloride flux across the membrane changes as a function of electrochemical and concentration gradients according to the Goldman Hodgkin Katz current equation for a single ion species at constant field (2). Under these simplifying assumptions, f was determined as the voltage dependent factor of the synaptic current at a given membrane potential (3). The experimentally derived IPSP amplitude at -90 mV in the presence of 5mM CsCl was chosen as reference, in order to calculate expected IPSP amplitudes at different membrane potentials in the absence of I_h activation (4). I_h is blocked under these conditions and most likely no other voltage dependent channels are active. The extracellular chloride concentration $[Cl]_o$ was 510mM, and the intracellular chloride activity $[Cl]_i$ was assumed to be 37mM at 20°C, based on the IPSP reversal potential and documented values in seawater crustaceans (Freel, 1978, Theander et al, 1999, Cleland and Selverston, 1995, 1998, Marder and Eisen, 1982, Hashemzadeh-Gargari and Freschi, 1992, Doolin et al., 2001).

$$(1) \quad V_{IPSP} = \frac{I_{IPSP}}{g_m}$$

V_{IPSP} : postsynaptic inhibitory potential, recorded in the soma; I_{IPSP}: synaptic current; g_m : overall membrane conductance.

$$
(2) \quad I = \frac{p(zF)^2(V_m)}{RT} \cdot \frac{[Cl]_o - [Cl]_i \cdot e^{\frac{-zF(Vm)}{RT}}}{1 - e^{\frac{-zF(Vm)}{RT}}}
$$

I: ionic flux*; p:* opening probability of GluR*; F:* Faraday number*; z:* charge*; V_m:* membrane potential*; $[Cl]_o$ and $[Cl]_i$:* extracellular and intracellular chloride concentrations*;*

$$
(3) \quad f_{(Vm)} = \frac{(V_m) \cdot ([Cl]_o - ([Cl]_i \cdot e^{\frac{-zF(Vm)}{RT}})}{1 - e^{\frac{-zF(Vm)}{RT}}}
$$

$$
(4) \quad V_{IPSP(Vm)} = \frac{V_{IPSP(-90)} \cdot f_{(-90)}}{f_{(Vm)}}
$$

2.4 Immunocytochemistry

Selected neurons were filled with 4% neurobiotin (NB) in 50mM Tris and 0.5M KCl. For neurobiotin injection, tips of low resistance electrodes (3-5 MΩ when filled with 3M KCl) were backfilled with the NB solution for 10 minutes. The shaft was then filled with 2 M KCl, leaving a small (1cm) gap between the NB in the tip and the KCl in the shaft. The resistance of the filled electrode was 25-90 MΩ. Neurobiotin was injected for about 40 minutes with 500ms,+5nA pulses at 1Hz. Preparations were left for 1 hour for individual neuron staining, or for 3-16 hours for additional gap junction-mediated staining of electrically coupled neurons. For example, after three hours of incubation of a neurobiotin injected VD cell ,the VD, AB, both PD neurons and INT1 were strongly stained and both LPG neurons were more weakly stained. Interestingly, neurobiotin crosses rectifying electrical synapses only in the direction of the rectification. In PD neurons, thirty minutes to one hour of incubation after neurobiotin injection caused no staining of other

28

neurons, whereas longer periods of incubation resulted in additional filling of the other PD and the AB neuron.

STGs were fixed in 3.5% or 2% paraformaldehyde in phosphate buffered saline (PBS) for 90 minutes at room temperature. The fix was washed out with 8 changes of PBST (PBS + 0.3-1 % triton X100) over 2-8 hours. The tissue was then blocked for 3 hours with 5% normal goat serum and 1% BSA in PBST at room temperature and incubated overnight in a rabbit anti-shal (1:2000) , rabbit anti-synaptotagmin (1:1000), or mouse anti-pentaHis (1:20) primary antibody in PBST +5% normal goat serum and 0.1% BSA. The primary antibody was washed out with PBST for 2 hours. The tissue was then incubated for 2 hours with alexa 488-, alexa 568- or alexa 635-conjugated goat anti-rabbit, goat anti-mouse or streptavidin secondary antibodies (Molecular Probes) at 1:500 dilution in PBST + 5% normal goat serum and 0.1% BSA. The secondary antibody was washed out with PBS for 2 hours. All incubations were performed at room temperature with constant shaking. The STG was mounted and cleared on a slide with Vectashield mounting media (Fluka). In several experiments, fixed ganglia were imbedded in 40°C warm, 4% low melting point agarose (Sigma) in *Panulirus* saline prior to antibody treatment. Slices (40-70 µm) were made with a vibrating microtome (Leica Microsystem, speed 4; frequency 9) and transferred to PBST filled wells. Antibody treatment was performed on the floating agarose sections or individual ganglion slices on a slide. Antibody staining in images of x-y planes or series of z-stacks were visualized and collected with a Leica TCS SP2 confocal system. For multiple staining, sequential imaging and narrow emission settings were used to prevent bleed-through effects. Image analysis and 3D reconstructions were performed with Volocity Visualization and Classification Software.

3 I_A-I_h Homeostasis in Pyloric Neurons

Previously, our lab found a homeostatic relationship between expression of the slow hyperpolarization-activated inward current I_h and the fast transient outward current I_A (MacLean et al. 2003, Zhang et al. 2003a). In the lobster, the *shal* gene encodes I_A in all six classes of pyloric neurons (Baro et al., 1996; Baro et al., 2000). An artificial increase of I_A in one of the two electrically coupled Pyloric Dilator (PD) neurons, by intracellular injection of *shal-GFP* RNA, was accompanied by a compensatory increase of I_h, such that the firing properties of the PD neurons did not change despite significant increases in both I_A and I_h. This homeostatic up-regulation of I_h appeared to be independent of activity changes, as overexpression of a mutated, non-functional form of I_A still caused an increase of I_h current. A novel molecular mechanism was proposed which could detect the presence of additional I_A RNA or protein and consequently trigger the compensatory increase of I_h.

To understand this interaction, and to determine if it is unique to PD neurons, in collaboration with Dr Jason MacLean, I over-expressed I_A via *shal-GFP* RNA injection in three pyloric neurons, the Pyloric Dilator (PD), the Lateral Pyloric (LP) and the Ventricular Dilator neuron (VD), and performed preliminary studies of the Inferior Cardiac (IC) neuron. This allowed me to examine in detail several properties of the system.   1) I studied the voltage dependence and kinetic properties of I_A and I_h in each pyloric neuron type, to determine whether the newly inserted channels were modified to generate neuron-specific I_A current properties, or whether a similar current is generated in all neuron types. 2) I studied the overall effect of shal-GFP overexpression on pyloric network activity patterns. 3) I characterized a low threshold, non-I_h component of the hyperpolarization

30

activated inward current. 4) I studied the effects of ectopically expressing a non-functional mutant of I_A, with an altered pore region that prevented ion flux through the channels, to examine whether the homeostatic response could be elicited by the presence of I_A protein alone. 5) I described a large variability in I_A amplitudes, but a positive correlation of I_A and I_h, among non-injected PD neurons. 6) I confirmed the localization of new I_A protein. 7) Previous work has shown that the homeostatic upregulation of I_h appeared to be uni-directional, since overexpression of the I_h gene from the related species *Panulirus argus* did not increase A-type currents in PD neurons (Zhang et al. 2003b). To examine if this result was caused by species-specific limitations, I studied the response of over-expressing *Panulirus interruptus* I_h splice variants in oocytes and in PD neurons in collaboration with Dr Qing Ouyang in our lab, to see if over-expression of a species–specific form of I_h could lead to an up-regulation of I_A.

3.1 Properties of Increased I_A after Shal-GFP Overexpression

I compared the amplitude and conductance/voltage relationships of I_A in different pyloric motoneuron types, before and after expression of shal-GFP. Following *shal-GFP* RNA microinjection into PD, LP, VD and IC neurons, I consistently found large changes in I_A in neurons that exhibited bright GFP fluorescence. Seventy two hours after microinjection of *shal-GFP* RNA, the I_A amplitude at a depolarizing step to 30 mV was increased by 72% to 400% compared to the I_A amplitude in control neurons that were injected with *GFP* RNA or with a dye (Figure 3.1A).

Peak conductance/voltage relationships for activation and inactivation were only slightly altered. Two consistent changes were observed in all neuron types following expression of *shal-GFP*. First, the V_{act} shifted significantly in a depolarized direction in the expressing neurons. With a third order Boltzmann fit

to the data, the V_{act} values of the individual gating particles of all four neuron types shifted by a range of 3.9 to 10.7mV, corresponding to depolarizing shifts of 2.5 to 6.2 mV in the voltage at which half of the channels open (Figure 3.1B, Table 3-1). The slope of the activation curve was somewhat steeper in the shal-GFP expressing cells, though not significantly so. Second, while shal-GFP expression did not change the V_{inact} values, the slope of the inactivation curve became significantly shallower in PD and VD neurons, increasing the slope parameter for inactivation by 1.4 to 2.5mV (Figure 3.1B, Table 3-1). This parameter was not measured in IC neurons.

In general, the *shal-GFP*-evoked current in the pyloric neurons had properties more similar to the current expressed in Xenopus oocytes after lobster *shal-GFP* RNA injection than the endogenous pyloric currents. The slope of the inactivation curve in oocytes was shallower than in control pyloric neurons, and all three *shal-GFP* RNA injected neuron types showed slope values that were intermediate between the neuronal and oocyte values (Figure 3.1 C, Table 3-1; this was not measured in IC neurons). The addition of the GFP tag did not affect the properties of the current: RNA injection of *shal* and *shal-GFP* generated currents with identical properties, both in oocytes (Figure 3.1 C) and in PD neurons (MacLean et al., 2003).

The properties of endogenous I_A vary significantly between different pyloric neuron types under control conditions (Table 3-1; Baro et al. 1997). However, after expression of shal-GFP, this variance decreased and I_A properties became more homogeneous. Analysis of variance (ANOVA) of V_{act} ($F_{(2,43)} = 2.6$; $p = 0.9$), V_{inact} ($F_{(2,39)} = 0.7$; $p = 0.5$), the slope of activation ($F_{(2,18)} = 1.4$; $p = 2.7$), and the slope of inactivation ($F_{(2,43)} = 2.2$; $p = 0.12$) showed that the new current became statistically indistinguishable between the different neuron types. These data suggest that the newly expressed protein in pyloric neurons may not have been sufficiently modified in cell-specific ways, and therefore retained properties more similar to the current in shal-GFP expressing oocytes.

The time course of I_A inactivation in pyloric neurons is best fit with a double-exponential relation. In PD, LP, and IC neurons under control conditions, the majority of the current inactivates with the slower time constant (τ_{slow}, varying between 80 and 110 ms), whereas a smaller fraction ($< 50\%$) inactivates rapidly (τ_{fast}, varying between 7 and 25 ms). Control VD neurons have exceptionally rapid inactivation kinetics with four- to five-fold faster decay of both the fast and the slow component (Baro et al. 1997; Table 3-1). After expression of shal-GFP, the inactivation kinetics of I_A were accelerated, and the majority of the current inactivated with the fast time constant (Figure 3.2 A; Table 3-1). In PD and LP neurons during a voltage step to -20 mV, the percentage of amplitude-normalized, rapidly inactivating current increased from below 40 % to above 50 %, while the time constants did not change. Conversely, I_A inactivation kinetics in the VD neuron decelerated and the time constants assumed values similar to those seen in the other pyloric neurons after shal-GFP expression (Figure 3.2, Table 3-1). The properties of the additional current dominated over its small, rapidly inactivating endogenous I_A. As in shal-GFP expressing LP and PD neurons, the major component of the new current inactivated rapidly. This shift in the current inactivation kinetics rendered the I_A in pyloric neurons more similar to the current in shal-GFP expressing oocytes (Table 3-1). The variance of τ_{slow} and τ_{fast} values between the different neuron types significantly decreased, as the current in the VD neuron became more similar to the IC, LP, and PD neuron (ANOVA: $F_{(1,33)} = 0.02$; $p = 0.8$), suggesting again that the expressed protein may not have been completely modified to the neuron-specific parameters.

The kinetics of recovery from I_A inactivation were examined using hyperpolarizing voltage steps to -120 mV of increasing duration (range 40–800 ms). This protocol gradually removes the inactivation of I_A that is present when the neuron is clamped at -50 mV (Figure 3.2, B). The curve generated by measuring maximal current amplitude against time of hyperpolarization was fit with a single exponential time constant (Figure 3.2 C). In non-injected PD, LP, and VD neurons, recovery from inactivation was rapid and essentially complete after 200 ms. After shal-GFP

expression, complete removal of inactivation was significantly slower and took > 500 ms at -120 mV (Figure 3.2 B and C; Table 3-1; PD, p = 0.001; LP, p = 0.004; and VD, p = 0.03; this parameter was not measured for IC neurons). This shift resembles the even slower kinetics of I_A recovery from inactivation in shal-GFP expressing oocytes, further suggesting that the new current in pyloric neurons was not modified to neuron-specific parameters.

3.2 Properties of the Hyperpolarization-Activated Inward Current I_h after Shal Expression

The increased I_A in shal-GFP expressing PD, LP, VD and IC neurons was accompanied by a significant increase in the hyperpolarization activated I_h current (Figure 3.3A, Table 3-2). As previously seen in PD neurons (MacLean et al., 2003), the enlarged inward current slowly activated during long hyperpolarizing voltage steps from -40 mV and was blocked by 5 and 10 mM Cs^+, characteristic features of I_h. To minimize contamination of I_h measurements at large hyperpolarizations with a current of unknown origin (see below for details), I_h amplitudes were compared at -90 mV, and the analysis of I_h was limited to steps between -40 mV to -100 mV. Unfortunately, activation of I_h does not approach saturation at these more depolarized potentials, and values obtained from a first order Boltzmann fit of the data need to be read with caution due to the difficulty in performing this fit. I was able, however, to make preliminary assessments of the effects of shal-GFP overexpression on the voltage dependence of the modified I_h. During a voltage step to -90 mV, I observed an average 94 % increase in I_h amplitude, and a 94 % increase in maximal conductance (both p < 0.001) in shal-GFP-expressing PD neurons (Figure 3.3 A, Table 3-2). I_h amplitude and maximal conductance also increased in shal-GFP expressing VD, LP and IC neurons, however the difference only approached significance for the 32% conductance increase in VD neurons (p = 0.13) due to large variance within this data (Table 3-2). The change of I_h amplitude in the VD neuron became significant when data

was pooled between Dr MacLean and me, leading to a 235 % increase after shal-GFP expression at the step to -100 mV (p = 0.03, Table 3-2). The mean normalized conductance/voltage relationships of control neurons and neurons expressing shal-GFP are shown in Figure 3.3 B. In general, despite the increase in maximal conductance of I_h, there was no significant change in the channel properties at the voltages tested in PD, LP and VD neurons. V_{act} in these neurons, as well as the slope of activation were not significantly modified following the expression of shal-GFP (Table 3-2). In the IC cell, overexpression of I_A appeared to hyperpolarize the V_{Act} of I_h (Table 3-2), but the sample size for this cell type was quite small (Table 3-2). Although the voltage dependence of channel gating of the shal-GFP-evoked I_h was unmodified, I found significant differences in the kinetics of channel activation (Table 3-2, Figure 3.3A). The enhanced I_h in shal-GFP expressing PD, VD and IC neurons showed somewhat slower activation parameters: activation showed a trend to be slower when measured at steps to -100 mV, with τ_{act} increasing slightly for PD neurons and more dramatically for VD and IC (Table 3-2). However, I did not observe a change in the activation kinetics of LP neurons. Even in non-injected neurons, activation of I_h was so slow that it was essentially not measurable at potentials more depolarized than -60 mV, and became slower still in most shal-GFP expressing neurons. Deactivation after returning to the holding potential also appeared to be slower in the shal-GFP expressing neurons (see tail currents in Figure 3.3).

3.3 Firing Properties of Shal-GFP Expressing Pyloric Neurons

Heterogeneity of I_A amplitude and kinetic properties among the different pyloric neurons has been proposed to play a role in determining their functional roles in the pyloric network, as subtle changes of 10-25% in I_A cause strong alterations in neuronal firing (Hartline, 1979; Tierney and Harris-Warrick, 1992; Baro et al.,

1997; Kloppenburg et al, 1999). Accordingly, a 125 – 400 % increase of I_A by overexpression of shal-GFP should dramatically alter the firing properties of the neurons. However, when comparing the rhythmic activity of control and shal-GFP expressing neurons, most of the activity parameters remained unchanged (Figure 3.4). Despite the large increase in I_A in VD, PD and LP neurons, there were only subtle changes in rhythmic neuronal activity, consistent with previous data for the PD neurons (MacLean et al., 2003). The cycle frequency, oscillation amplitude, membrane potential at the trough of the oscillation, and the number of spikes per burst were not significantly changed, though there were some subtle, non-significant trends, especially in LP and VD neurons that might be explained by an increase in I_A (Figure 3.4). Only two parameters changed in a statistically significant way. In the VD neuron, shal-GFP expression led to a significant (p = 0.02) decrease in the slope of the rise phase from 0.1 ± 0.02 mV/ms to 0.06 ± 0.01 mV/ms. Second, following expression of exogenous I_A, the PD neuron's overall spike amplitude decreased significantly from 9.7 ± 0.5 mV to 7.3 ± 1.7 mV, (p = 0.008). These changes were consistent with an increase in I_A.

3.4 An Unidentified Component of the Inward Current

During large hyperpolarized steps well below the resting potential, in addition to I_h, I often observed an unidentified component of the inward current with unexpected jumps (Figure 3.5, Table 3-3). The effect occurred mostly in RNA-injected neurons, and more often with large hyperpolarizations than small hyperpolarizations. On occasion, I also found irregular jumps in untreated neurons (Figure 3.6 A). It is unlikely that current flow through I_h channels was causing these jumps, as several properties distinguish it from typical I_h behavior. I_h generally activates gradually with a smooth exponential time course. However, when the unidentified current was present, it activated abruptly, causing large irregular steps superimposed onto the current trace, so that I_h activation no longer

36

could be fit with a single exponential curve. Moreover, the unidentified current deactivated much slower than I_h, with recovery times ranging from 20 s up to several minutes. Last, classic I_h-blockers, for instance Cs^+ (5 and 10 mM) and ZD 7288 (50 μg), did not block these jumps (Figure 3.6 B).

Typically, jumps were first noticeable during steps to membrane potentials below -90mV. RNA-injected neurons were more likely to display jumps in the current trace than untreated neurons (Table 3-3). In RNA-injected PD neurons, shal-GFP expressing cells were more likely to exhibit this current, and generally at less hyperpolarized voltages than cells that were expressing GFP alone (Table 3-3). I compared the proportion of shal-GFP expressing, GFP expressing and untreated PD neurons exhibiting the current jumps at steps to -100, -110, and -120 mV (Table 3-3). At steps to -100 mV, jumps occurred primarily in shal-GFP expressing neurons, occasionally in GFP expressing cells, and never in untreated neurons. The difference was significant between shal-GFP expressing and untreated neurons (*Fisher's exact* chi-square test, $p < 0.05$), and approaching significance between shal-GFP and GFP expressing cells ($p = 0.07$). When neurons were hyperpolarized to -110 mV, jumps were noticeable in both shal-GFP expressing and GFP expressing PD neurons, but not in untreated neurons. The difference was highly significant for both RNA-injected groups when compared to the untreated cells ($p < 0.01$), but not when compared with each other ($p = 1$). At very hyperpolarized steps to -120 mV, jumps occurred in all three groups, with no significant difference between them ($p > 0.3$ for shal-GFP and GFP expressing compared to untreated neurons; $p = 1$ for shal-GFP compared to GFP expression).

3.5 Expression of a Nonfunctional Mutant of Shal-GFP in PD Neurons

In a previous study, a non-functional mutant of shal-GFP (mshal) was expressed in PD neurons to determine whether the up-regulation of I_h depended on the

functionality of the newly expressed I_A channels, or depended on the simple presence of *shal-GFP* RNA or shal protein (MacLean et al., 2003). To generate the mutant, the sequence of the pore region was altered from GYG to AFA (aa 372-374) to create a channel protein with a non-functional pore.

In order to separate a potential increase in I_h from the unidentified inward current described in Section 1.5, I repeated these experiments but limited analysis to voltage steps only down to -100 mV. The two PD neurons were injected with the mutant *shal-GFP* (*mshal-GFP*) and *GFP* RNA, respectively, providing a within-animal control. After 72 hours in organ culture, protein expression was confirmed by GFP fluorescence of both PD neurons, and I_A and I_h were measured in voltage-clamp (Figure 3.7 and Figure 3.9).

As expected, the amplitude of I_A was not affected by the expression of mshal-GFP. However, while the previous study had shown an increase of I_h in mshal-GFP expressing PD neurons using large hyperpolarizations, I did not find a statistically significant difference when using only smaller hyperpolarizations (n = 4 pairs). The g_{max} for I_h was 0.2 ± 0.05 μS in mshal-GFP expressing cells, with average current amplitudes of 6 ± 2.2 nA at -90 mV, and 0.2 ± 0.09 μS in control GFP expressing neurons, with average amplitudes of 8 ± 2.9 nA at -90 mV (n = 4 PD pairs). It is worth mentioning however, that these values were relatively large in both mshal-GFP and GFP expressing neurons, when compared to the I_h amplitudes in control PD neurons of the first section (Table 3-2). Re-evaluation of activation parameters obtained in the previous study also showed no significant difference when the data were re-analyzed with the same restrictions to I_h measurements, excluding hyperpolarized steps below -100m. While it appeared that the mshal expressing cells in fact had a larger Ih (Figure 3.10), this was only the case at lower (more hyperpolarized) voltages.

I_h activation parameters remained unchanged between mshal-GFP and GFP expressing PD neurons, and both showed the same firing properties after 72 hours (Figure 3.8). These results were also in contrast with the previous data, where

38

changes in firing properties were reported after expression of mshal-GFP (MacLean et al. 2003).

3.6 Positive Correlation between I_A and I_h in Non-injected PD Neurons

In my experiments, the maximal conductance of I_A and I_h varied considerably between control, uninjected PD neurons in different animals. Golowasch et al. (1999) have described similar variance of I_A and other currents within a cell type. In fact, a comparison of I_A conductance from experiments recorded during the time course of three years, showed fluctuations of I_A amplitude, which were larger at the beginning of the year, and significantly decreased between the months of May and October (*Pearson's* correlation test, $p < 0.05$).

Interestingly, analysis of I_A conductances at +15 mV and I_h conductances at - 90 mV in a 29 control neurons showed a statistically significant positive correlation: neurons with a higher baseline level of I_A also tended to have a higher baseline level of I_h ($r = 0.608$ for a linear relationship, $p < 0.001$; Figure 3.11). The cell's capacitance, and thus size, does not vary greatly between PD neurons: Baro et al. (1997) reported that the input capacitance of 10 PD neurons was 1.2 ± 0.07 nF. Therefore, the variability of current amplitudes between the neurons was more likely due to different current densities than to differences in size. These results strongly suggest that the up-regulation of I_h after overexpression of I_A is not simply an experimental artifact, but reflects a relevant interaction between I_A and I_h in pyloric neurons, which might normally lead to co-regulated expression levels of these two channels within a defined ratio.

3.7 Localization of I_A and the Implications for Neuronal Cycling

It has been previously hypothesized that the homeostatic compensatory increase in I_h accounts for the failure to change the firing properties of PD neurons after shal-GFP expression (MacLean et al., 2003). However, an inappropriate targeting of the new shal channels in the injected neurons was observed, which might also contribute to the lack of effect of the increased I_A. shal-GFP fluorescence and increased shal immunocytochemical labeling were localized only to the soma and the proximal initial neurite (Figure 3.12); the injection-evoked increase in I_A label disappeared before or near the initial neurite's first branch in the neuropil. This is in marked contrast to the normal pattern of shal expression in uninjected neurons (see results in Chapter 4): the protein was found in both the soma and all the neurites within the STG, where synaptic integration and spike initiation occur (Baro et al., 2000). In order to verify that the labeling procedure did not discriminate against central neuropil labeling, two separate RNAs were co-injected into a PD neuron, one encoding cytoplasmic GFP and the other encoding shal (without the GFP tag). GFP labeling in two injected pyloric neurons was found in the soma, throughout the neurites and in the axon leaving the STG. In contrast, antibody labeling of shal protein in the same neurons shows that the new intense labeling was localized only to the soma and initial neurite of the injected neurons (Figure 3.12).

3.8 Directionality

Previous work showed that the I_h upregulation response to I_A overexpression appeared to be uni-directional. Overexpression of PAIH, the I_h gene from the related species *Panulirus argus,* did not increase A-type currents in PD neurons and consequently their firing activity was altered by the uncompensated elevation in I_h (Zhang et al. 2003). However, this result may have been flawed by the use of the I_h gene from a different species, since PAIH is different from the endogenous *Panulirus interruptus* I_h gene *PIIH.* This gene undergoes extensive alternative splicing of its RNA (Ouyang et al., 2007). Functional expression of 10 different PIIH splice forms in *Xenopus* oocytes produced currents with very different voltage dependencies, kinetic properties, and cAMP sensitivity, which were all blocked by the Ih channel blockers Cs+ and ZD7288 (Ouyang et al., 2007). There are significant sequence differences between all PIIH splice variants and the single PAIH sequence so far reported (Gisselmann et al. 2005). I collaborated with Dr. Qing Ouyang in studying the effects of PIIH overexpression in PD neurons to further explore the question of directionality of the homeostatic response, and to understand how I_h contributes to pyloric motor pattern generation. We injected RNA for two of the ten functional splice variants, PIIH ABS-I or PIIH A-II, into PD neurons and measured how this altered the neurons' electrophysiological properties. We chose these two variants because they contain most of amino acid sequences that are not found in PAIH (e.g., segment A, C1, and pore II), they cover all C-terminal amino acid differences, and their currents activated quickly at significantly more positive potentials when they were expressed in *Xenopus* oocytes (Ouyang et al., 2007).

One PD was injected with PIIH ABS-I or PIIH A-II RNA, whereas the other was injected with GFP RNA as a control. Both spice variants produced very similar results; only data for *PIIH AB$_S$-I* are shown, as it had a much higher rate of successful expression. Our results with PIIH ABS-I were similar to those

previously found with PAIH RNA injections (Zhang et al. 2003). Hyperpolarizing steps from -40 mV to more negative values (-45 to -120 mV) produced a much larger I_h in PIIH ABS-I overexpressing PD neurons than in GFP-expressing cells (Fig. 6A): the average maximal conductance was increased nearly threefold (n = 16 paired PDs, Table 3-4). Consistent with the rather depolarized V_{act} of PIIH ABS-I in oocytes (Ouyang et al., 2007), the current in PIIH ABS-I-expressing PD neurons was activated at significantly more depolarized potentials than in control PD neurons: the voltage for half-maximal activation was shifted by 9 mV to more depolarized voltages (-81 ± 4 vs. -90 ± 6 mV; p < 0.01), whereas the slope factor decreased by 3.8 mV (10 ± 1.1 vs. 6.2 ± 0.8; p < 0.01). Furthermore, the current had a significantly faster time constant of activation than the current in control neurons. For example, at -100 mV, τAct was 2.2 ± 0.5 s for PIIH ABS-I expressing PD neurons and 3.4 ± 0.8 s for control neurons (Table 3-4, Figure 3.13, A and B). The I_h in PIIH ABS-I expressing PD neurons was blocked by 5 mM Cs+ or 100 μM ZD7288, indicating that the increased inward current is a typical H-current (Figure 3.13E).

Although overexpression of PIIH ABS-I in PD neurons produced an average threefold larger Ih, this current did not evoke any compensatory increase of IA (Figure 3.13, C and D). The average peak current at +30 mV was 580 nA in control and 540 nA in PIIH ABS-I-expressing PD neurons (Table **3-5**). There were no significant differences in the amplitude, voltage dependence of activation and inactivation, or kinetics of I_A between the PIIH ABS-I-expressing PDs and the GFP-expressing controls (n = 16 paired PD neurons; Figure 3.13, C and D, Table **3-5**).

To verify this result, we tested the effects of second variant, PIIH A-II, which differs by the lack of the BS segment and the insertion of pore II segment in the P region. Expression of this variant in PD neurons produced an average twofold increase in I_h, depolarized the V_{act} by 4 mV, decreased the activation slope factor by 1.2 mV, and accelerated the time constant for activation, when compared to I_h in control cells (p = 0.05, for all comparisons). However, the amplitude of I_A did

not change significantly after expression of this splice variant either (560 ± 140 nA for control vs. 580 ± 110 nA for PIIH A-II-injected PD neurons at +30 mV; $p > 0.05$; $n = 7$ paired PD neurons). Thus, overexpression of PIIH produced an increase in I_h but did not cause a compensatory increase in I_A in PD neurons.

As predicted for an uncompensated elevation of I_h, PIIH ABS-I overexpression altered the firing properties of the PD neurons in a manner that depended on the relative increase in I_h. In the presence of modulatory inputs from other ganglia, the PD neurons in the pyloric network oscillate and fire rhythmic bursts of action potentials with a characteristic oscillation amplitude, number of spikes per burst, duty cycle, and phasing relative to other pyloric neurons. When Zhang et al. (2003) overexpressed the homologous PAIH from P. argus in a PD neuron, these firing properties changed, compared to the control, Fast Green-injected PD neuron in the same ganglion. Increased I_h depolarized the minimum membrane potential of the cell, reduced the oscillation amplitude, decreased the time to the first spike, and increased the duty cycle and number of action potentials per burst. We tested whether overexpression of PIIH ABS-I would cause similar changes in PD neurons when compared to the paired GFP-injected control in the same ganglion. Seven of 13 PD neurons showed little change in firing properties after PIIH expression. On the other hand, the remaining six PD neurons showed significant changes in firing properties (Figure 3.14 A). In these preparations, the PIIH ABS-I expressing PD neuron fired more action potentials per burst (9 ± 2 vs. 7 ± 1) with longer burst duration (0.21 ± 0.07 vs. 0.18 ± 0.05 s), increased duty cycle (0.30 ± 0.09 vs. 0.25 ± 0.08), had more depolarized V_{min} (-56 ± 3 vs. -60 ± 3 mV) and V_{max} (-40 ± 5 vs. -44 ± 6 mV), and showed a decreased time from the oscillation minimum to the first spike (0.35 ± 0.1 vs. 0.38 ± 0.1s; $p = 0.05$, for all comparisons). We sought an explanation for the difference between these two groups of experiments and proposed that the degree of change in firing properties might vary with the level of overexpression of PIIH. Indeed, the amount of I_h did vary widely between the different PIIH ABS-I expressing PD neurons, with twofold to more than ninefold

increases in maximal Ih conductance (Figure 3.14, B–D). As predicted, the neurons that showed a greater increase in Ih also showed greater changes in their firing properties. We analyzed the changes in firing parameters as a function of the Ih conductance increase, the shift in V_{act}, and the change in activation slope factor, to examine possible correlations. As seen in Figure 3.14, B–D, the number of spikes/burst, the burst duration and the duty cycle all showed a significantly positive relationship with the level of I_h overexpression ($R \geq 0.7$, $p < 0.01$). Interestingly, there was a threshold effect for the increase in Ih conductance needed to change these parameters: neurons with less than two to threefold increase of Ih showed no detectable changes, whereas neurons with larger increase showed a significant correlation between Ih amplitude and change in firing properties. As the overexpression of Ih increased, it was accompanied by a decrease in the PD neuron's slope factor and depolarization of its Vact; this presumably arises from the greater fraction of total Ih channels in the neuron membrane arising from PIIH ABS-I, with its steeper slope factor and depolarized Vact. As a consequence, there was also a positive relationship between the change in slope factor and Vact and the changes in firing properties (R values ≥ 0.7), but only the relationships between slope factor and the changes in firing properties (the number of spikes/burst, burst duration and the duty cycle) were statistically significant ($P < 0.05$). These results show that an increase in PIIH changes the firing properties of PD neurons; however, the change had to be large, with a threshold of two-to threefold increase in Ih before the neuron changed its activity pattern.

The absence of any measurable change in the I_A amplitude and kinetics confirms our earlier tentative conclusion that the homeostatic compensation between I_A and I_h is uni-directional. However, it remains possible that overexpression of one of the other PIIH splice variants might confer the ability to simultaneously up-regulate I_A.

44

A

PD

LP

200 nA

VD

IC

200 ms

-50 mV ⌐ +20 mV
      └─ -120 mV

C

Oocyte

|1 A

-70 mV
        +10 mV
    -90 mV

B

45
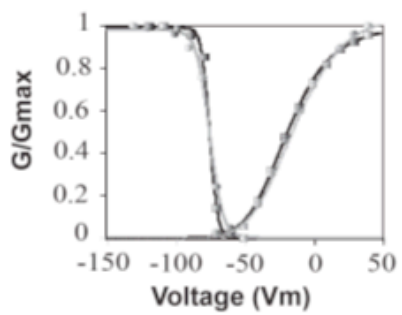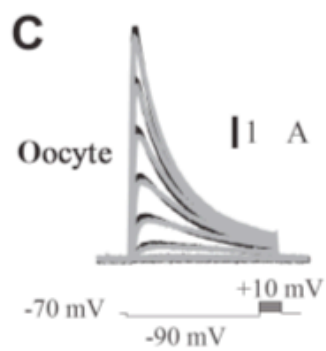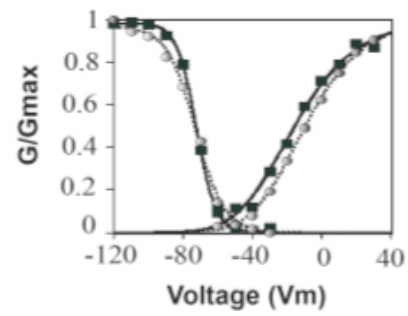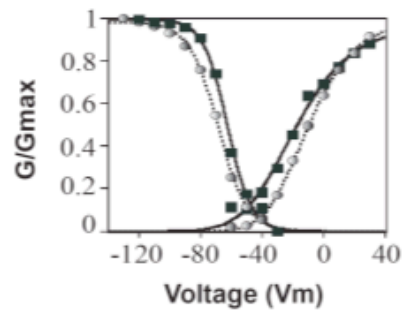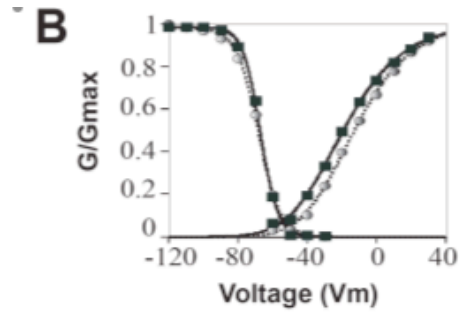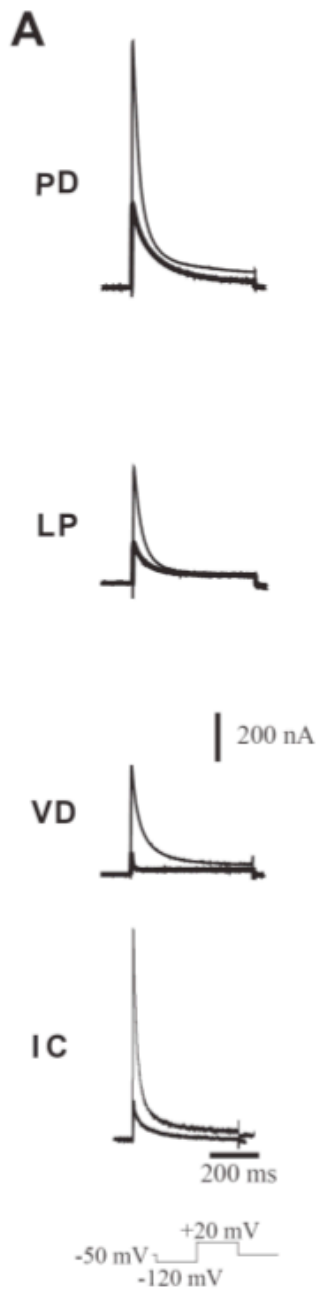
Figure 3.1 IA amplitude increased 72 hours after microinjection of *shal-GFP* RNA. A) IA current response to a depolarizing voltage step to +30 mV, 72 hours after microinjection of RNA. IA amplitude in shal-GFP expressing neurons (thin) was increased by 72% to 400% over IA amplitude in control neurons (solid). PD; Pyloric Dilator neuron; LP: Lateral Pyloric neuron; VD; Ventricular Dilator neuron; IC: Inferior Cardiac neuron. B) Peak conductance/voltage relationships for activation and inactivation were slightly changed in neurons expressing shal-GFP (dashed) compared to control (solid). C). shal K+ current in response to graded voltage steps in shal (black) and shal-GFP (gray) expressing oocytes are overlaid. B) Peak conductance/voltage relationship for activation and inactivation were unmodified in currents evoked by the shal-GFP construct (gray) when compared to shal (black) in oocytes.

46
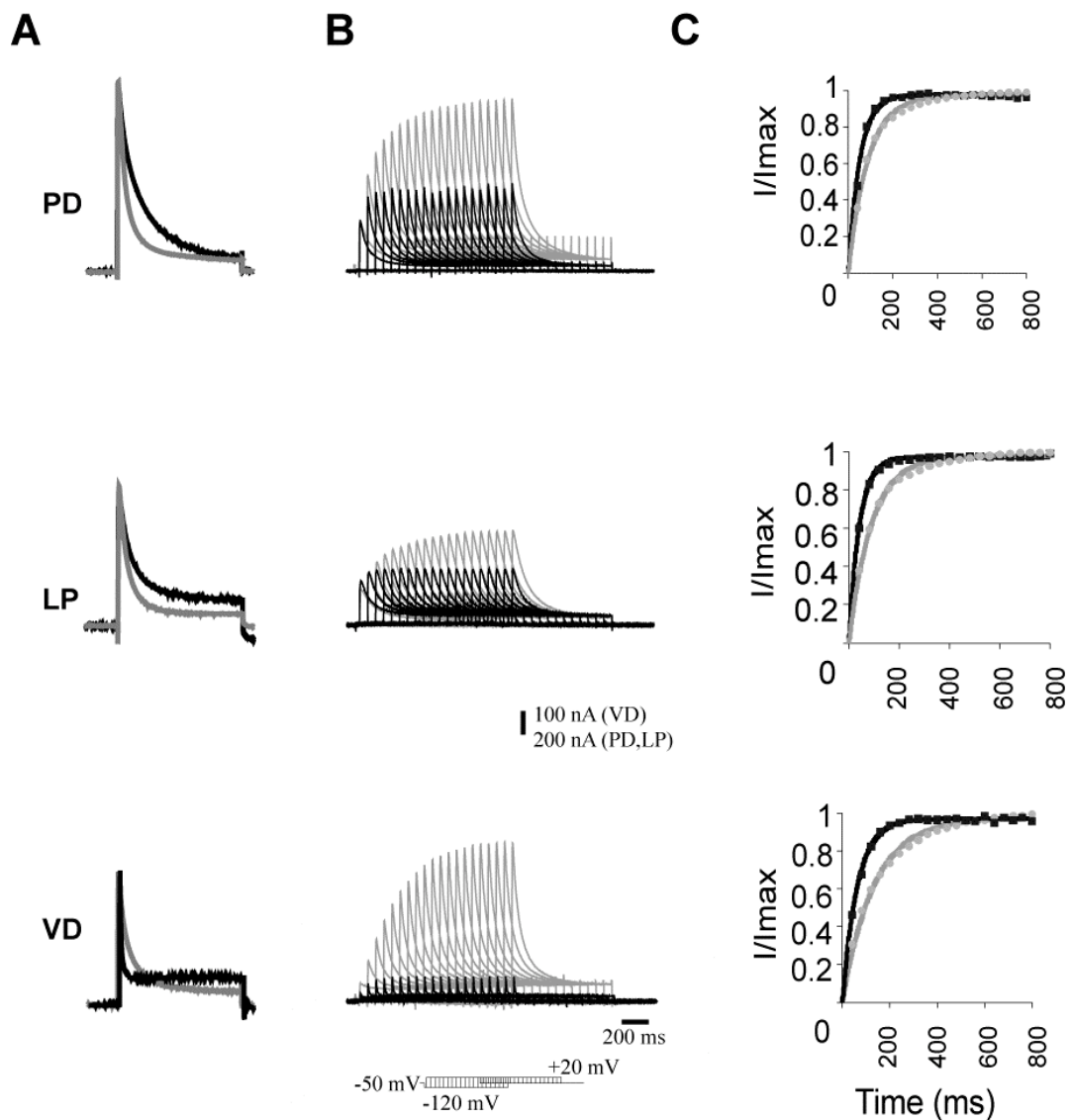
Figure 3.2 The kinetics of the expressed channel were modified in shal-GFP expressing neurons. A) The rate of inactivation of I_A was increased in shal-GFP expressing neurons. The amplitude-normalized I_A in a control neuron (black) and a neuron expressing shal-GFP (grey) are superimposed to show the more rapid rate of inactivation in the shal-GFP expressing neurons.   B) Release from inactivation of I_A was modified in shal-GFP expressing neurons. I_A was evoked by depolarizing steps to +20 mV, following hyperpolarizing steps to -120 mV of varying durations, in control (black) and shal-GFP (grey) expressing neurons. C) Comparison of plots of I/Imax vs. time in control (black) and shal-GFP expressing (grey) neurons.

Cell Type	Imax (nA)	Gmax (μS)	Act $V_{1/2}$ (mV)	Act slope factor (mV)	Inact $V_{1/2}$ (mV)	Inact slope factor (mV)	Inact τ_{fast} (ms)	Inact τ_{slow} (ms)	% peak IA (τ_{fast})	% peak IA (τ_{slow})	Release from Inact τ (ms)
PD control *n=37*	405.11 ± 97.4	4.2 ± 1.1	-41.9 ± 6.3	-17.7 ± 4.5	-67.2 ± 4.9	4.2 ± 0.3	20.6 ± 5.8	101.9 ± 31.5	33.6 ± 1.5	66.4 ± 1.5	51.6 ± 11.3
expressing *n=38*	696.3 ± 156.5**	6.8 ± 1.7**	-39.0 ± 4.3*	-18.4 ± 2.7	-68.6 ± 7.6	5.6 ± 1.3**	23.7 ± 5.8	101.0 ± 20.2	53.2 ± 1.0**	46.8 ± 1.0**	89.4 ± 34.4**
LP control *n=9*	201.8 ± 49.6	2.0 ± 0.4	-41.5 ± 5.2	-21.4 ± 8.2	-62.1 ± 6.0	7.0 ± 1.3	24.2 ± 3.6	107.6 ± 29.5	41.9 ± 1.0	58.1 ± 1.0	43.6 ± 17.4
expressing *n=9*	491.2 ± 101.7**	5.1 ± 1.3**	-34.4 ± 5.6**	-19.4 ± 4.5	-70.0 ± 10.9	8.2 ± 1.2	28.1 ± 13.0	104.6 ± 27.5	56.9 ± 2.8*	43.1 ± 1.0*	91.8 ± 23.7**
VD control *n=9*	82.6 ± 33.3	0.8 ± 0.3	-45.2 ± 8.0	-20.7 ± 6.2	-71.8 ± 6.1	4.2 ± 0.6	4.7 ± 2.4	41.4 ± 33.1	46.9 ± 2.0	53.1 ± 2.0	62.3 ± 9.6
expressing *n=12*	358.9 ± 124.2**	3.6 ± 1.1**	-35.6 ± 7.1**	-19.1 ± 2.5	-72.1 ± 7.7	6.7 ± 1.7**	22.4 ± 11.4**	103.5 ± 39.2**	59.3 ± 1.0	40.7 ± 1.0	197.0 ± 132.1*
IC control *n=4*	68.1 ± 28.2	0.7 ± 0.3	-40.6 ± 3.8	-18.0 ± 1.8	NA	NA	7.5 ± 1.2	81.7 ± 37.8	50.4 ± 4.6	49.6 ± 4.6	NA
expressing *n=2*	358.5 ± 205.7	3.8 ± 1.9	-33.6 ± 4.8	-17.3 ± 7.3	NA	NA	15.3 ± 3.8	80.9 ± 9.6	64.7 ± 20.7	35.3 ± 20.7	NA
Lobster I_{shal} Oocyte	NA	NA	-42.9 ± 2.3 *n=6*	-21.1 ± 2.7 *n=6*	-68.6 ± 2.5 *n=8*	7.4 ± 2.2 *n=8*	37.7 ± 5.0 *n=5*	184.9 ± 117.4 *n=5*	53.3 ± 1.8 *n=5*	46.7 ± 1.8 *n=5*	889.0 ± 597.3 *n=5*
Lobster $I_{shal\text{-}GFP}$ Oocyte	NA	NA	-41.6 ± 5.4 *n=6*	-20.1 ± 1.5 *n=6*	-68.9 ± 6.1 *n=9*	8.4 ± 1.0 *n=9*	56.9 ± 19.2 *n=11*	192.0 ± 54.1 *n=11*	62.4 ± 9.9 *n=11*	37.6 ± 10.3 *n=11*	1012.1 ± 598.1 *n=8*

Values indicate averages± S.D.
* significantly different (p<0.05)
** significantly different (p<0.01)

Table 3-1 Properties of I_A in control and shal-GFP expressing neurons.

48
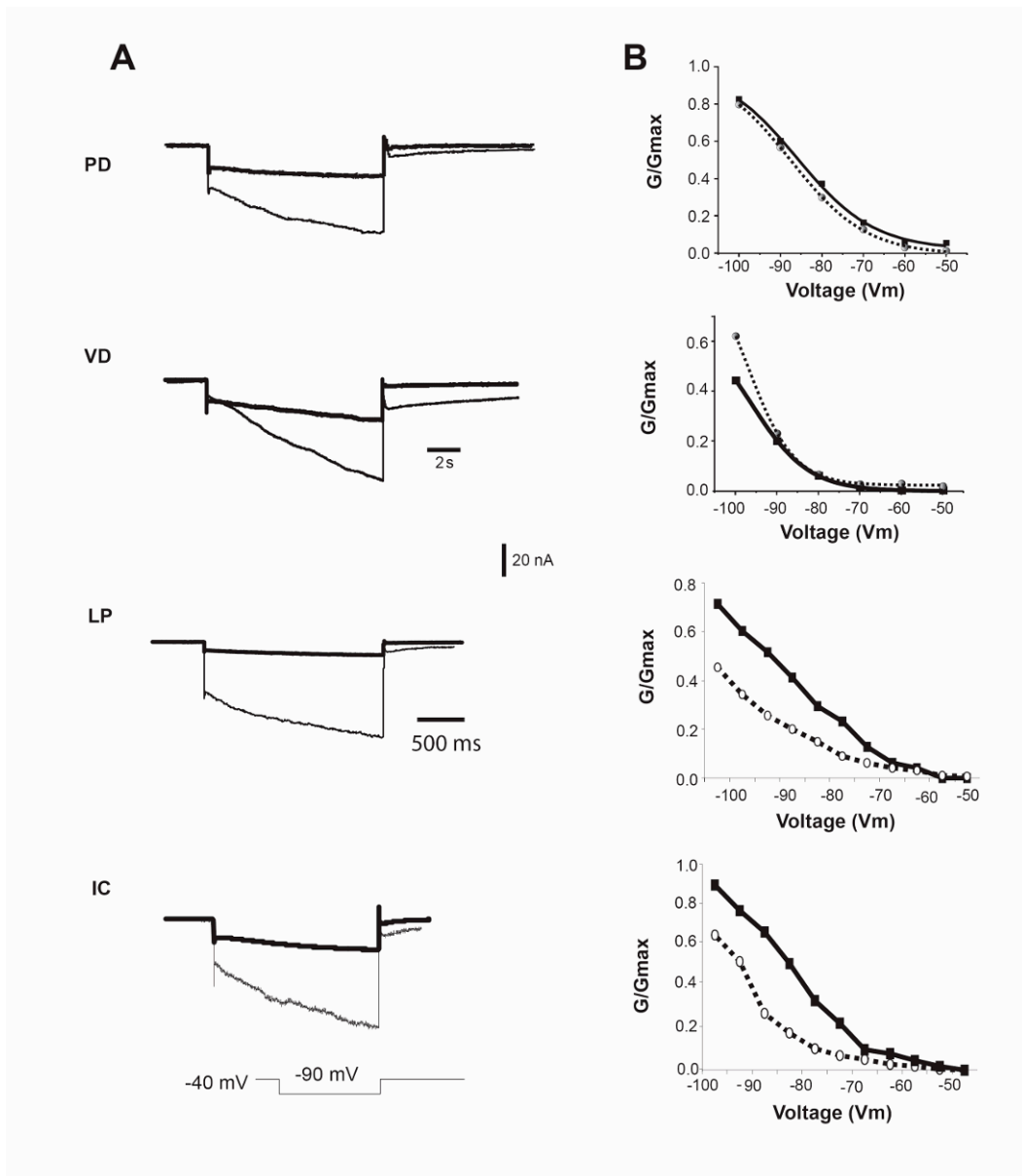
Figure 3.3 shal overexpression evoked a compensatory increase of inward I_h in all pyloric neurons tested A) Top pair of traces: I_h measurement at -90 mV in a PD pair within the same ganglia, one of which is control (thick line) and one which is expressing increased I_A (thin line).   Bottom three pairs of traces: I_h measurement at -90 mV in control and expressing VD, LP and IC neurons, from different preparations, since there is only one neuron of each type per ganglion. B) Peak conductance/voltage relationships for activation of I_h in neurons expressing shal-GFP (dashed) compared to control neurons (black).

Table 3-2 Properties of I_h in control and shal-GFP expressing neurons.

Cell type	$I_{max,}$, nA (-90 mV)	G_{max}, µS	Act $V_{1/2}$, mV	Act Slope Fct, mV	Act τ, s (-100 mV)
PD control (24)	-4.9 ± 2.5	-0.17 ± 0.0	-88.6 ± 5.6	8.0 ± 1.6	3.7 ± 2.0
expressing (7)	$-9.5 \pm 3.1^{**}$	-0.33 ± 0.1	-88.8 ± 4.9	9.7 ± 2.7	2.5 ± 0.6
expressing (22)***	$-43.3 \pm 33.$	$-1.9 \pm 1.8^{**}$	-88.7 ± 4.4	9.6 ± 2.5	$6.8 \pm 1.9^{*}$
VD control (4)	-8.3 ± 2.3	-0.19 ± 0.0	-82.4 ± 2.3	9.0 ± 0.5	1.8 ± 0.4
expressing (2)	-11.0 ± 2.5	-0.25 ± 0.0	-83.9 ± 3.0	7.1 ± 2.2	2.5 ± 0.3
expressing (5)***	$-12.9 \pm 2.7^{*}$	$-1.4 \pm 1.2^{*}$	-83.9 ± 2.3	6.9 ± 1.5	5.8 ± 4.2
LP control (3)	-4.8 ± 0.7	-0.12 ± 0.0	-85.6 ± 1.9	9.3 ± 1.0	2.6 ± 0.6
expressing (3)	$-13.6 \pm 12.$	-0.70 ± 0.9	-90.8 ± 10.8	9.1 ± 2.7	2.7 ± 1.0
IC control (4)	-5.9 ± 2.0	-0.13 ± 0.0	-85.6 ± 1.8	6.3 ± 1.0	1.8 ± 0.8
expressing (2)	-12.0 ± 7.1	-1.07 ± 0.0	-102.5 ± 10.1	7.9 ± 1.4	2.7 ± 0.1

Values indicate averages $\pm$ SD with number of cells in parentheses. $^{*}p < 0.05$; $^{**}p < 0.01$; *** Data pooled (MacLean and Goeritz), I_{max} at -100 mV
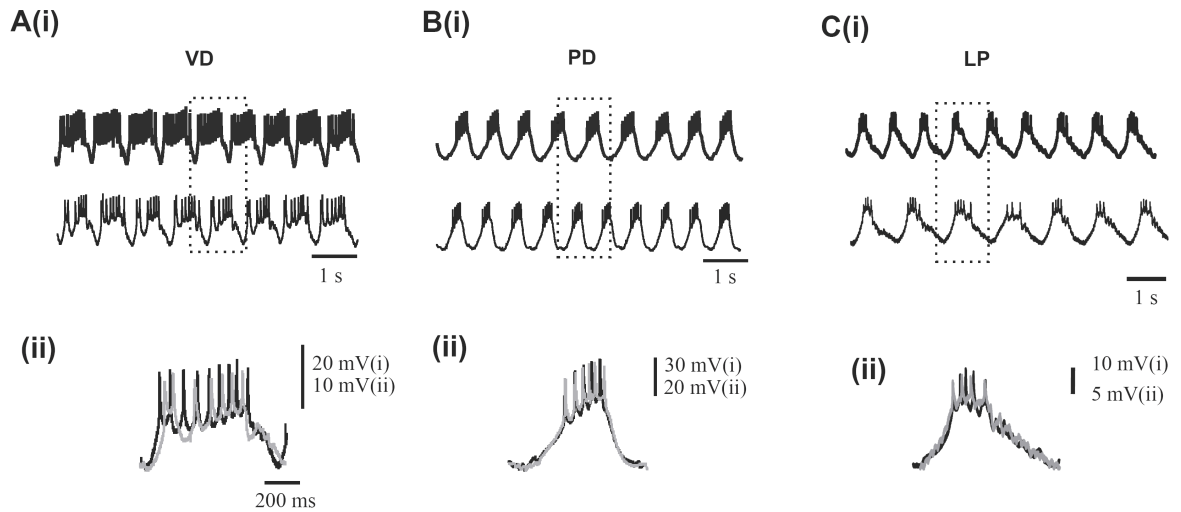
Figure 3.4 Rhythmic activity of neurons expressing shal-GFP was only slightly modified. A) Comparison of activity during the pyloric rhythm in a control VD (thick) and a VD expressing shal-GFP (thin) 72 hours after injection of *shal-GFP* RNA. Single cycles of activity, as indicated by the dashed line box are overlaid in A(ii). Note the slower rise time of the oscillation in the neuron expressing shal-GFP (gray). B. Comparison of activity during the pyloric rhythm in a control PD (thick) and a PD expressing shal-GFP 72 hours after injection of *shal-GFP* RNA (thin). Single cycles of activity, as indicated by dashed line box are cycle normalized and overlaid B(ii). C. Comparison of activity during the pyloric rhythm in a control LP (thick) and a LP expressing shal-GFP 72 hours after injection of *shal-GFP* RNA (thin). Single cycles of activity, as indicated by dashed line box are cycle normalized and overlaid (shal-GFP expressing gray) C(ii).

51

A untreated

B GFP

5nA
2s

Ci shalgfp

Cii shalgfp
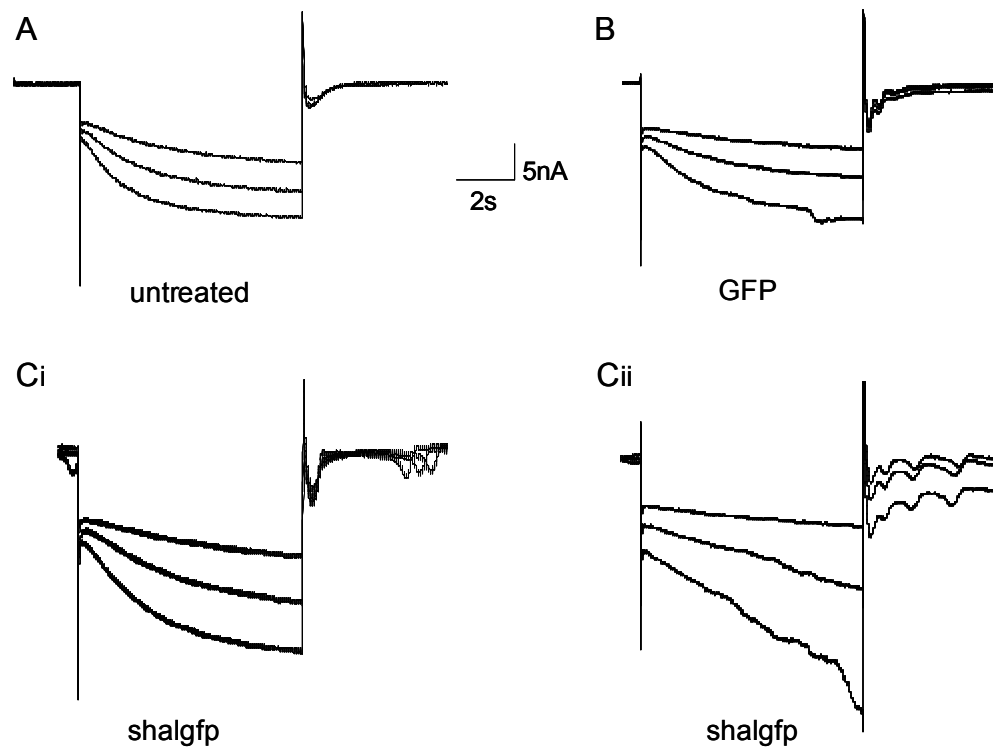
Figure 3.5 I_h and low threshold unidentified inward current at voltage steps to - 80, - 90 and - 100 mV. A. Untreated PD neurons with typical activation of Ih upon hyperpolarization. B. GFP expressing PD neuron with I_h activation and superimposed unidentified current at the last voltage step to -100 mV. C. Inward current in shal-GFP expressing neuron, Ci example for a mostly I_h-like current. Cii. Example for larger fraction of unidentified inward current, superimposed onto I_h activation.

52
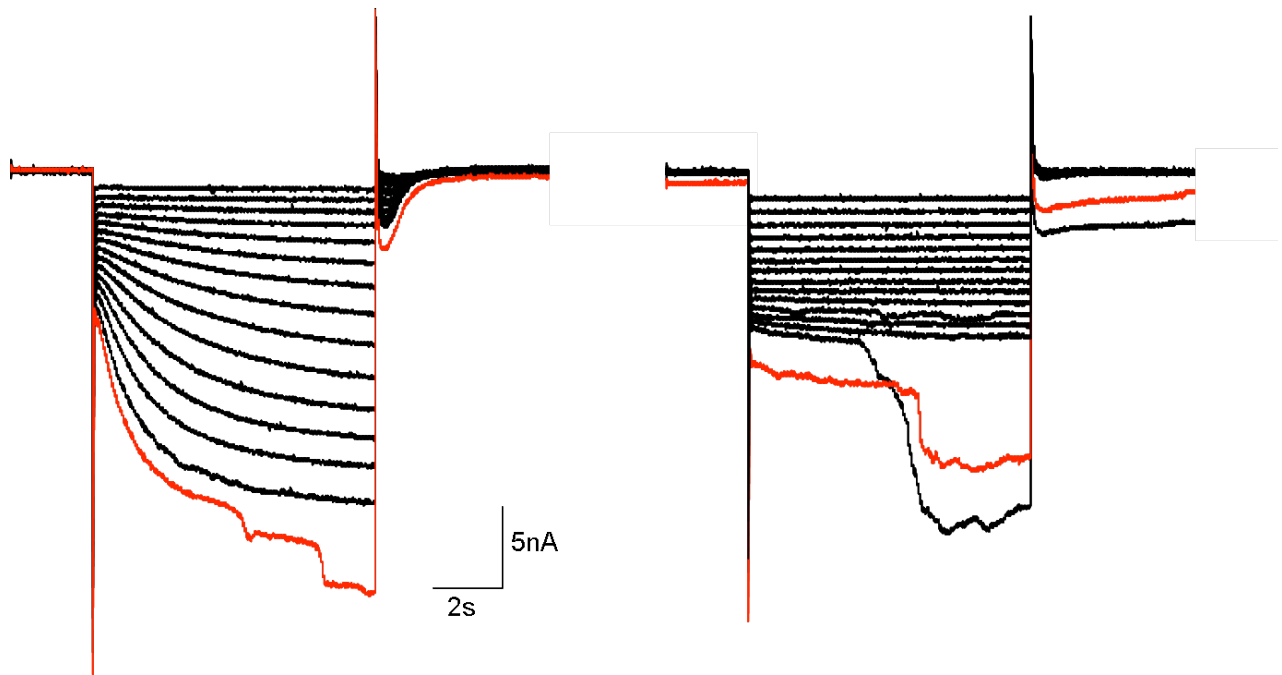
Figure 3.6 Unidentified current jumps in an untreated PD neuron under A. control conditions and B. after pharmacological block of I_h. Red traces indicate identical voltage steps (-115 mV).

Table 3-3 Rate occurrence of the slow threshold current jumps in RNA-injected and untreated PD neurons.

	% occurrence	% occurrence at -110mV	% occurrence at -120mV	n
shal-GFP	42.9	57.1	71.4	7
GFP	8.7	52.2	65.2	23
untreated	0	0	46.1	13
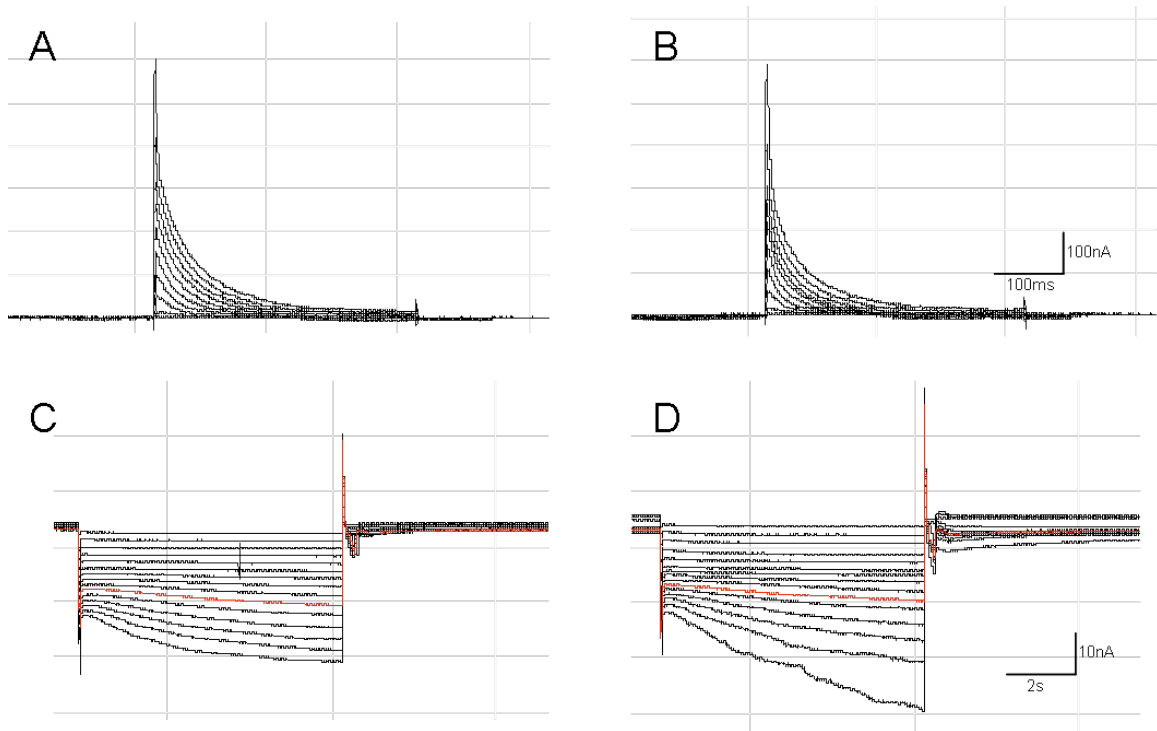
Figure 3.7 Expression of GFP (control; A and C) and of the mutant mshal-GFP (B and D) in a pair of PD neurons in one ganglion. The sequence of mshal-GFP contained a non-functional pore region, which did not cause a change in I_A between the GFP control (A) and the mshal-GFP expressing PD neuron (B). No significant up-regulation of I_h was found after mshal-GFP expression (D) compared to the GFP expressing control (C). Red traces indicate I_h at -90mV. Note the large apparent inward current at more hyperpolarized potentials in the mshal-GFP expressing PD neuron, which could not be contributed exclusively to I_h.

A

PD1 GFP

PD2 mshal

20mV

2 s

B

PD1 GFP

PD2 mshal

20mV

2 s

C

10mV

0.4s

D

10mV

0.4s
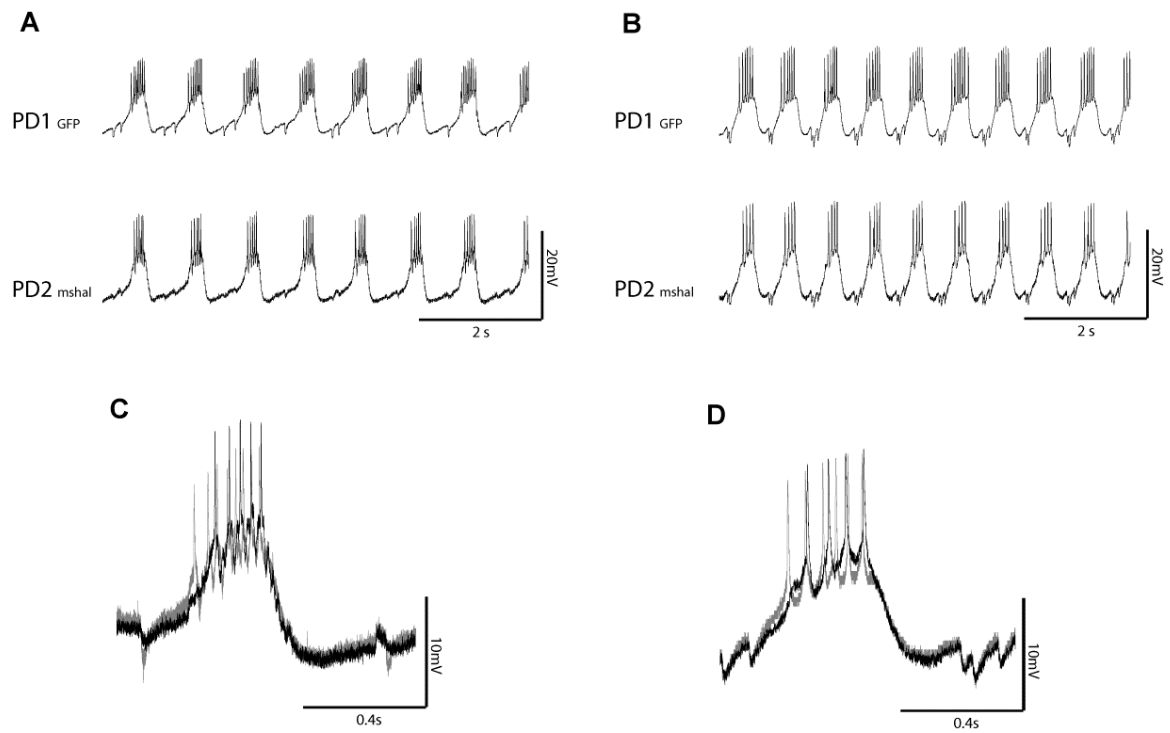
Figure 3.8 Rhythmic activity of neurons expressing mshal-GFP was only slightly modified. A. Activity during the pyloric rhythm in a pair of PD neurons before RNA injection. Single cycles of activity are overlaid in C. (control: black trace; non-functional mshal-GFP: grey trace). B. The same pair of PD neurons 72 hours after injection of *mshal-GFP* RNA. Single cycles of activity are overlaid in D.
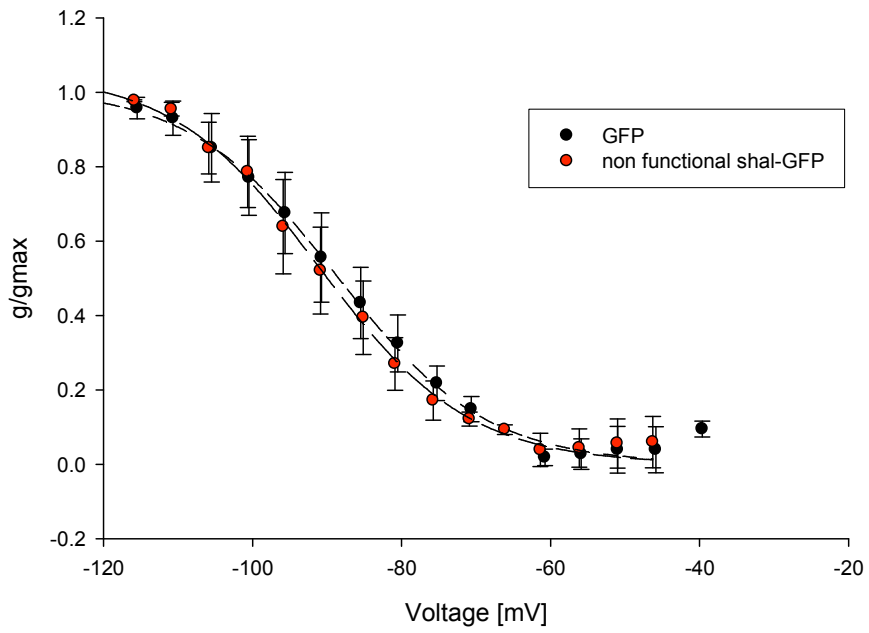
Figure 3.9 Peak conductance/voltage relationship for activation of I_h is not significantly different in PD neurons expressing a non functional form of shal-GFP (red) compared to GFP expressing control neurons (black). N = 4 PD pairs.
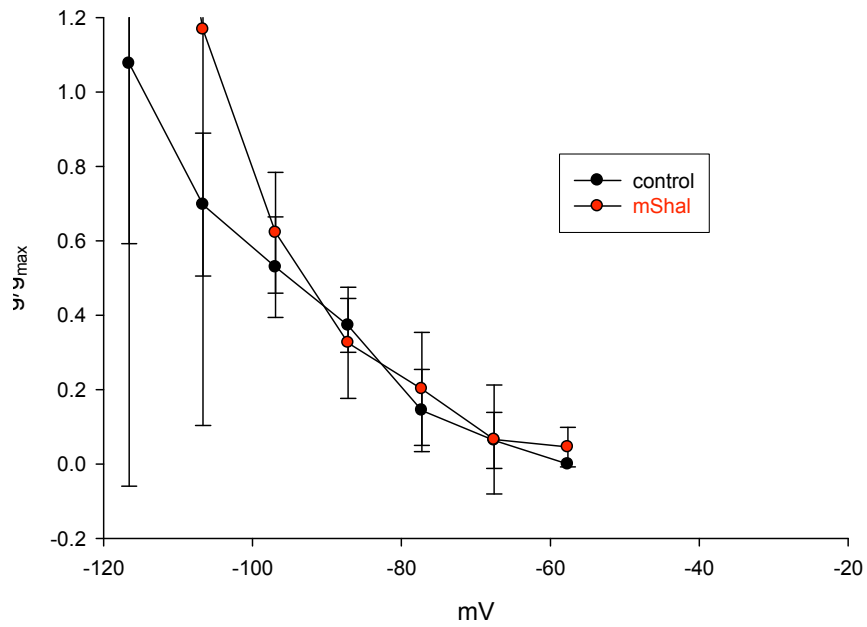
Figure 3.10 Re-evaluation of I_h in 4 PD pairs from a previous study, expressing a non functional form of shal-GFP (red) compared to *GFP* expressing control neurons (black). Peak conductance/voltage relationship for activation of I_h was not significantly different.
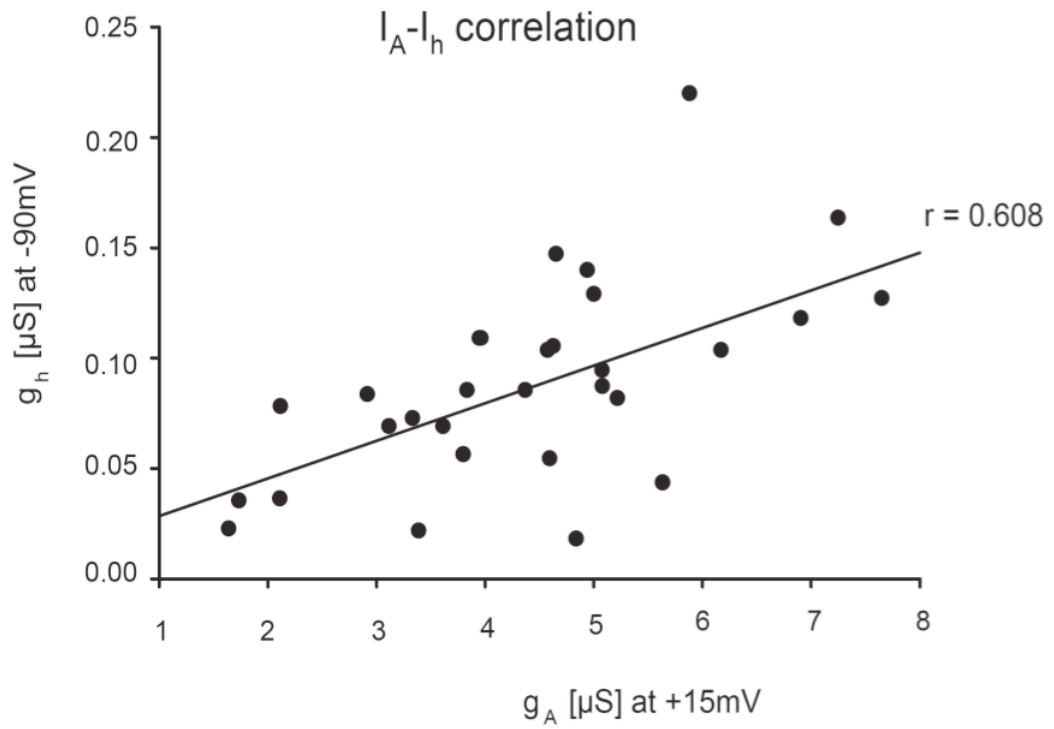
Figure 3.11   Relative relationship between I_A amplitude (measured at +15mV) and I_h amplitude (measured at −90mV) in control, non-injected PD neurons.   Each point represents the ratio of currents in the same neuron.   The line represents a linear regression of the data.

A

GFP

B

Anti-shal
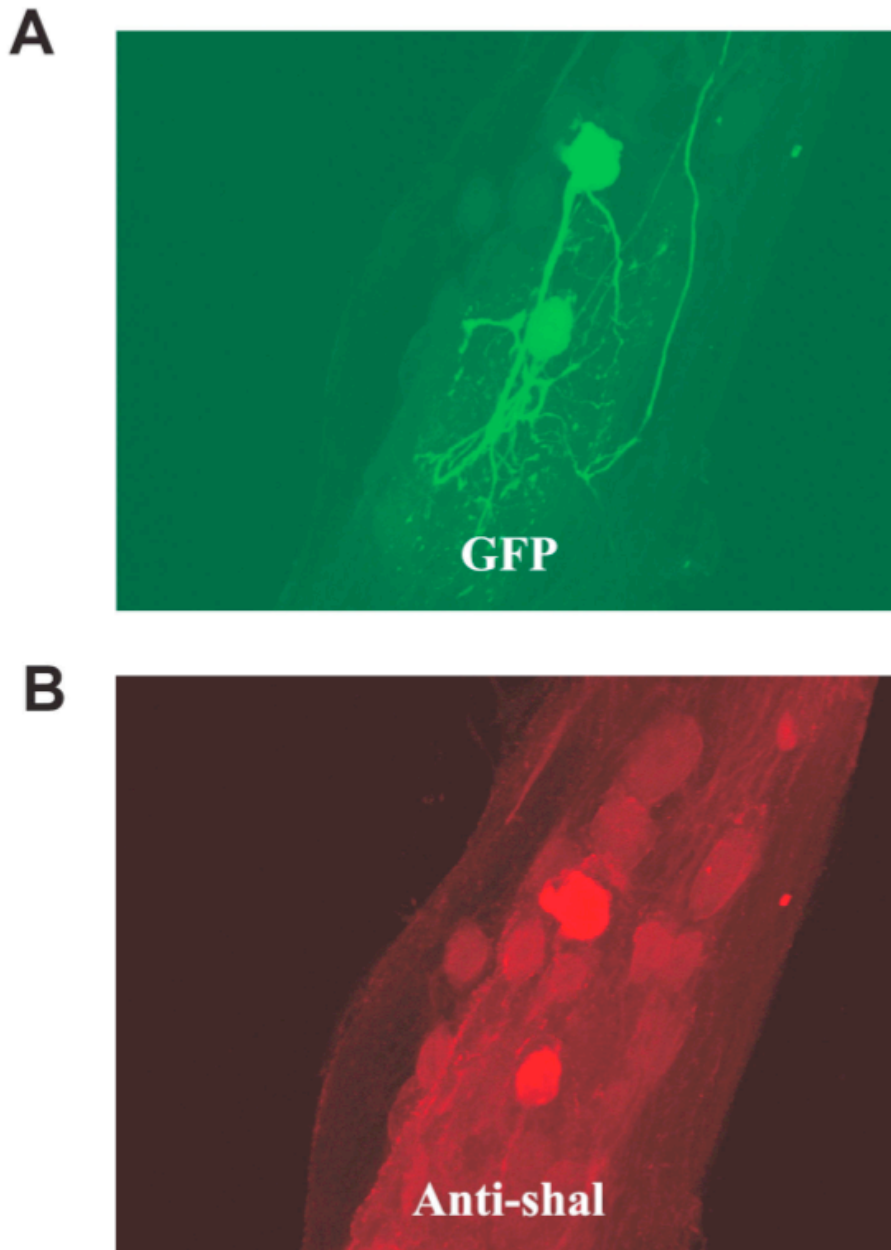
Figure 3.12 Shal protein is localized to the somata of injected neurons. Confocal images of neurons co-injected with *shal* RNA and *GFP* RNA. The GFP fluorescence (A) extended throughout the neurites and the axons of injected neurons, while shal antibody labeling (B) was localized only to the soma and initial segment of the injected neurons.

60
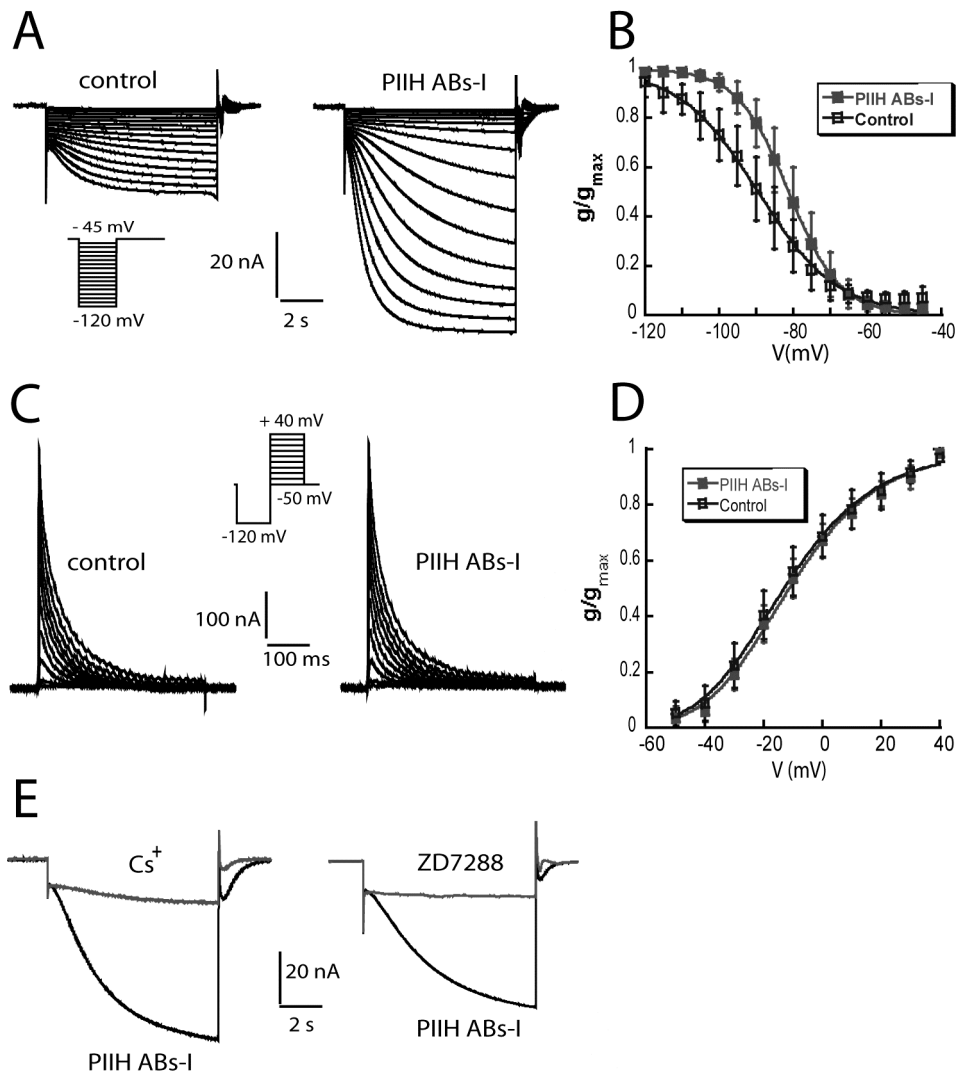
Figure 3.13 Over-expression of PIIH AB_S-I in PD neurons caused an increase of I_h amplitude without affecting the expression of I_A. (**A**) I_h recorded in control and *PIIH AB_S-I*-injected PD neuron in the same ganglion. The cells were held at –40 mV, and a series of 8 sec pulses was applied from –45 mV to –120 mV in 5 mV increments. The insets show the voltage protocols. (**B**) Plots of g/g_{max} versus voltage for activation of I_h in control (□) and PIIH AB_S-I-expressing (■) PD neurons (n=13 pairs). (**C**) A-currents recorded in control and *PIIH AB_S-I*-injected PD in the same ganglion. The cells were held at –50 mV, and after a 400 ms deinactivating prepulse to -120 mV, a series of 400 ms voltage steps were given from –50 mV to + 40 mV in 10 mV increments. The insets show the voltage protocols. (**D**) Peak conductance/voltage relationships for activation of I_A in control (□) and PIIH AB_S-I-expressing (■) PD neurons (n=13 pairs of PDs). (**E**) The PIIH AB_S-I currents could be blocked by 5 mM Cs^+ and 100 μM ZD7288.

Table 3-4 Properties of Ih in control and PIIH ABS-I-expressing PD neurons.

	g_{max} (µS)	$V_{1/2}$ (mV)	Slope factor (mV)	τ_{act} (s) (at -100 mV)
Control (n = 13)	0.24 ± 0.07	-89 ± 6	10.1 ± 1.2	3.5 ± 0.8
PIIH AB$_S$-I (n = 13)	0.65 ± 0.3 [**]	-81 ± 4 [**]	6.4 ± 0.7 [**]	2.3 ± 0.6 [**]

[**] $p < 0.01$.

Table 3-5 Properties of IA in control and PIIH ABS-I-expressing PD neurons.

	I_{max} (nA)	g_{max} (μS)	Act $V_{1/2}$ (mV)	Act slope factor (mV)	Inact τ_{fast} (ms)	Inact τ_{slow} (ms)	% peak I_A (τ_{fast})	% peak I_A (τ_{slow})
Control (n = 13)	562 ± 159	5 ± 2	-41 ± 6	17 ± 2	12 ± 3	70 ± 14	42 ± 7	58 ± 7
PIIH AB$_S$-I (n = 13)	523 ± 119	5 ± 1	-38 ± 5	16 ± 2	13 ± 2	74 ± 13	44 ± 10	56 ± 10
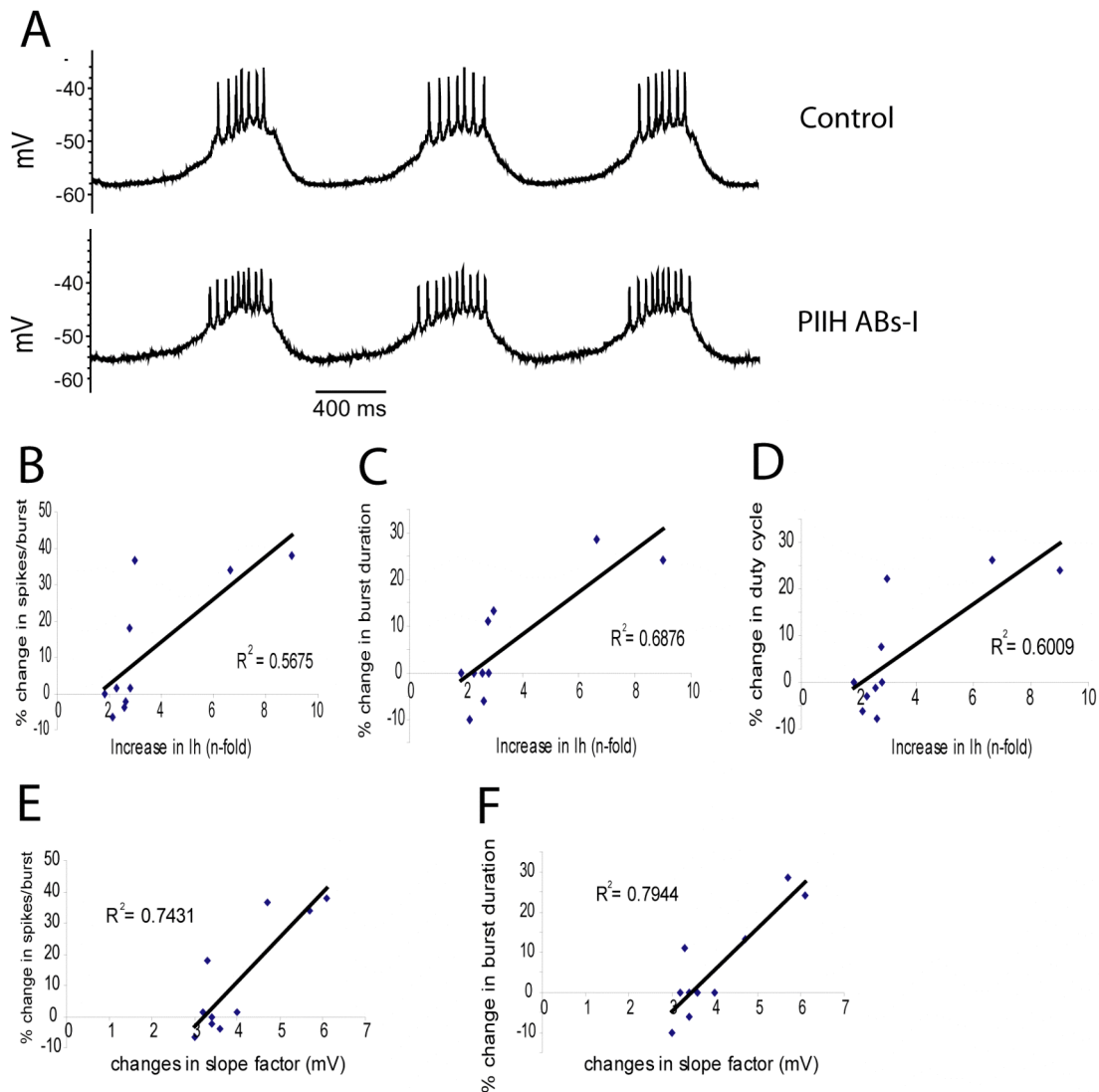
Figure 3.14 PIIH AB$_S$-I overexpression altered the firing properties of the PD neurons in an amplitude-dependent manner. (**A**) Representative rhythmic activity recorded in paired control and PIIH X-expressing PD neurons from the same ganglion. (**B**-**D**) The changes in spikes/burst, burst duration and duty cycle were correlated with I$_h$ conductance in PD neurons. (**E**-**F**). The changes in spikes/burst and burst duration were also correlated with the change in the activation slope factor. Each point represents the ration changes in a PIIH AB$_S$-I-expressing PD to a control PD neuron from the same ganglion (n=10).

Discussion

Properties of Increased I_A are Similar to Endogenous I_A

I over-expressed the I_A channel protein shal by injecting *shal-GFP* RNA into identified pyloric neurons. Interestingly, *shal-GFP* RNA was translated with approximately equal efficiency in all the pyloric neurons examined, as the total amount of increased I_A was similar in all neurons. The endogenous expression of I_A differs between the six pyloric neuronal classes in its amplitude, voltage dependence and kinetics (Tierney and Harris-Warrick, 1992; Baro et al., 1997). This variability of I_A helps to set the phase relationships and firing frequency of each neuron within the pyloric motor pattern. The different properties of I_A between pyloric neuron types under control conditions (Table 3-1) have been hypothesized to result from alternative splicing of the *shal* gene, from post-translational modifications such as phosphorylation, and/or from different levels of auxiliary subunit expression, which modify the biophysical properties of the shal channel (Baro et al., 2001; Zhang et al., 2003).

Shal-GFP expression increased I_A in all pyloric neurons (Figure 3.1). The relative increase was more pronounced in neurons with little endogenous I_A, such as the VD cell. In general, the I_A kinetics after *shal-GFP* RNA injection were similar but not identical to the endogenous I_A. With an increasing contribution of exogenous current to total current, the shal-GFP-evoked current became more similar to the current evoked by *shal-GFP* RNA injection into oocytes and the variability of I_A between neuron types decreased. The V_{act} shifted significantly in a depolarized direction, and in PD and VD neurons the slope of the voltage inactivation curve became more shallow (Figure 3.2, Table 3-1). A likely interpretation for this result is that the neurons were unable to synthesize sufficient quantities of auxiliary subunits, other regulatory proteins, or additional post-translational modifications, when a high density of shal-GFP protein was expressed, and consequently the

65

exogenous channels might have been unmodified. Work from our lab showed in a different study that co-expression and co-assembly with proteins in the KChIP family restored normal baseline properties of the exogenous I_A in PD neurons (Zhang et al 2003, An et al., 2000), supporting this interpretation.

I_A Overexpression is Accompanied by an Increase in I_h

Increased I_A after microinjection of *shal-GFP* RNA was accompanied by an increase of the hyperpolarization-activated inward current I_h in all pyloric neuron types examined (Figure 3.3, Table 3-2). The increased I_h might counteract the action of the overexpressed I_A channels, as previously seen in PD neurons (MacLean et al 2003; Zhang et al 2003). Despite very large increases in I_A following *shal-GFP* RNA injection in PD neurons, only very subtle changes in pyloric cycle activity were observed (Figure 3.4, MacLean et al., 2003, 2005). The neurons were hyperpolarized for less than half of the normal period of the pyloric rhythm (about 1-2 sec), which appears too short to significantly alter the conductance of the new I_h in the normal voltage range. As a result, I propose that the additional I_h may function by acting as a tonic depolarizing leak conductance. I_A operates in the subthreshold range of membrane potentials and is activated by depolarization after a period of hyperpolarization that removes resting inactivaction (Graubard and Hartline 1991). A-type potassium channels have been shown to be critical in determining neuronal activity during the pyloric cycle. When reduced by as little as 25% by 4-AP, the cycle frequency, spike frequency and slope of the rise phase of the oscillation are all increased, leading to marked phase changes in firing of the neurons within the pyloric cycle (Tierney and Harris-Warrick 1992). Due to the heterogeneity of I_A between neurons, these effects are quantitatively different in each of the six pyloric neurons. I_A is also a major target for dopamine (DA) modulation, which dramatically alters the pyloric cycle (Flamm and Harris-Warrick 1986a,b, Harris-Warrick et al., 1998; Harris-Warrick et al., 1995a, b; Kloppenburg et al., 1999). For example, the I_A amplitude in the PD neuron is increased by only 10% during bath application of DA (Kloppenburg

66

et al., 1999). As a result there is a decrease in the slope of the rise phase of the PD voltage oscillations, and a decrease in spike number and spike amplitude; sometimes the PD stops firing altogether (Flamm and Harris-Warrick, 1986a, b). Hence, the changes in firing properties following an artificial increase in I_A via *shal-GFP* RNA injection were surprisingly small, and only two statistically significant changes were seen, a decrease in spike amplitude in PD and a decrease in the slope of the rise phase of the oscillation in VD. These are consistent with an increased I_A, but are very modest changes for an increase of $125 - 400\%$ in I_A amplitude. One possible explanation for this very small physiological response is the compensatory increase in I_h.

Up-regulation of I_h following *shal-GFP* RNA injection occurred in all the pyloric neurons tested, suggesting that a linkage between these two competing channels may be a general property among pyloric neurons and not unique to any one cell type.   Like I_A, the increased I_h had somewhat different properties than the endogenous currents, perhaps also due to lack of sufficient quantities of auxiliary subunits or use of new alternative splice variants of the I_h gene (Figure 3.2, Table 3-2).   A recent report suggests that the Min-K-related peptide can act as an auxiliary protein for HCN channels (Yu et al. 2001, Decher et al. 2003), specifically accelerating the kinetics of channel activation and deactivation.

An Unidentified Component of the Inward Current

At more hyperpolarized voltages, I often observed an unidentified, low threshold component of the inward current, including large inward jumps superimposed onto the I_h current trace (Figure 3.5, Figure 3.6) This current behaved atypically for I_h, as it did not activate with a single exponential time course, deactivated very slowly, and could not be blocked by classic I_h blockers such as Cs^+ or ZD7288. It

occurred especially after RNA-injection, but was occasionally also seen in untreated neurons. Shal-GFP expressing PD neurons were more likely to exhibit this current than GFP-expressing cells. This suggests that even if it is not identical to I_h, the current was still a response to shal-GFP, from either the RNA, the protein or the expression and subsequent increase in leak conductance of the neuron. However, the current generally appeared to be linked to indicators of cell damage, such as a depolarized resting potential, low input resistance, or cloudy appearance after culturing. This damage may have resulted from bacterial or fungal infection, to which cells are particularly sensitive after RNA-injection. Mechanical stress can also cause injury, for instance multiple penetrations due to blocked or blunt electrodes during RNA-injections or during set-up of the voltage clamp. In experiments with repeated I_h trials, the current jumps were frequently more prominent and manifested at less hyperpolarized potentials during later protocol repetitions, indicating further that declining cell health might be related to their occurrence. Interestingly, I also observed a much higher rate of cell death in *shal-GFP* than in *GFP* RNA injected neurons.

The reversal potential of this current could not be clearly determined. However inward tail-current observation suggests that it is more depolarized then the resting potential, suggesting that it is not a pure chloride or potassium current. Similar large inward currents that are only observed at very negative, non-physiological voltages, have been seen following injection of RNA for other membrane proteins in *Xenopus* oocytes (Kuruma et al., 2000). The source of this current is at present unknown; however, in *Xenopus* oocytes, the current is not detectable at voltages more depolarized than -130 mV. In contrast, the increased I_h in pyloric neurons after shal-GFP expression became active at physiologically relevant subthreshold voltages and was easily seen at voltages more hyperpolarized than -100 mV (Figure 3.3).

Another possible explanation is that the current reflects physical properties of the membrane. The lipid bi-layer functions as a capacitor. Due to its thinness, the

molecules in the membrane are subject to a strong electric field when a voltage is applied across the membrane. Prolonged and extensive hyperpolarization might eventually lead to local ionization or dissociation of polar membrane molecules (The Axon CNS Guide, 1993-2006, Molecular Devices Corporation, p.10). This could eventually cause a temporary or permanent breakdown of the capacitor, when the membrane suddenly becomes locally conductive. This would be seen as sudden increase in current in the voltage clamp current traces. If this is the cause for the non-I_H inward currents I observed, it remains unclear why cells were more likely to exhibit capacitive breakdown after expressing RNA, and why shal-GFP expression caused more breakdown than GFP expression alone.

It is important to remember this unidentified current when analyzing changes of I_h in neurons, especially after RNA injection. The large variance of I_A and I_h between different experiments, which appeared to be affected by seasonal changes, demonstrates the importance of examining both PD neurons within one ganglion to estimate whether I_h increased. Further, cells that were dye-injected with Fast Green instead of RNA showed high survival rates and little occurrence of this current, which make Fast-Green injection, used in some of our previous experiments, a less suited control than GFP-RNA-injection.

Expression of a Nonfunctional Mutant of shal-GFP in PD Neurons

So far, our data suggested that the homeostatic response of I_h increase after shal-GFP expression was activity-independent. We never detected a change in firing properties of the neurons after *shal-GFP* RNA injection. Further, MacLean et al. showed that overexpression of a nonfunctional mutant in PD neurons still caused an increase of I_h, indicating that the presence of the RNA or protein itself, and not

a change in firing properties was sufficient to trigger the compensatory increase of I_A. However, with the discovery of the non-I_h component of the inward current in RNA-injected, I chose to reinvestigate this result in order to eliminate a potential contamination of the measured I_h increase with the unidentified current.

Overall, I did not find an increase of I_h in mshal expressing PD neurons compared to paired GFP expressing control PD neurons, when analysis was restricted to voltage steps between -40 and -100 mV (Figure 3.7, Figure 3.8). Re-evaluation of the data from the previous study also did not reveal a statistically significant increase of I_h, when analysis was restricted to -40 to -100 mV, and traces with obvious non-I_h current jumps were discarded (Figure 3.10). A possible explanations for this difference in both studies is likely the existence of the low threshold, slowly activating current described in the previous section, which may have counted towards the total I_h in the original analysis of the first study.

However, this unexpected result has to be interpreted with caution. Unlike successful experiments with injection of other RNA (*GFP* or *PIIH)*, I had generally a high rate of cell death and a very low rate of successful ectopic channel expression of *shal-GFP* as confirmed by larger A-currents in the *shal* RNA injected cells. This indicates that there may have been a general problem with the shal-GFP clone I used, which may have accumulated mutations causing these problems. The *mshal* RNA was derived from the same clone, and the same problems may have flawed the outcome of this experiment in an unpredictable way. With the mutated sequence of *mshal-GFP,* it was not possible to conf irm good expression electrophysiologically, and we had to rely on observation of strong fluorescence in the injected cell. Monitoring protein expression by fluorescence levels introduces a caveat, as visible fluorescence might generally require lower levels of shal-GFP protein than the amount that is required to affect channel insertion into the membrane in a physiologically relevant manner. While it appears unlikely that only the GFP tag could have been expressed in fluorescent cells, it is possible that low expression levels of mshal-GFP were still sufficient to produce a weak fluorescent signal in the soma but were not high enough to reach a

necessary threshold to trigger the homeostatic regulation of I_h or other channel proteins. In support of this, on rare occasions after *shal-GFP* RNA injection we observed weakly fluorescent neurons without measurable changes of I_A. In addition, the inability of I_h to reach full activation at more depolarized steps, especially in shal expressing cells, limits the meaning of Boltzmann fits in the process of estimating the maximal conductance g_{max}. This affects the normalization in g/g_{max} plots and leaves data from different neurons less comparable.

However, keeping these limitations in mind, the presence of increased mutant shal protein alone still appeared not to be sufficient to trigger a compensatory response in this study. I also found no change in the firing properties of paired PD neurons after the expression of mshal-GFP.

The homeostatic response I observed after injection of *shal-GFP* RNA may still occur independently of changes in firing properties, since we never detected any significant changes in neuronal firing properties after *shal-GFP* RNA injection. In the shal-GFP expressing neurons, when both I_A and I_h were significantly increased, blocking either current alone can unmask the hidden effects of the other current (MacLean et al, 2003). However, without further experiments, closely monitoring the activity of both PD neurons after RNA-injection, it cannot be concluded whether the homeostasis of I_A and I_h is activity-independent or not.

Consistent Ratio of I_A and I_h

While the numbers of transcripts for a particular ion channel appear to vary significantly between animals, the ratio of certain channel combinations like I_A and I_h is remarkably constant. I found the level of I_A to vary quite dramatically, following a significant, time-dependent trend throughout the year, which may reflect seasonal changes in channel expression. Most notably, even in control, non-injected PD neurons, a positive relationship exists between the amount of I_A and I_h (Figure 3.11), suggesting that under normal conditions the expression of

these channels is in some way co-regulated. This may add flexibility and the ability to generate relatively stereotyped patterns by a potentially very large number of combinations of channel expression. Quantitative expression of multiple ion channel genes in STG neurons have been estimated by single cell RT-PCR based on their number of mRNA transcripts (Schulz et al., 2006a; 2006b; 2007). These studies support evidence for neuron class-dependent co-regulation of different ion channels. Whether or not this is a functional mechanism within rhythmic networks is still subject to debate (Prinz et al., 2005; Selverston et al., 2007) and requires further examination. In my study, the relative ratio of I_A and I_h in control PD neurons (Figure 3.11) supports the hypothesis that a certain ratio of these currents might be important for a neuron's firing pattern, although the large variance suggests that additional currents or their modulation also contribute to the functional role of this ratio. Consistent findings of similar I_A and I_h conductance or mRNA transcripts within the two PD neurons of individual ganglia seem to indicate that this variance is not an experimental artifact caused by different levels of injury to the cell, but instead might be the result of a developmental mechanism to establish neuron identity.

The Homeostatic Response is Uni-Directional

I have not found the homeostatic interaction between the two channel proteins to be reciprocal. We previously showed that in pyloric neurons the rate of postinhibitory rebound and the initial interspike interval (ISI) after large hyperpolarizing pre-pulses are co-regulated by I_h and I_A (Harris-Warrick et al., 1995). While overexpression of I_A failed to change the neurons' firing properties due to the homeostatic up-regulation of I_h, results from our lab showed that the overexpression of a non-native I_h gene, *PAIH*, did not alter the expression of I_A (Zhang et al., 2003) and thus did lead to significant changes in the membrane potential and firing properties of the PD neurons. In the present study, we overexpressed two splice variants of the native gene, *PIIH ABS-I* and *II,* into PD

72

neurons. Despite 2- to 9-fold increases in I_h, the amplitude and properties of I_A were not significantly changed. This confirms our earlier tentative conclusion that the homeostatic compensation between I_A and I_h is uni-directional. The reasons for this uni-directionality are not clear, but the result suggests that the neuron monitors I_A more carefully and compensates for variation in I_A to a greater extent than it does for I_h. This may arise because in the lobster STG I_h has extremely slow kinetics of activation and deactivation. Thus, it is probably a component of the leak current that helps maintain the resting potential, and could in theory be compensated by a large number of other currents.

As with *PAIH* (Zhang et al., 2003), overexpression of PIIH AB_S-I and *A-II* did change the firing properties of the injected PD neurons, but only when the maximal conductance was increased over a threshold level of 2- to 3-fold (Figure 3.14). It therefore appears that I_h can only affect the pyloric motor pattern when a large number of its channels can be activated in the normal voltage range. Even twofold overexpression of I_h, combined with depolarizing shifts of the $V_{1/2}$ to a more positive potential, and steeper slope factors, did not significantly change the firing pattern of PD neurons. Above this threshold increase in I_h, PD neuron firing parameters increased as a function of increasing I_h expression. There are several possible interpretations of this result. First, under normal conditions the endogenous I_h may play a rather limited role in shaping the firing properties of pyloric neurons as suggested by our recent work (Peck et al. 2006). Second, it is possible that most of the exogenously expressed I_h channels were inserted into the membrane in the soma, far away from the firing pattern generation sites located in the distal neuropil, as was the case after *shal-GFP* RNA injection (Fig. 1-12, MacLean et al. 2005). In both dynamic-clamp studies and a simple two-cell-model, selectively raising I_h fourfold caused the neuron to depolarize, to phase advance and to fire additional spikes per burst (MacLean et al. 2005; Zhang et al. 2003). These modeling results mimic the effects of upregulating I_h through

overexpression of the *PAIH* gene (Zhang et al., 2003) and the *PIIH* gene in our present paper.

Similarly, it was reported earlier that overexpression of GFP or of the lobster *shaker* gene, which encodes an I_A selectively targeted to the axons of STG neurons, did not produce an increase in I_h in the relevant voltage range (MacLean et al. 2003).

These results all suggest that the link between expression levels of shal and I_h is physiological relevant and not simply an artifact of channel RNA injection.

New I_A Channels are inappropriately targeted in shal-RNA injected Neurons

An alternative explanation for unchanged firing properties after overexpression of I_A could be a failure to target the exogenous channels to the neuropil, where synaptic integration and spiking occur. The new protein appeared to be selectively targeted to the soma and initial neurite (Figure 3.12). Analysis of the PD neuron's firing properties using a three compartment mathematical model has shown that spike activity is much more sensitive to increases in I_A amplitude in the neuropil/axon compartment compared to the soma and primary neurite compartments (MacLean et al., 2003). This is consistent with the fact that both synaptic integration and spike initiation occur in the neuropil, electrically remote from the soma. However, when I_A parameters were adjusted to those observed in the *shal-GFP* injected neurons only in the soma and primary neurite compartments, the model neuron's spike activity and spike amplitude were still very significantly reduced. These results suggest that even inappropriate targeting of I_A after *shal* RNA injection should lead to observable changes of firing properties, and that additional compensatory processes like an increase of I_h must be activated to maintain normal firing properties in the injected neurons.

74

Functional Implications for the Homeostatic Response

The homeostasis described here co-regulates two currents that are active in the critical voltage range below spike threshold; they have opposing effects and their ratio has been previously demonstrated to regulate neuronal spike and pacemaker activity (Angstadt and Calabrese, 1989; Harris-Warrick et al., 1995b). In pyloric neurons, the rate of post-inhibitory rebound and the initial spike interval after inhibition are co-regulated by I_h and I_A (Harris-Warrick et al., 1995b); pharmacologically induced decreases in I_A led to more rapid post-inhibitory rebound and shorter first ISIs, while pharmacologically induced decreases in I_h had the opposite effect. The interactions of I_A and I_h have been modeled in a simple 2-cell model (MacLean et al, 2003). Selectively increasing I_A in one of the model neurons caused it to hyperpolarize and fall silent, showing only electrotonic coupling depolarizations from action potentials in the other neuron. On the other hand, selectively raising I_h caused the neuron to depolarize, to phase advance and to fire additional spikes per burst. Finally, when both I_A and I_h were raised to the extents and in the ratio seen in the experimentally injected neurons, the firing properties of the neuron were largely unchanged, just as in the experiments. A more detailed study of the interaction between I_A and I_h in the control of spike number per burst showed a set of "stripes" in the parameter space, which are linear regions where correlated increases in both I_A and I_h in a constant ratio do not alter the firing properties of the neuron. This model suggests that the compensatory up-regulation of I_h is by itself sufficient to cancel the effects of the *shal-GFP*-induced up-regulation of I_A, retaining normal firing properties in the injected neurons. The model of course cannot prove that this is also necessary, nor can it eliminate additional compensatory changes that might contribute to the homeostatic response. However, both experimental and modeling approaches (Goldman et al., 2001; Prinz et al 2004) have indicated that similar parallel changes in linked channels can maintain normal activity over a broad range of channel expression.

4 IH protein localization

Knowledge of a protein's localization within a cell can be very useful in better understanding its functions. I showed in chapter 3 that I_h can play a role in maintaining stable firing properties in pyloric neurons by compensating changes of another current in a homeostatic response. I_h has been electrophysiologically characterized in STG neurons, and its cell specific regulation by monoamines makes it a likely regulator of network or cellular activity. However, its functional roles within the STG remain unclear. Knowing the localization of I_h channels in pyloric neurons might help us to understand its role in regulating network activity. An ongoing debate about whether or not I_h channels regulate synaptic integration in addition to their depolarizing effect on the resting potential (Kaupp, Seifert 2003, Yu et al 2004, Genlein et al 2007) made it especially interesting to examine the distribution of PIIH protein at in regions of the neuron that do or do not contain synaptic sites. I was also interested in comparing the expression pattern of endogenous Shal and PIIH protein to gain more insight into possible mechanisms underlying the homeostatic interactions of I_A and I_h. I therefore characterized the PIIH protein distribution in the STG by immunocytochemical methods. The somata of *Panulirus interruptus* STG neurons are located on the dorsal and to a lesser extend on the ventral surface of the ganglion. They send a large primary neurite towards the interior of the ganglion. This central interior region is called the coarse neuropil, where primary neurites broaden and wrap around each other or run parallel for short stretches. They then branch into secondary neurites, which send many small and further branching processes into the fine neuropil. The fine neuropil partially surrounds the coarse neuropil and often forms concentrated areas of extensive fine branching on the dorsal and ventral surface below the ganglion sheath or even between the STG somata. (King 1976, Ayali et al., 1998). Essentially all the synaptic interactions in the STG occur at the level of the fine

neuropil. The spike initiation zones are thought to be located in the posterior regions of the coarse neuropil, near where the axons leave the ganglion (Raper, 1979; Miller, 1980).

Mapping the distribution of I_h channels might also help to understand the mechanism behind the homeostatic response to *shal* RNA injection. If I_h and I_A channels were interacting physically on the protein level, in multi-protein complexes, co-localization of Shal and PIIH protein would be expected. I examined the localization and potential co-localization of IH protein with the synaptic marker, Synaptotagmin, and the A-channel protein Shal by immunocytochemistry, followed by confocal imaging. To monitor I_h protein distribution, I took advantage of an unusual continuous sequence of eight histidines in the carboxyl terminus of the lobster PIIH sequence, which could be specifically bound by a monoclonal anti-penta His antibody. This antibody is normally used in molecular biology to help purify proteins that have been tagged with an artificially introduced sequence of histidines. A GenBank BLAST search did not detect any other crustacean proteins with a continuous sequence of five or more histidine residues, allowing us to use a commercially available anti-penta-His antibody to visualize I_h protein in the STG. Recognition of PIIH and antibody specificity was confirmed with Western blot staining (Figure 4.1). An antibody raised against I_h protein of the related species *Panulirus argus*, anti-PAIH (gift of Dr B. Ache) did not show enough specificity to be reliably used in tissue staining. Confocal images of slices and z-series from whole or sectioned ganglia were processed with Volocity imaging software for contrast enhancement, noise reduction and 3D reconstructions. In order to distinguish between different neuron types, I identified the pyloric neurons with intracellular recordings and filled one neuron with neurobiotin for 15 to 45 minutes. Neurobiotin filling not only helped with post-fixative ganglion orientation and cell identification, but also helped me to distinguish the small processes of the filled neuron in the fine neuropil.

4.1 Overall Expression Pattern

I consistently found I_h protein expression in the soma and membranes of pyloric neurons (Figure 4.2, Figure 4.3 and Figure 4.4). The amount of soma labeling varied between different neurons of the same ganglion. However, I did not find a statistically significant correlation between neuron type and PIIH staining intensity (Figure 4.2, Figure 4.6). The PIIH staining of the soma membranes was not distinctly different from the overall soma staining, but often a concentric pattern of higher intensity was located intracellularly around the nucleus (Figure 4.4A, Figure 4.16), perhaps arising from protein still bound in the Golgi apparatus or endoplasmic reticulum. The neuropil region revealed strong but often diffuse reactivity for I_h protein (Figure 4.3). In sectioned ganglia, and occasionally in whole mount ganglia with good penetration, some PIIH protein appeared to be localized in the central coarse neuropil on the primary and secondary neurites (Figure 4.3, Figure 4.5 to Figure 4.8). However, in most intact ganglia, almost no PIIH immunoreactivity was noticeable in the coarse neuropil, possibly because of penetration difficulties of the primary antibody (Figure 4.3). Occasionally, structures on the dorsal and ventral surface of the ganglion showed intense PIIH staining. These structures often spanned across the whole ganglion with a sparse branching pattern, and may be of neuronal or non neuronal origin (Figure 4.6, Figure 4.7). When present, the PIIH labeling in the coarse neuropil appeared to be unevenly distributed in the form of large patches in or on the secondary processes, frequently very close to branching points (Figure 4.7, Figure 4.8). Volume rendered 3D-reconstructions of confocal image stacks helped to reveal this distribution (Figure 4.8, Figure 4.9). The strongest PIIH labeling was observed in the area of the fine neuropil, where it appeared in clouds at the ends of very fine branches, in bulbous or fingerlike structures (Figure 4.5, Figure 4.6, Figure 4.8, Figure 4.10, Figure 4.11) as larger spots of intense labeling between neurobiotin-filled processes, presumably on another process that was not filled (Figure 4.10, Figure 4.11, Figure 4.20, Figure 4.21,).

78

4.2 IH Protein in the Synaptic Neuropil

To determine whether the areas of high intensity PIIH labeling were related to regions of synaptic contacts, I performed co-staining with a *Drosophila* anti-synaptotagmin antibody, which labels both synaptic vesicles and dense-core vesicles in crustacea (Skiebe and Wollenschlaeger, 2002; review: Marqueze et al., 2002). Dr Pat Rivlin donated the Synaptotagmin antibody, which was raised in rabbit. Anti-synaptotagmin labeling occurred in large clusters and punctuated staining throughout the fine neuropil with several areas of concentrated staining in the ganglion, (Figure 4.12). Co-staining for PIIH protein revealed an increased likelihood for I_h protein in areas of strong synaptotagmin labeling. At higher magnifications, adjacent (but only rarely overlapping) labeling of the punctate synaptotagmin and PIIH signals could be found (Figure 4.13, Figure 4.14), indicating the presence of I_h channels at pre- or postsynaptic sites.

I observed patches of strong PIIH labeling on very small processes of neurobiotin filled neurons in close vicinity of synaptotagmin, often close to branching points. The anti-synaptotagmin labeled structures were often not labeled with neurobiotin, suggesting that they were terminals of a different neuron (Figure 4.13, Figure 4.14, **Error! Reference source not found.**C). From these data, without the higher gain analysis of electron microscopy, we cannot determine whether I_h channels are localized at pre-or postsynaptic terminals. However, my experiments suggest that at least a fraction of I_h channels are expressed in close vicinity to synaptic proteins and may therefore be involved in the regulation of synaptic transmission. The virtual absence of membrane-bound double labeling for PIIH and synaptotagmin, despite the large occurrence of synaptotagmin-labeled structures, suggests a primarily postsynaptic distribution of PIIH.

4.3 IH and IA Protein Localization

G-protein receptors and ion channels have been shown to physically interact with regulatory proteins, subunits and transport molecules in multi-protein complexes.

The homeostatic interaction of I_h and I_A could in theory be mediated by their participation in such a complex, where up-regulation and surface expression of Shal proteins could activate a coupled surface expression of PIIH proteins as well. In this case, one would expect to find similar patterns of PIIH and Shal immunoreactivity with co-localization of their immunocytochemical signals. I therefore used a rabbit polyclonal lobster anti-Shal antibody, which was previously designed and tested in our lab. Co-staining revealed different patterns of soma-bound protein by anti-Shal and anti-PIIH labeling. The large anti-Shal signal in the membranes of the soma and primary neurites was not matched by a similar localization of PIIH signal. The high amount of membrane-bound Shal protein caused ring-like staining in cross-sections of the soma (Figure 4.16) and intense labeling along primary neurites (Figure 4.15). These regions generally showed very low I_h immunoreactivity. In the fine neuropil, labeling of I_h and Shal protein revealed similar overall expression pattern with high concentrations in the densest part of the synaptic neuropil. However, at high magnifications it was apparent that the I_h and Shal labeled structures were not identical (Figure 4.18-Figure 4.22). Shal staining in the membranes of the fine branches was usually homogenous and diffuse. This is different from PIIH which, as stated above, often showed patchy staining patterns throughout the secondary neurites and within the fine neuropil (Figure 4.5, Figure 4.8) or was highly concentrated at the end of fine branches (Figure 4.7, Figure 4.8B).

80
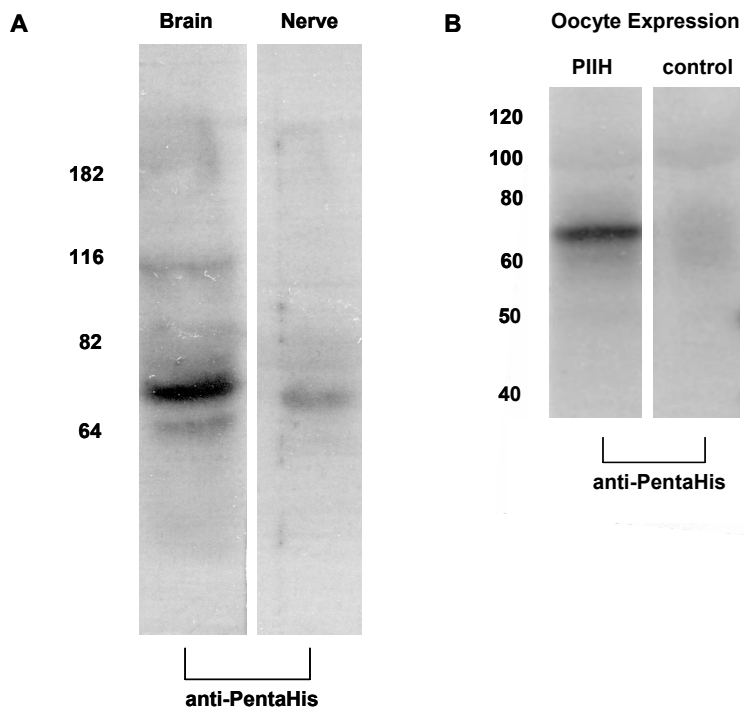
Figure 4.1 Western blot staining for the pentaHis antibody against I_h protein. A. Anti-PentaHis specificity in protein extracts of lobster brain and nerve tissue. Scale on the left hand side indicates apparent weight (kDa). The antibody recognizes bands in the weight range of the 10 cloned PIIH splice forms (77 and 82 kDa). The source of an additional band of higher molecular weight is likely residual subunit binding. B. Positive control of antibody recognition in protein extract from PIIH-expressing and untreated Xenopus oocytes.
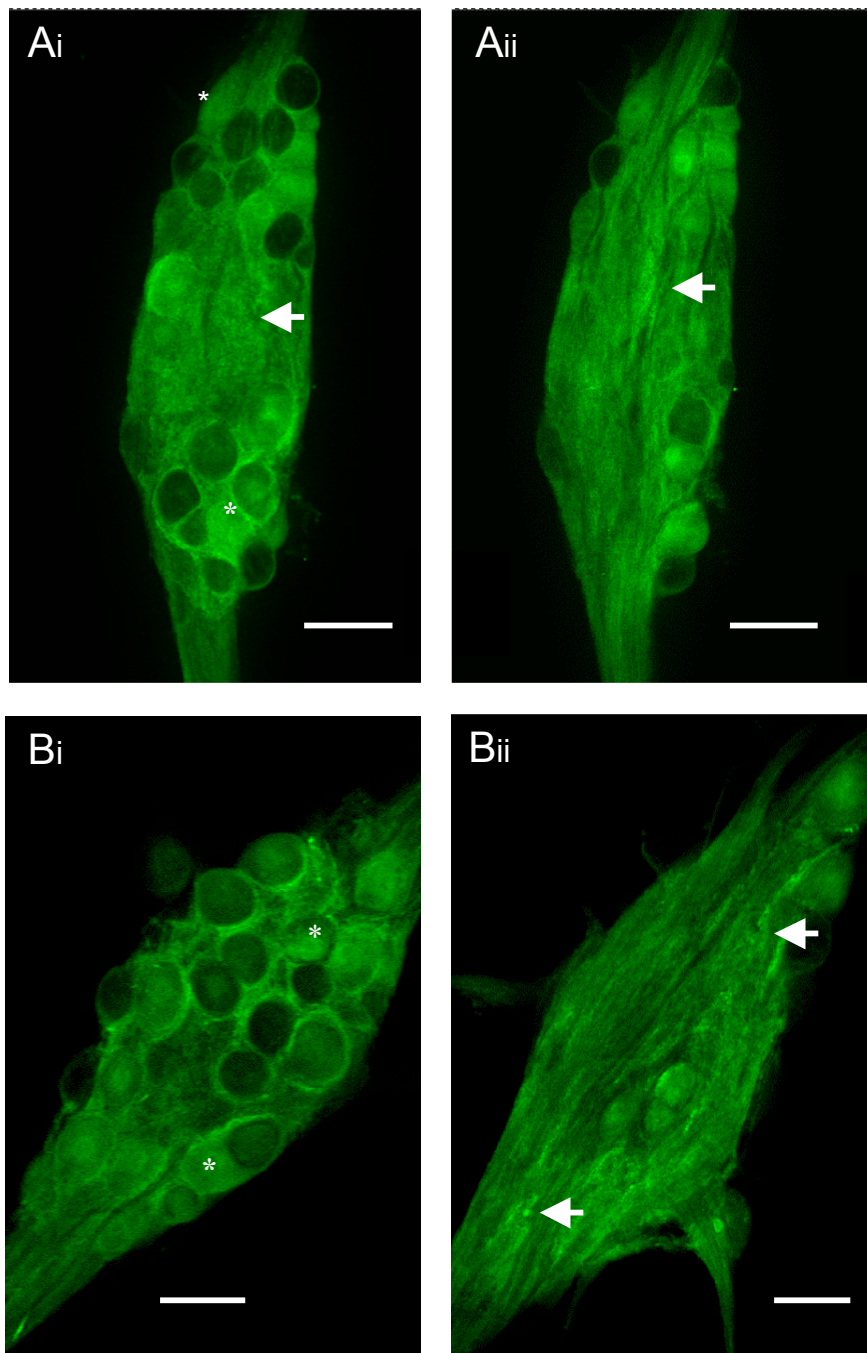
Figure 4.2 PIIH staining in different confocal planes of two STGs. A and B show different ganglia.The stn is located at the top, the dvn towards the bottom of the pictures. Scale bar 200 μm. Ai and Bi show dorsal planes near the surface of the ganglia, at the depth of most of the cell bodies. PIIH immunoreactivity varied within neurons from very strong (asterisks) to very weak (dark cells). Aii and Bii are show more ventral planes towards the middle of the same ganglia, at the level of the fine neuropil. Gain and background subtraction were not changed between sections. In the neuropil and between somata, localized areas of strong punctuate and clustered anti-PIIH immunoreactivity could be seen (arrowheads).
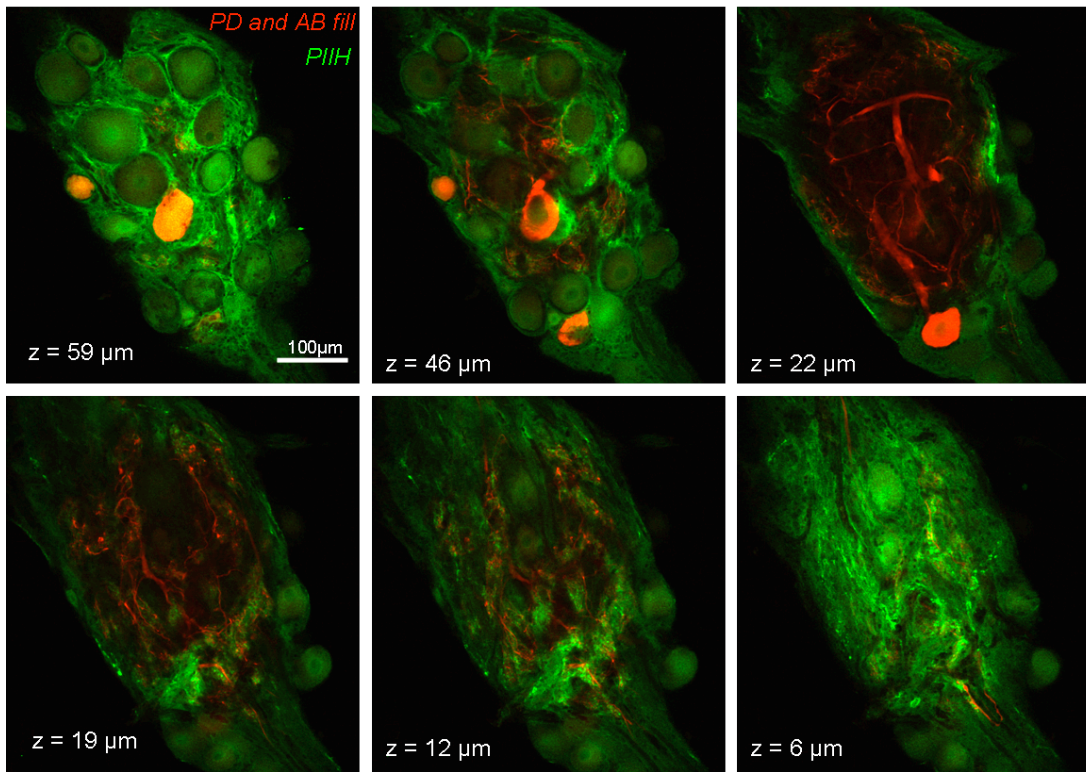
Figure 4.3 PIIH protein localization (green) in the STG. Confocal images from z-stack from the most dorsal (z=59μm) to ventral (z=6μm) plane. A PD neuron was injected with neurobiotin for better orientation and resulted in the fill (red) of both PDs and the AB neuron (smaller cell on the left side at z=46μm). Notice almost complete lack of PIIH signal in the coarse neuropil in the middle sections, which is likely due to limited penetration of the antibody (compare to sectioned ganglion in Figure 4.5).

83
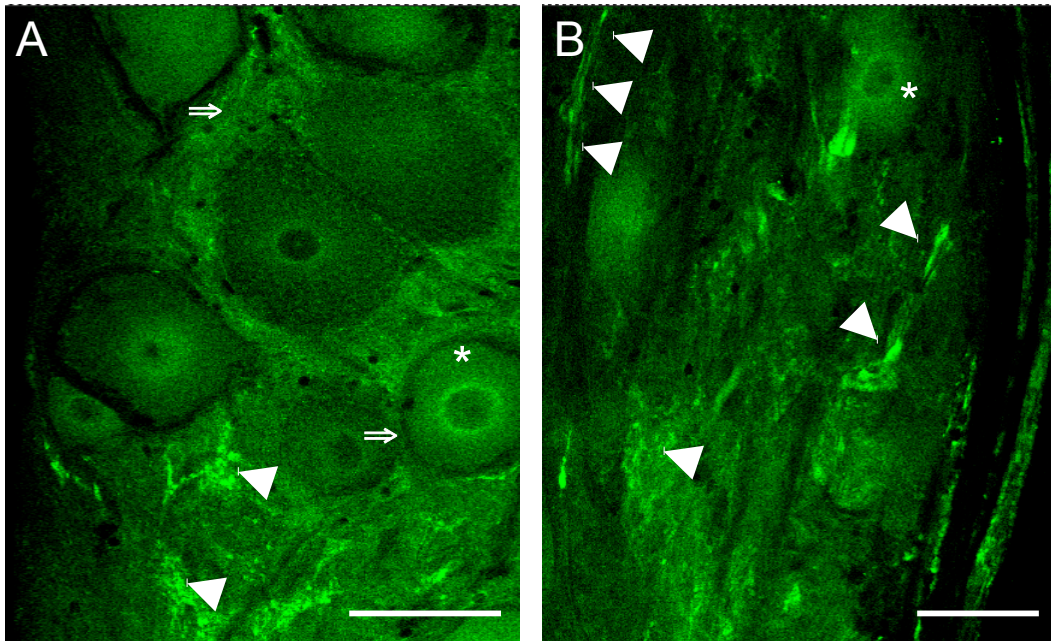
Figure 4.4 PIIH expression in the STG. Confocal slice of different planes from the same ganglion as in the previous figure. Scale bar 75 μm. Several somata showed strong PIIH staining (asterisks). The somatic anti-PIIH staining was usually concentrated around the nucleus. Notice the absence of ring-like immunoreactivity at the surface of most neurons (open arrowhead), indicating only weak surface expression in the soma. Punctuate anti-PIIH signal and areas of concentrated or clustered staining were seen outside of cell bodies (closed arrows in A and B), which might be part of the neuropil but could also arise from glial cells surrounding the neurons. I often observed fiber like structures of various thicknesses throughout the ganglion, which showed high affinity for anti-PIIH staining (arrowheads in B). Sosa et al. (2004) observed similar structures in anti-5HT receptor staining in crustaceans.
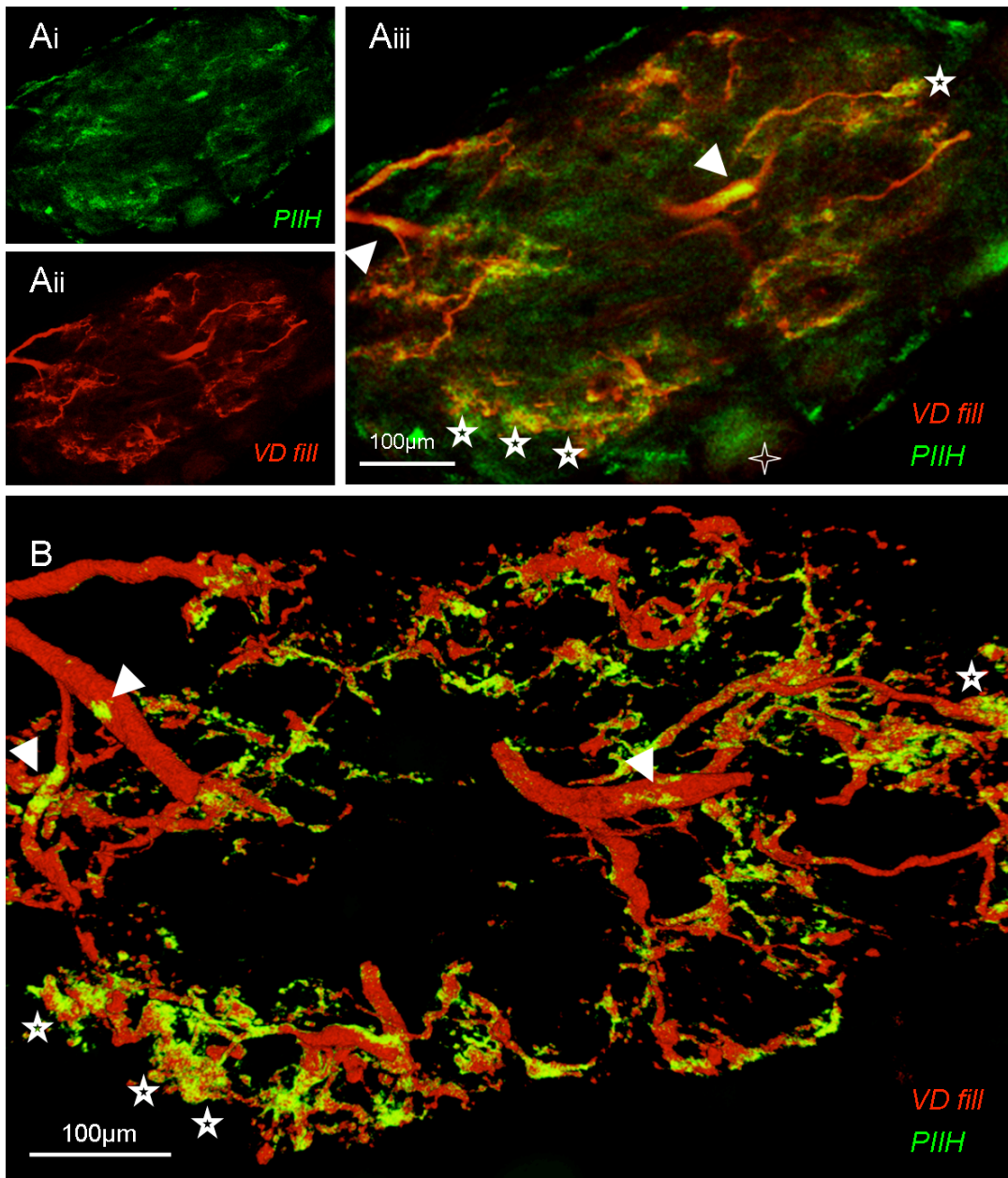
Figure 4.5 Ai. PIIH staining (green) in the neuropil. Single plane of a cross-sectioned STG (45µm thick), in which the VD neuron was injected with neurobiotin (red, Aii). Overlay of VD neurobiotin fill and PIIH signal in Aiii, areas of overlap appear yellow. The section does not contain the soma of the VD neuron. Notice the cloudy distribution of PIIH signal in the fine neuropil (stars) and its patchy appearance on larger VD processes. B shows a 3D-opacity rendered reconstruction of the same section. Dense opacity setting for neurobiotin and transparent setting for PIIH emphasize PIIH signal in the coarse

(arrowhead) and fine (star in Aiii and B) neuropil. Notice concentrated intense PIIH signal in the surrounding fine neuropil, while PIIH reactivity in the coarse neuropil is sparse and patchy (arrrow heads in Aiii and B). The soma of a non injected neuron in Aiii (4-point star) does not show up in the redered image (B).
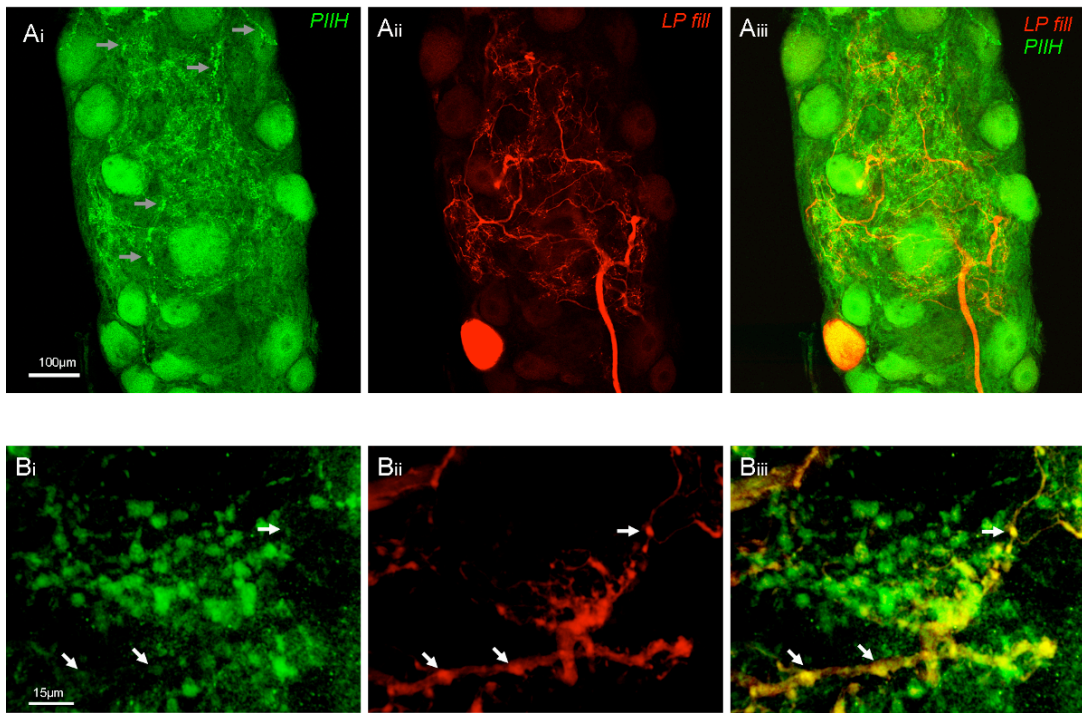
Figure 4.6 Ai. Overall distribution of PIIH protein in the STG in a z-series projection. Notice different intensities of somatic labeling. Strongly labeled structures were seen across the dorsal surface of the ganglion (grey arrows), that may be processes of a non identified or descending neuron, or could be non-neuronal structures. Aii Projection of the neurobiotin filled LP neuron. Aiii Overlay reveals PIIH labeling in the LP soma and throughout the neuropil. Bi 100xs magnification of PIIH labeling in the fine neuropil structures of the same ganglion. Bii Neurobiotin labeled LP neuropil. Biii Overlay of the PIIH and neurobiotin signal reveals overlap in bulbous varicosities of the LP neuropil (arrows in Bi, Bii and Biii).
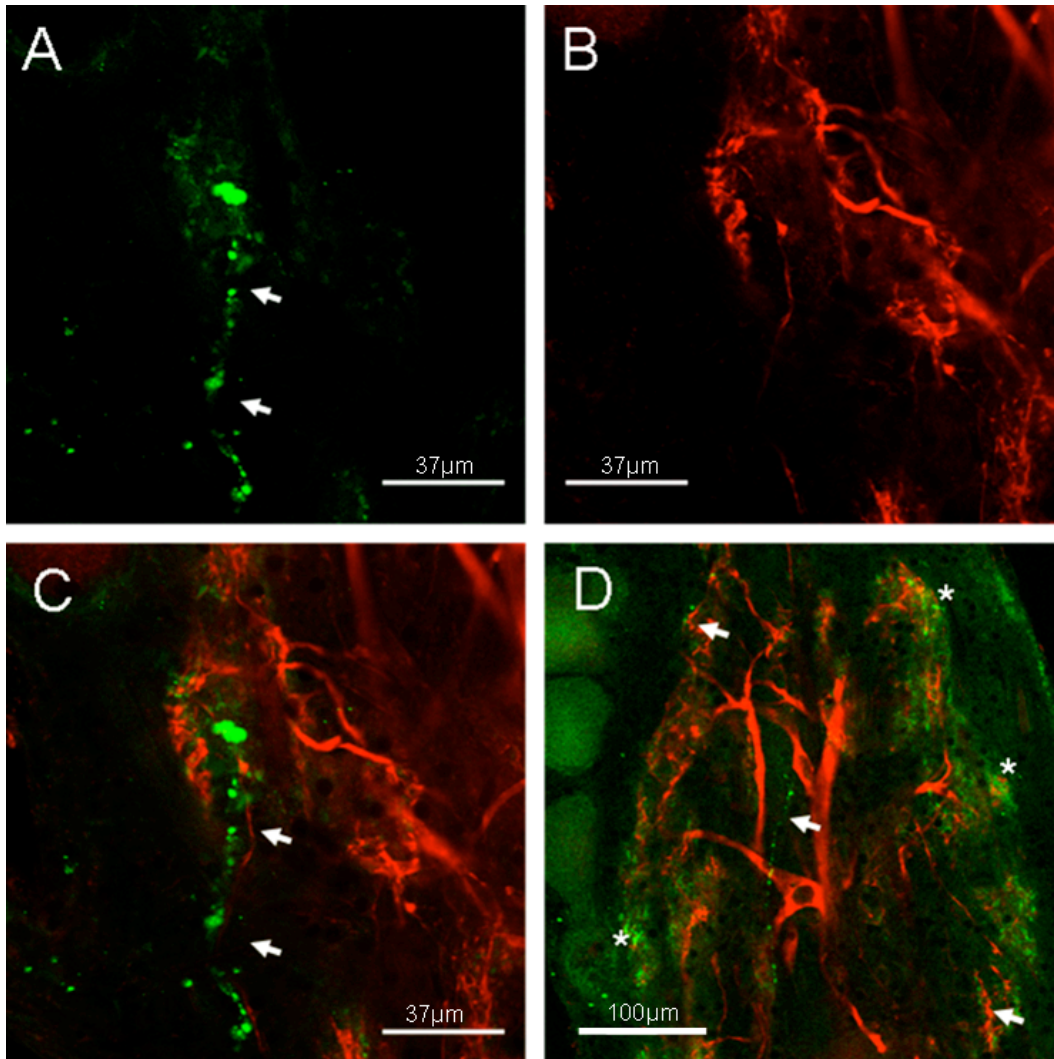
Figure 4.7 Individual optical sections of an STG in which a PD neuron was injected with neurobiotin. A. Unidentified Structures with PIIH immunoreactivity (green) in the neuropil. Multiple processes with bulbous varicosities were labeled with anti-PIIH antibody. B. Neurobiotin label of a portion of the PD neuron (red). C. Overlay of PIIH and neurobiotin signal reveal an organization of the PIIH labeled structures, which appeared to follow parallel to a small branch of the PD neuropil. D. Overlay of a different region in the same ganglion at lower magnification. Notice that the PIIH signal is largely absent in the middle of the coarse neuropil, and stronger in the region of the surrounding fine neuropil (asterisks). Also, notice multiple structures as the one shown in A at different locations in the ganglion (arrows).
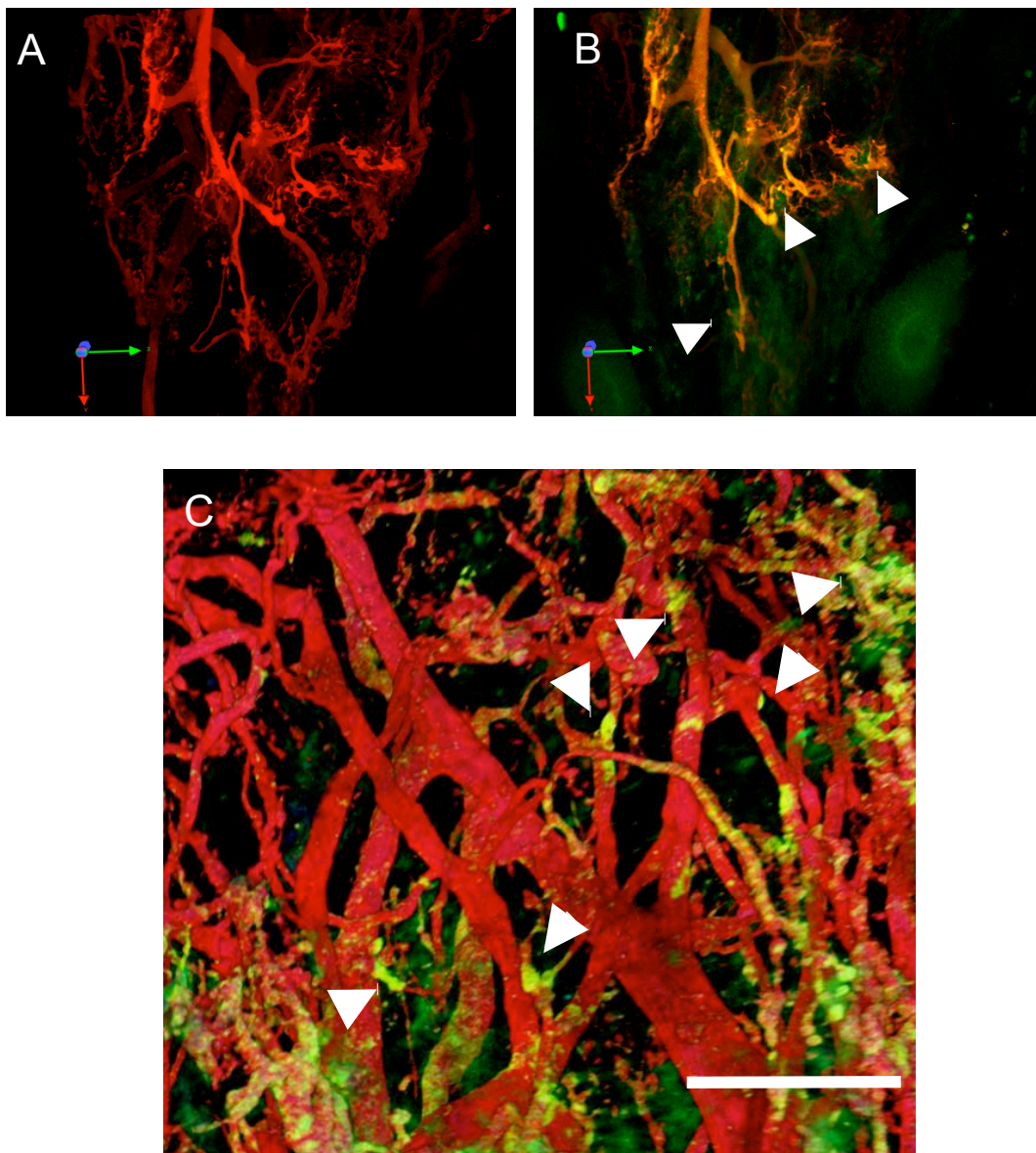
Figure 4.8 Anti-PIIH staining in 3D-opacity-rendered STG, in which an IC neuron has been filled with neurobiotin. A. 3-dimensional neuropil reconstruction of the IC neuron. B. Overlay of the PIIH signal (50% transparency, green) and the neurobiotin signal (76% transparency, red). Notice the overall orange tint of the neuropil which is a result of strong background PIIH staining in the tissue. Small processes of the neuropil appeared to end in hand- or basket- like structures with very strong PIIH staining in between. (Arrows in B). C shows a 3D reconstruction with higher density rendering settings and different clipping of black levels in both channels. PIIH staining on the neuropil processes are more apparent than the transparent PIIH signal without neurobiotin background. Notice the

unevenly distributed PIIH signal on different processes and patches of stronger labeling close to branching points (arrows). Scale bars 37μm.
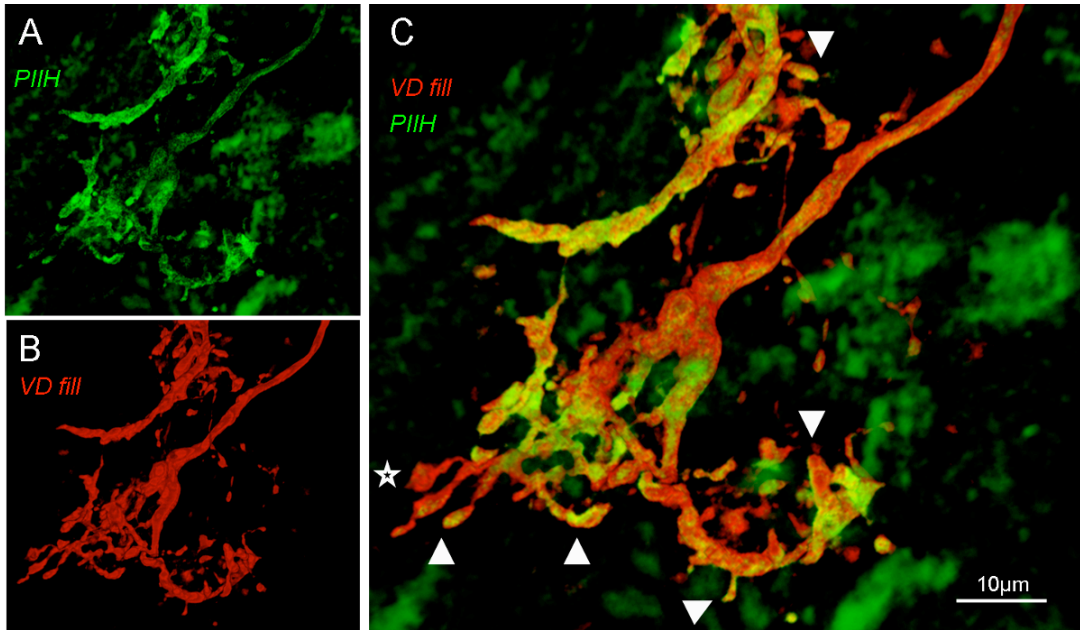
Figure 4.9 100x magnification of PIIH protein staining in a fine branch of the VD neuropil in a sectioned ganglion. A: Anti-PIIH staining (green) revealed small branch-like processes at high magnification (100 xs). Neurobiotin-double labeling (B, red) confirmed that some of the signal was located in the processes of the neurobiotin-filled neuron. Notice spiny and bulbous processes on the neuron, which often showed strong labeling for PIIH (arrow heads), however not always (star).
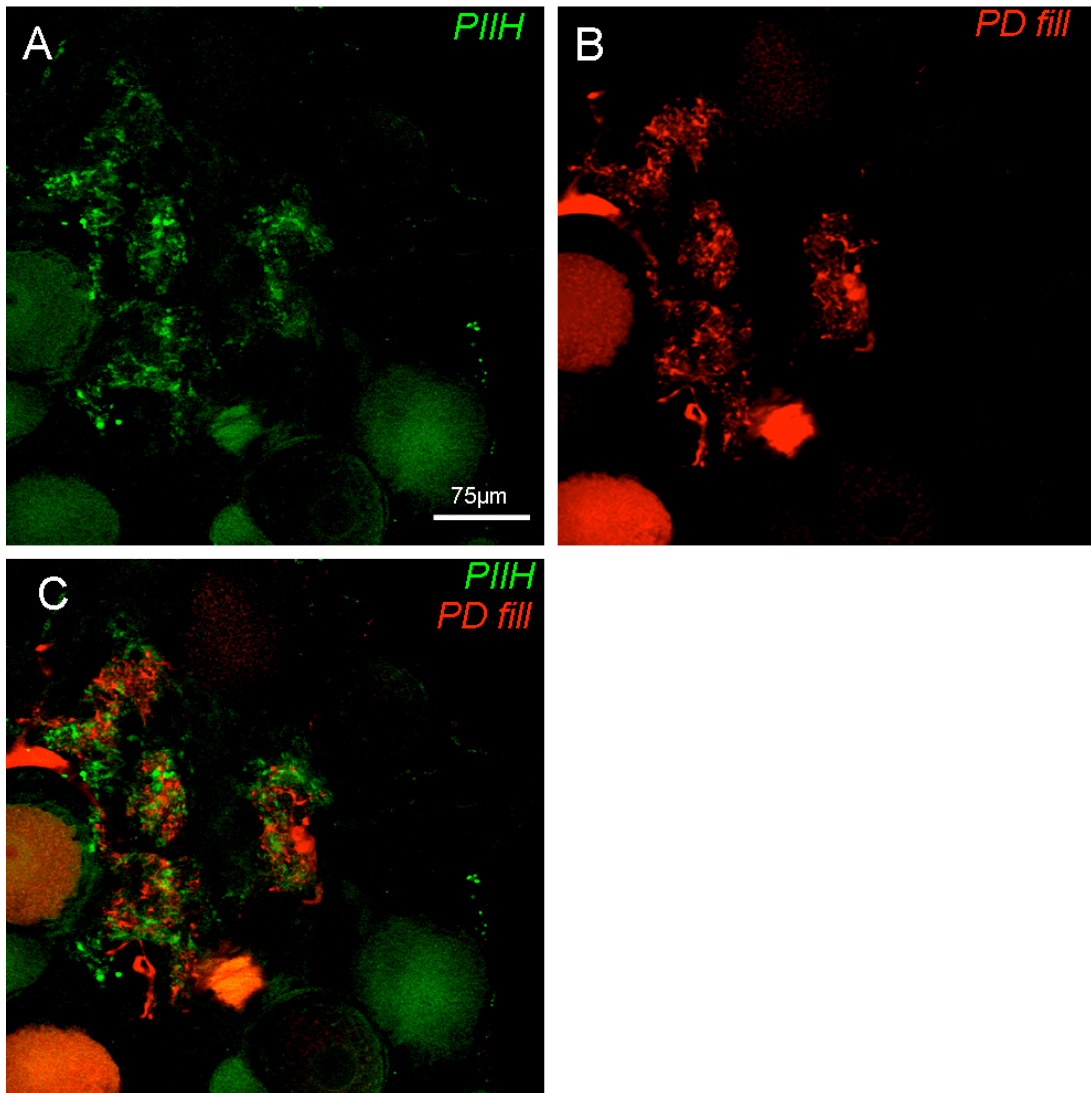
Figure 4.10 PIIH staining in the neuropil. A. Intense PIIH protein staining in very fine processes of the PD neuropil in a sectioned ganglion. Anti-PIIH staining (green) revealed small bulbous and branch-like structures. B. Neurobiotin labeling (red) of the PD neuropil. C. The lack of PIIH/Neurobiotin double-labeling shows that very little PIIH is located in the PD neuropil. Process-like PIIH stained structures in A therefore belong to other neurons, potentially physically interacting with the PD neuron.
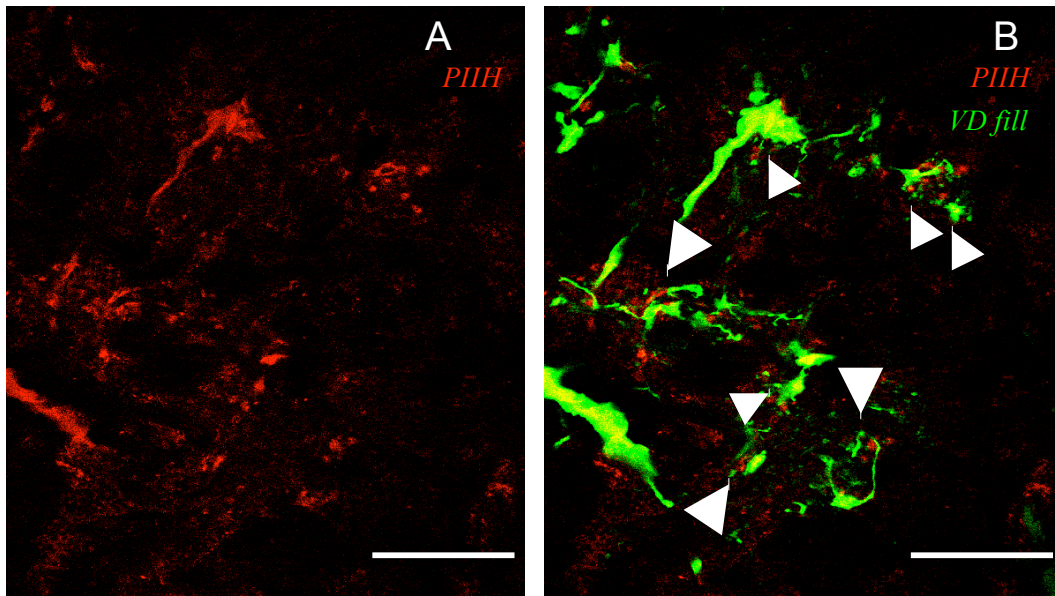
Figure 4.11 PIIH protein staining in very fine processes of the VD neuropil in a sectioned ganglion. A. Anti-PIIH staining (red) revealed small branch-like structures at high magnification (100 xs). B. Neurobiotin-double labeling (green) confirmed that some of the signal was located in the processes of the neurobiotin-filled neuron. Note that some process-like structures in A did not belong to the VD neuron but appeared very close and potentially physically interacting in B (arrowheads), although higher resolution than light microscopy can provide would be required to further examine this. Both scale bars 9µm.
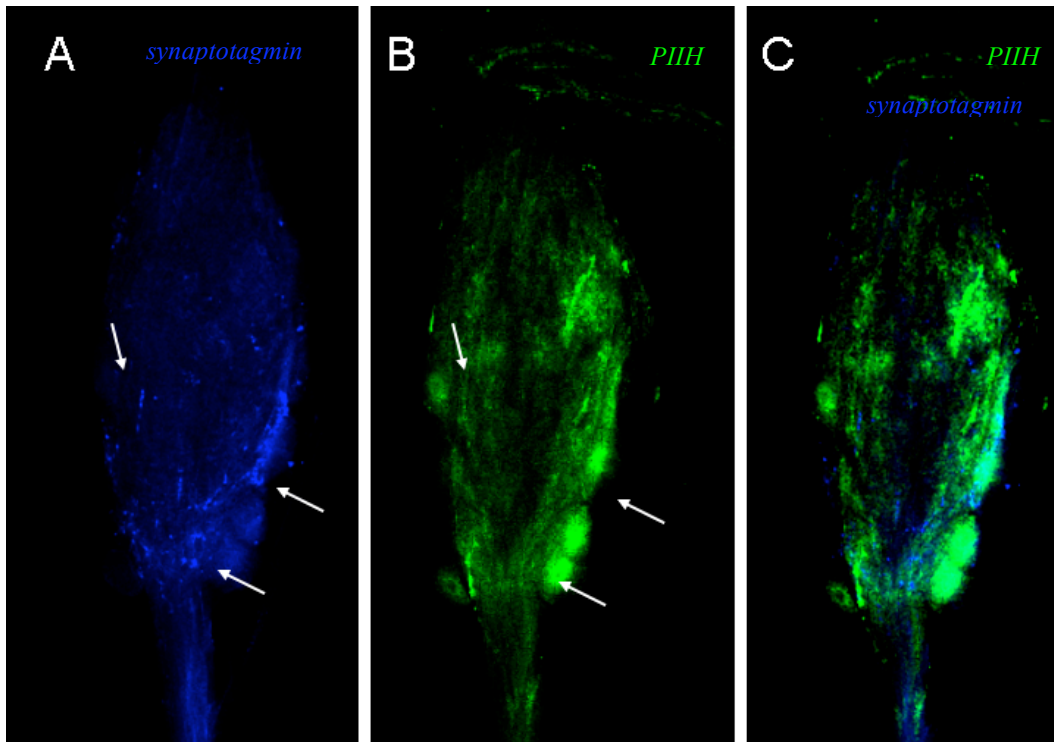
Figure 4.12 Overall localization of synaptotagmin (blue) and PIIH (green) protein in an optical section of the STG. The stomatogastric nerve (stn) is located at the top of the image. The optical section exposes the coarse neuropil in the middle ot the ganglion, with the most of the fine neuropil concentrated in a region of very fine processes at the right side of the ganglion (upper right arrow). A. Synaptotagmin immunoreactivity with bold labeling in the coarse neuropil and diffuse albeling in the fine neuropil. B. PIIH immunoreactivity with diffuse labeling of the coarse neuropil and intense diffuse labeling of the concentrated fine neuropil. C. The overlay of both channels shows that the dense area of the fine neuropil was strongly labeled for both proteins, whereas PIIH and Synaptotagmin distribution differed in other parts of the ganglion.
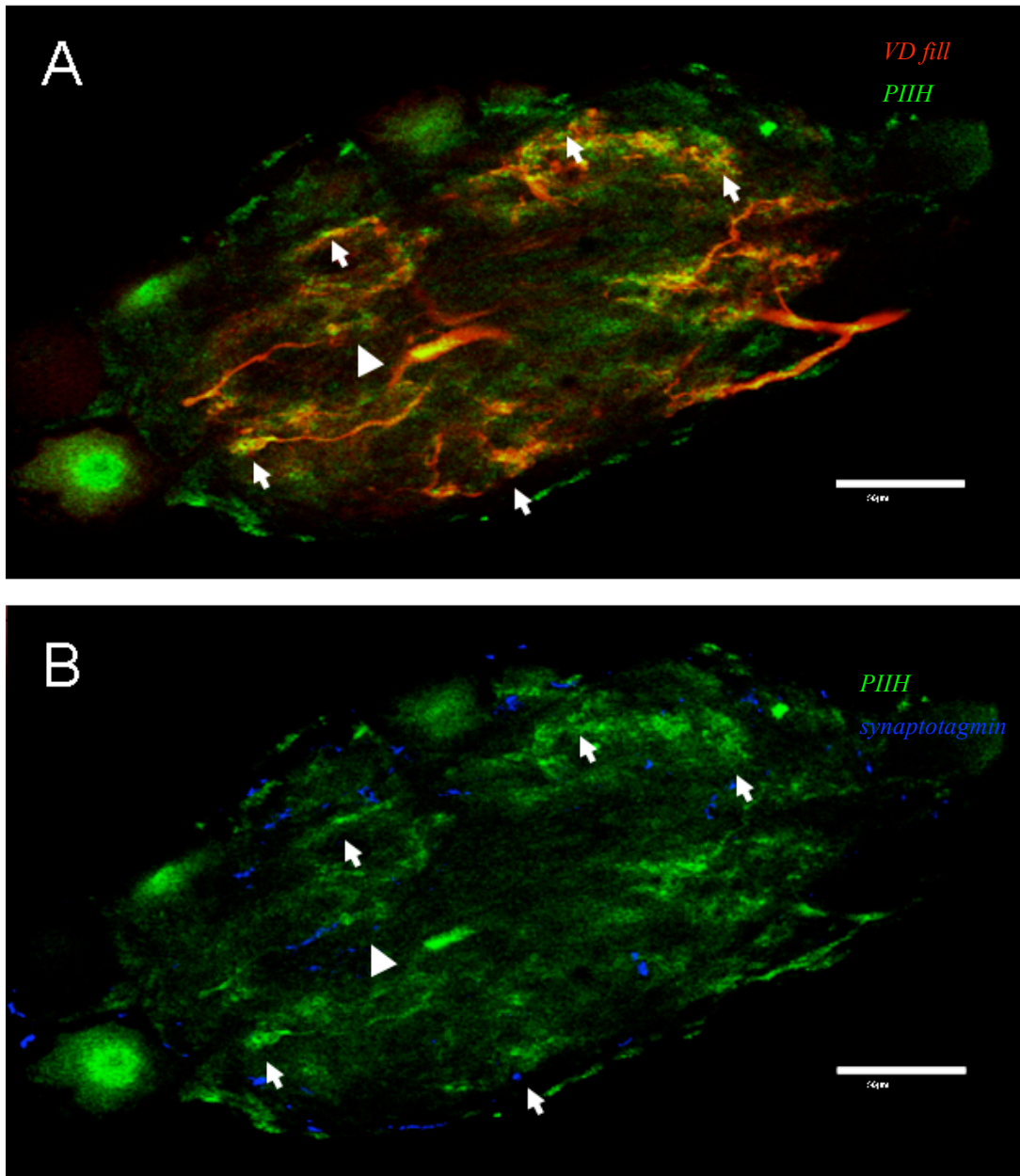
Figure 4.13 PIIH and synaptotagmin distribution in the STG. Single optical stack of a cross -sectioned STG (45µm thick). A. Coarse and fine neuropil of a neurobiotin-filled VD neuron (red). The arrows point at finely branched areas of the neuropil with high levels of PIIH (green). B Overlay of anti-IH staining (green) with anti-synaptotagmin (blue) reveals different expression pattern of both proteins in the coarse neuropil and most of the fine neuropil. However, notice occasional close vicinity of I_h protein and synaptic marker (arrowhead). Scale bar: 50µm.
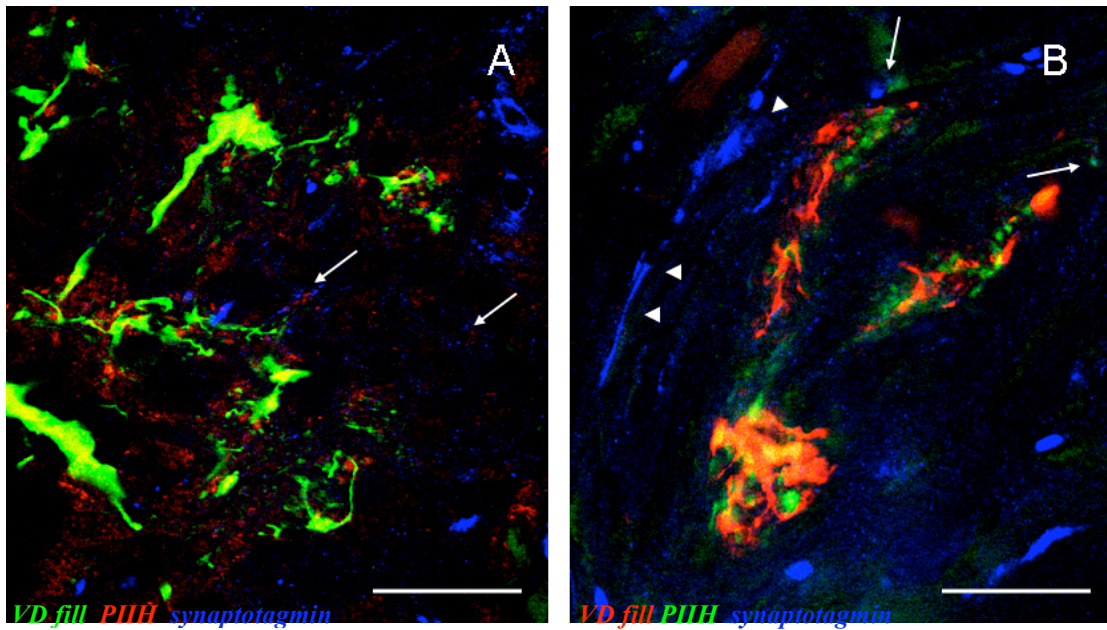
Figure 4.14 A. PIIH (red) and synaptotagmin (blue) in processes of the fine neuropil of a neurobiotin-filled (green) VD neuron in a sectioned ganglion at high magnification (100x). Large clusters and fine punctate staining of the synaptic marker can be found within the area, but almost never at the spots where the VD neuron came in close contact with PIIH (red). B. Different section shows the coarse and fine neuropil in the same ganglion. I typically observed long narrow marks of anti-synaptotagmin staining (blue, arrowheads) in the coarse neuropil. Very close proximity of PIIH and synaptic staining is seen at the arrow in the top center of B., but there is no overlap. The arrow on the upper right hand side points to one of the few globular spots of PIIH and synaptotagmin co-localization (appears cyan). Scale bars 9µm.
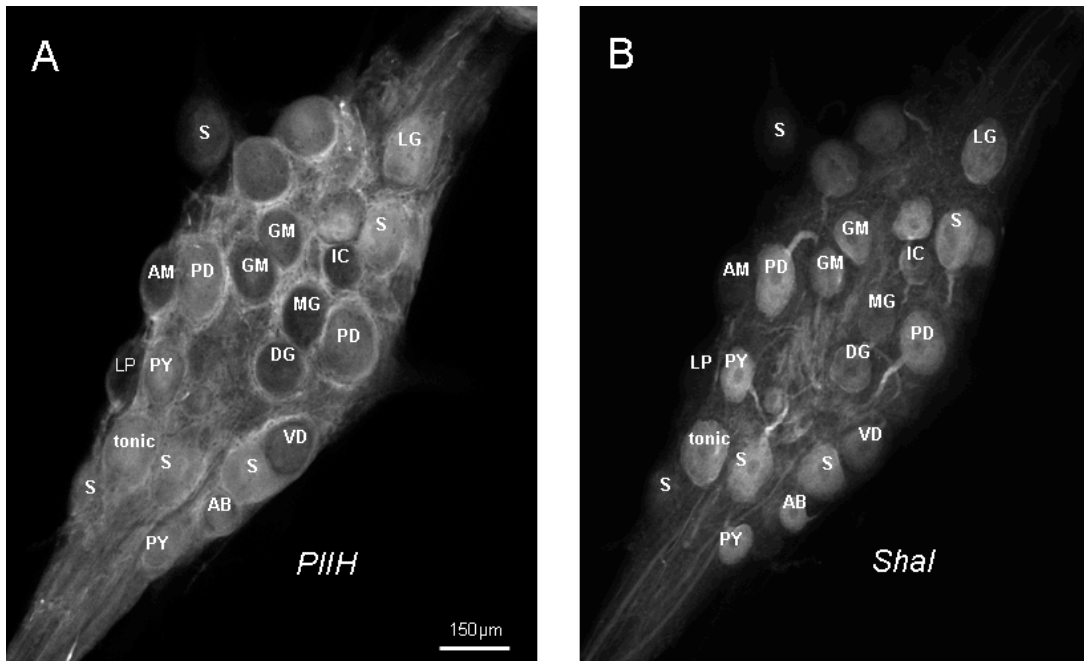
Figure 4.15 I_h (A, PIIH) and I_A (B, shal) protein are differently distributed in identified STG neurons: A. PIIH protein is variably expressed in the various somata, with strong extracellular staining around the soma that may be non-neuronal. Among identified neurons, the AB neuron and occasionally the IC neuron (but not in this example) tended to show high levels of PIIH staining compared to other cells.   B. Shal protein is strongly concentrated in the soma and primary neurite membranes of many neurons. Diffuse Shal staining was also found in the membranes of the fine neuropil.   Pyloric cells are abbreviated PD (Pyloric Dilator), LP (Lateral Pyloric), AB (Anterior Burster), VD (Ventral Dilator), PY (Pyloric); AM, GM, MG, DG, LG are gastric neurons.
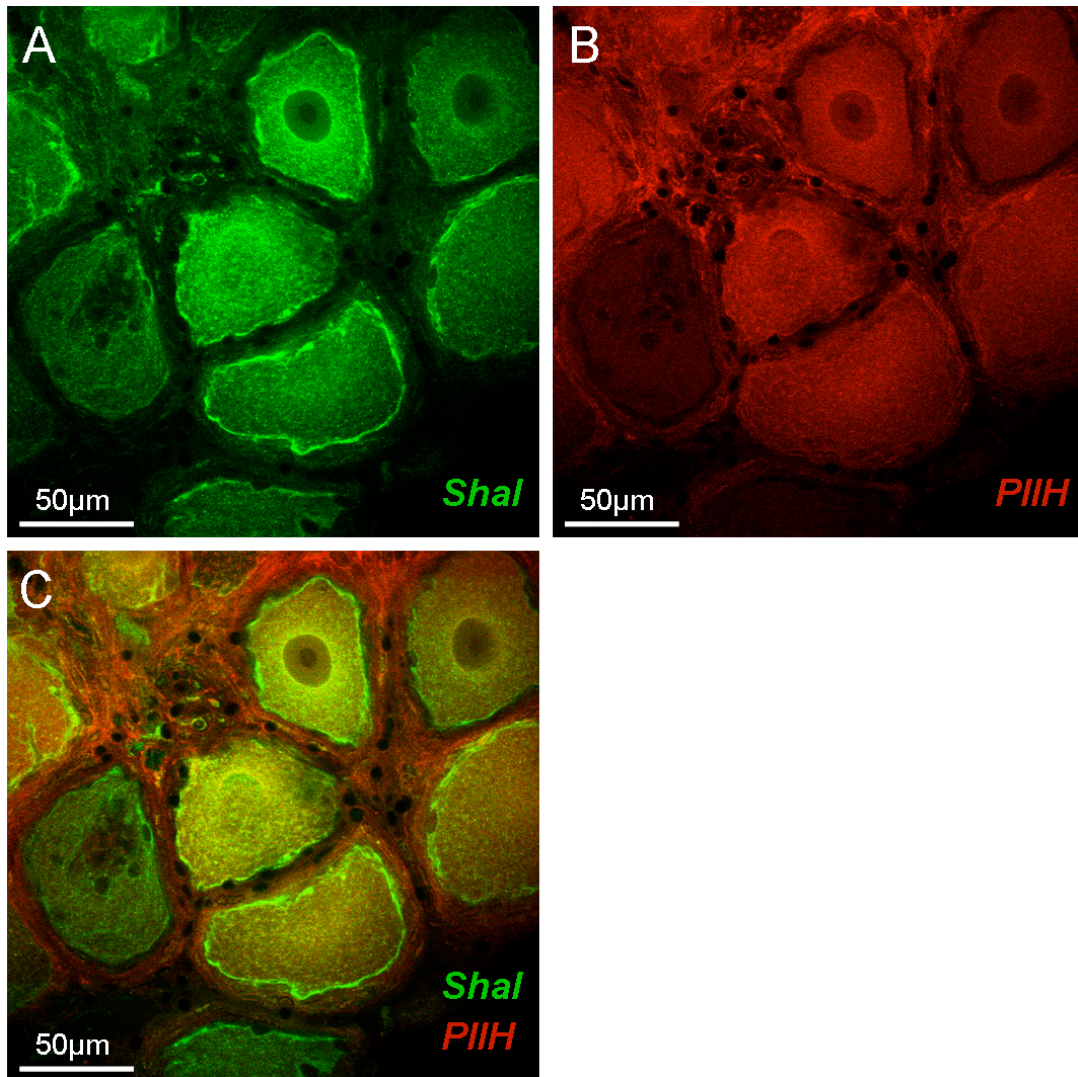
Figure 4.16 Shal (A) and PIIH (B) localization in STG somata. Notice high level of membrane-bound shal signal around the soma in A and the strong PIIH signal surrounding the nucleus and also in the perineuronal tissue surrounding the somata in B. Overlay in C shows colocalisation of Shal and PIIH (orange) in many, but not all neurons and in the perineuronal tissue.
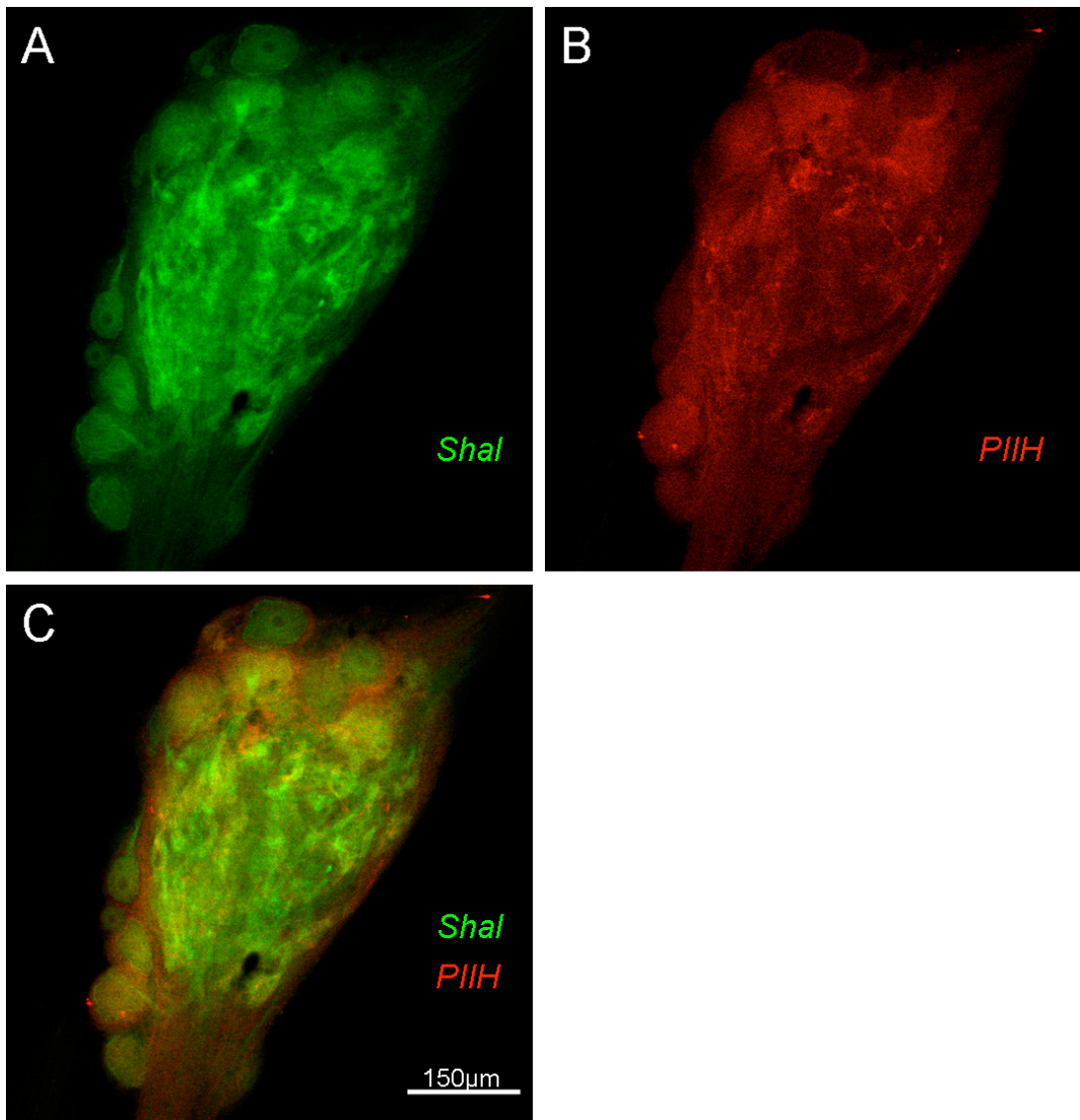
Figure 4.17 Comparison of Shal (A, green) and PIIH (B, red) distribution in the neuropil regions of the STG in single optical slice. C. Overlay, high level of yellow indicates presence of Shal and PIIH protein in the neuropil (middle of the ganglion).
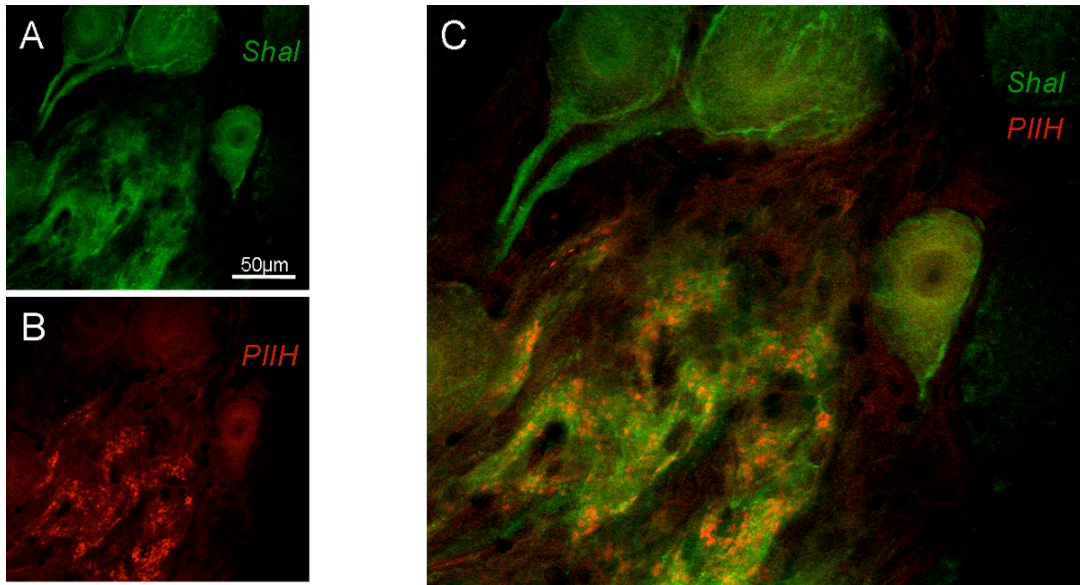
Figure 4.18 Higher magnification (40x) of unidentified STG somata and neuropil. Shal protein (A, green) is diffusely distributed in the fine neuropil, visible in the lower half of the image and concentrated in the membranes of the soma and primary neurite. PIIH protein (B, red) is only weakly expressed in the soma membranes, but notice intense and discrete staining in the neuropil area. C shows the overlay of both images, yellow in the neuropil and in the soma indicate presence of both proteins.
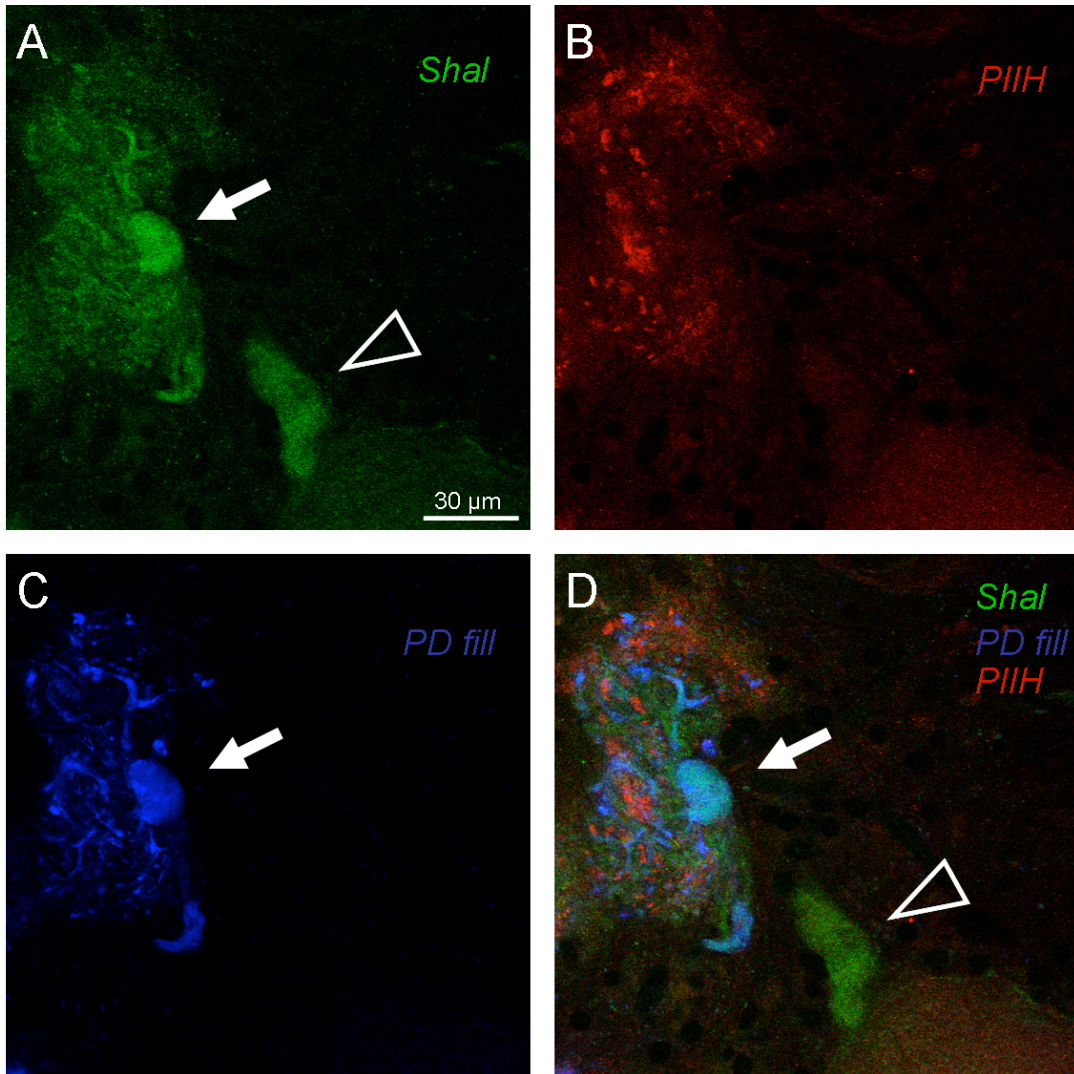
Figure 4.19 Shal protein (green in B and D) is localized in small processes of the PD/AB neuropil (blue in C and D). PIIH protein (red in B and D) is localized in neuropil structures in close vicinity of the PD/AB neuropil, with significant presence in the boutons of the PD neuropil (D: purple with neuropil and PIIH alone and white for overlap of all). PIIH (red) and Shal (green) appear not to colocalize in PD. Scale bar 30µm.
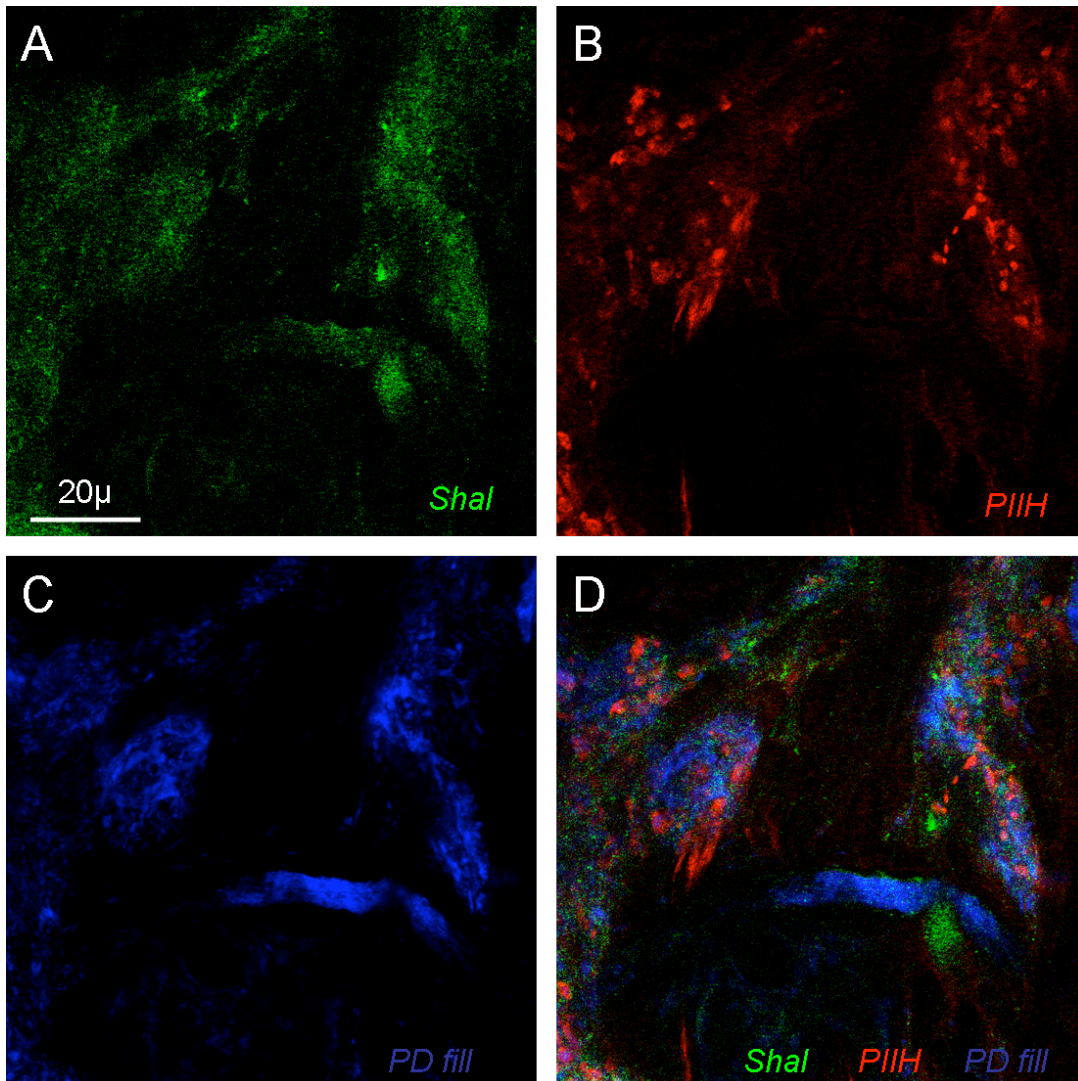
Figure 4.20 High magnification of the neuropil, shows small processes of the fine and larger processes of the course neuropil. A. Shal localization (green). B. PIIH localization (red). C. Neurobiotin filling of one PD neuron shows processes of the PD or the electrically coupled AB neuropil (blue). D. Channel overlay. Notice the Shal (green) and PD (blue) overlap, indicating the presence of Shal protein in many small branches of the neuropil. Also notice some overlap between PIIH (red) and neurobiotin (blue), which shows as purple, and between PIIH (red) and Shal (green), which shows as yellow or orange. The relatively lack of triple-labeled structures indicates that Shal and PIIH peak concentration are differently localized in the PD neuron.
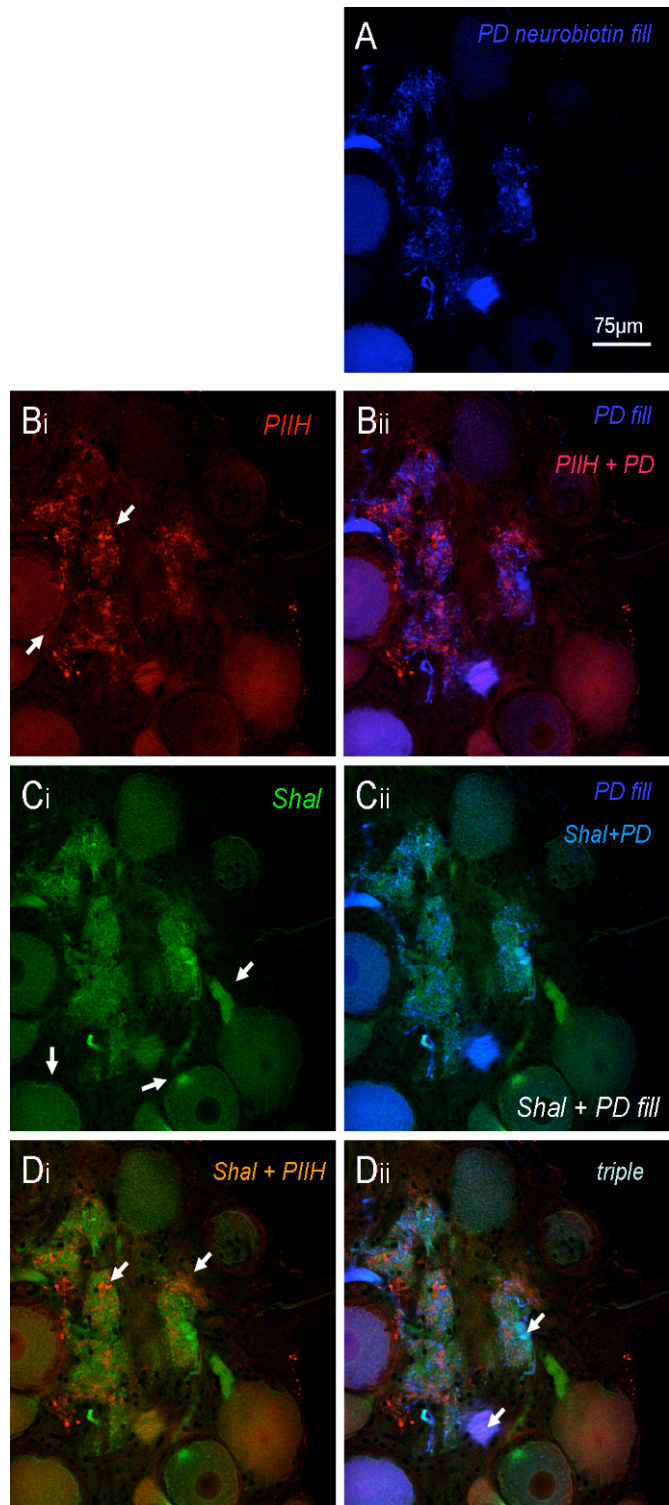
Figure 4.21 Localization of Shal and PIIH in somata, primary neurites and in the fine neuropil. A: Neurobiotin filling of the PD neurons. Bi. PIIH staining shows weak labeling in

the somata and strong labeling in tuftlike structures of the neuropil (arrows). Bii. Overlay of neurobiotin signal and PIIH signal shows PIIH in the neuropil region of the PD neurons (purple).Ci. Shal staining with distinct and intense labeling of the soma membranes and in the proximal primary neurites (arrows), and diffuse staining of the neuropil. Cii. overlay of Shal staining with PD neurobiotin labeling. Di. Double staining for PIIH (red) and Shal (green) shows some overlap (orange), but also distinctly (red, Aii) is more diffuse in the somata, very low or absent in the primary neurites and intense in the fine neuropil Dii.Overlap of all three signals shows as whitish color.and can be seen to a low degree in the somata and larger processes.
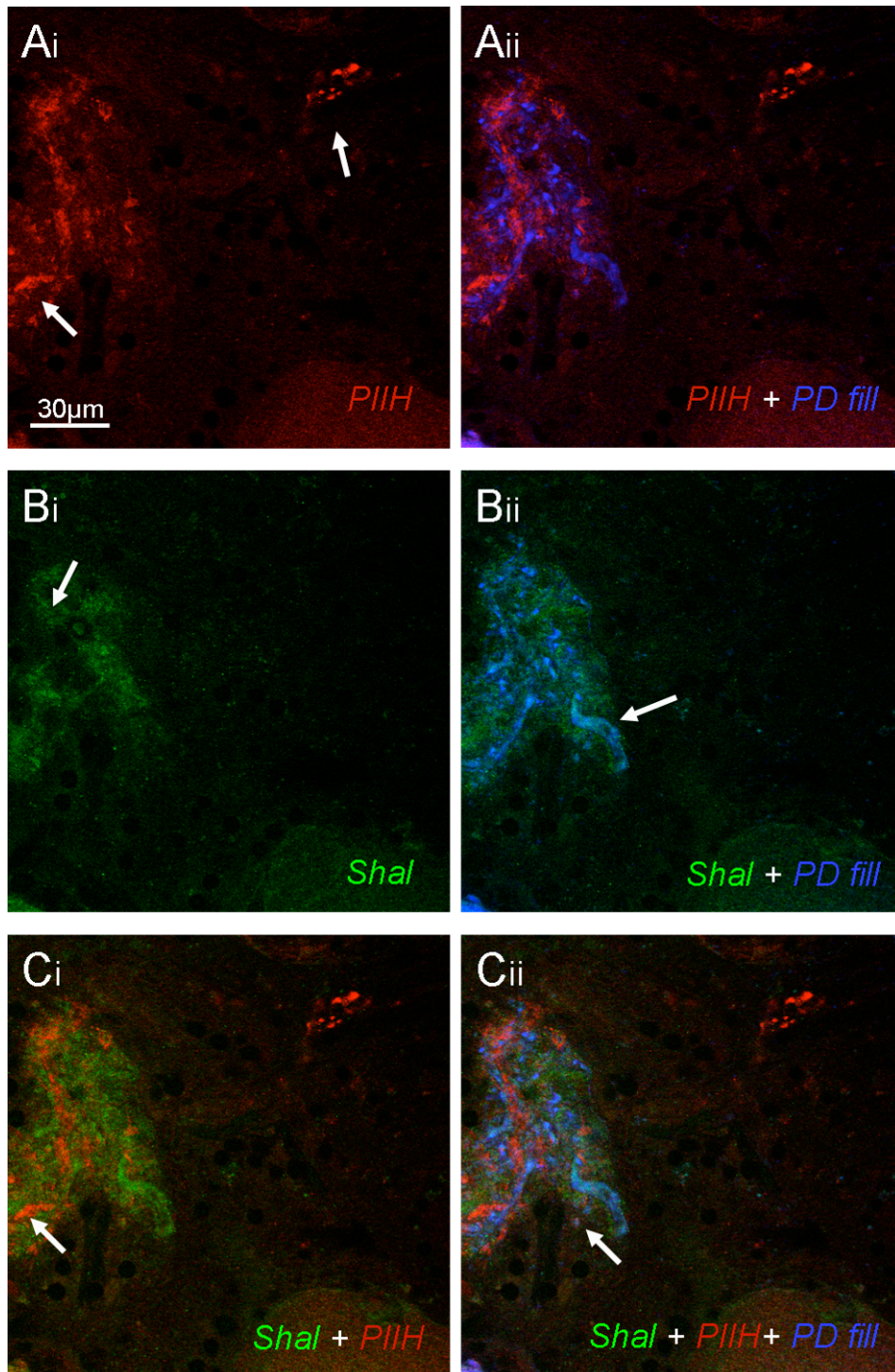
Figure 4.22 Example for Localization of PIIH (red) and Shal (green) in the fine neuropil. (100x) Ai. PIIH labeling in the fine neuropil. Aii Neurobiotin filling of the PD/AB neuropil (blue) reveals areas with PIIH immunoreactivity in the very close vicinity of the processes,

but only little overlap (purple).Bi. Shal labeling in the fine neuropil. Bii.Overlap of Shal signal with the neurobiotin labeling (cyan) shows that Shal protein appears to be localized in the PD/AB processes Bii). Ci. Overlay of the Shal and the PIIH signal shows some degree of overlap (yellow-orange) Cii.Triple overlay., Co-localization of PIIH with both Shal and neurobiotin would show as white.

Discussion

I examined the localization of I_h channels in identified STG neurons and their distribution in respect to a synaptic marker and to a different channel protein, Shal, which mediates the A-current in pyloric neurons (Baro et al, 1996; Baro et al., 2000). I could demonstrate I_h protein (PIIH) expression in the cell bodies and in the neuropil of STG neurons, with particularly high expression in the fine neuropil region. Pattern of strong PIIH localization were found in areas that were rich in synaptic contacts, however, only few spots of exact overlap with the synaptic marker (Synaptotagmin) could be identified. Similarly, stronly PIIH-labeled neuropil regions coincidated with strong Shal staining, however, at higher magnifications, Shal and PIIH signals were only localized in close vicinity but did not overlap. These results suggest that I_h channels may play an important role in dendritic signal processing. The lack of consistent co-labeling with the synaptic marker indicates that primary function of I_h channels is probably not tied to their localization at synaptic terminals. Instead, I_h may shape transmission and integration of synaptic signals by locally altering the input resistance (effectively shunting synaptic potentials) and/or by affecting the dendritic membrane potential. The lack of distinct co-labeling with Shal protein suggest that the homeostatic response may not be caused by a physical interaction of PIIH and Shal protein such as co-expression or co-insertion. However, the concentration of both proteins in the fine neuropils still supports a tight link in the expression and function of I_h and I_A channels.

I used used a monoclonal anti-pentaHis antibody to characterize PIIH localization in the STG. This commercially available antibody binds to an unusual continuous sequence of eight histidines in the lobster PIIH C-terminal sequence. A BLAST protein search detected less then ten proteins with a similar sequence of five or more histidine residues, which were all only putative protein-coding sequences with the exception of the *brakeless* gene product in *Drosophila*, which is required

for photoreceptor growth-cone targeting (Rao et al, 2000). In the STG, anti-pentaHis appeared to specifically label IH protein. I confirmed this finding with Western blot analysis (Figure 4.1A). The major band with an apparent molecular weight around 70kDa falls well within the expected accuracy range for PIIH protein, with sequence-based predictions between 77 and 82kDa for the various splice variants. Additionally, weak bands of larger molecular weight were found, that were most likely caused by incomplete denaturation or by residual protein binding. Anti-pentaHis is a commercially available monoclonal antibody, which was produced in cell cultures from a specific target sequence and a carrier protein. Therefore, incubation with a pre-immuno serum could not be used to exclude unspecific cross-reactivity. Another source for unspecific bands could be cross-reactivity with the carrier protein, however, pre-absorbtion with the carrier protein was not possible due to restricted information release from the company that created the antibody. Nevertheless, as a positive control, His labeled Panulirus IH reliably and specifically in Western blots staining of total protein from oocytes that had been injected with PIIH-RNA, but not protein from control oocytes (Fig 4.1B; Dr Q. Ouyang, unpublished data).

I_h channels have been linked to regulation of excitability through their role in setting the membrane potential and their contribution to rebound activity after hyperpolarization (Pape 1996, Robinson, Siegelbaum 2003, Kaupp, Seifert 2002). A uniform distribution of I_h channels throughout a complex neuronal structures like the STG might be evidence for a such a function in the STG, similar to other potassium currents. However, in many systems a non-uniform distribution of I_h additionally contributes to modulation of synaptic transmission via pre- and postsynaptic effects (see Chapter 5 for a more thourough dicussion of these effects).

I found a consistent pattern of IH protein expression in all ganglia studied. The strongest PIIH signal occurred in the areas of the fine neuropil (Figure 4.3, Figure

4.4, Figure 4.6). The somata of individual neurons revealed a wide range of PIIH staining intensity, which varied between different ganglia (Figure 4.2, Figure 4.6). Among pyloric neurons, the somata of the AB, VD and IC neuron were usually strongly labeled, while the PD neurons often exhibited weaker staining; however, overall there was not a statistically significant correlation between neuron type and PIIH labeling intensity in the soma. This result is inconsistent with data from voltage clamp recordings, where the largest I_h among pyloric neurons occurs regularly in VD neurons, followed by intermediate current amplitudes in the AB, and IC, relatively little I_h in the LP and PD, and varying I_h amplitudes in PY neurons (Peck et al., 2006; MacLean et al, 2005). My data suggest that the intensity of the somatic PIIH signal appears not to reflected in the level of functional channels at the surface membrane. Most of the label in my preparations was intracellular, and the very small amount of protein expressed at the cell surface may not be linearly related to the amount of intracellular protein. It is also possible, although less likely, that the current measured in voltage clamp experiments is affected by the neuron geometry, where somatic recordings of I_h might be attenuated more in cells with long primary neurites (like the PD and the LP neuron). Peck et al. also demonstrated that I_h is subject to strong modulation (Peck et al, 2006), which might obscure comparison of I_h recordings with somatic protein levels.

Tissue in-between and around somata on the dorsal and ventral side of the ganglion usually revealed strong labeling with the PIIH antibody (Figure 4.2A, Figure 4.3 (first and last sections), Figure 4.15, Figure 4.16). This connective tissue probably contains different types of glial cells (observed by M. Schmidt, personal communication), and small capillaries. Recent studies have demonstrated the presence of potassium and sodium currents in glial cells, they can affect the neuronal membrane potential, firing rates, and synaptic transmission (Yamazaki et al., 2005; Kang et al., 1998, Janigro, 1997, Bannerjee et al., 2007) Very little is known about glial physiology in the STG. The hypothesis that I_h channels may be expressed in glial cells is intriguing and might add a new approach towards

understanding the regulation of rhythmic firing in STG neurons. Specific PIIH staining of somatic and neurite membranes was weak, and showed no "railroad track" pattern in thin optical slices of neurites (Figure 4.15, Figure 4.16), as previously described for other potassium cannels in the STG like Shal, Shaw and Shab (Baro et al., 2000, French et al., 2004). These patterns are considered evidence for high rates of membrane insertion. However, their occurrence depends on a high ratio of membrane-bound protein versus cytosolic protein in the ER/Golgi-system and in trafficking vesicles. Therefore, their absence only indicates that membrane-bound levels of I_h expression are not particularly high compared to intracellular levels. A concentric pattern of intense PIIH signal was seen intracellularly in the soma around the nucleus, perhaps arising from protein still bound in the Golgi apparatus or endoplasmic reticulum (Figure 4.4A, Figure 4.16). I found neuropilar PIIH labeling to be sparse and patchy on larger primary and secondary neurites of the coarse neuropil (Figure 4.5, Figure 4.8). The fine neuropil showed cloudy areas of intense labeling with localized punctuate staining at higher magnifications (Figure 4.5, Figure 4.8). Labeling often occurred close to branching points, or on very thin, long branches (Figure 4.5). I used a synaptotagmin antibody to label the pre-synaptic terminals in the neuropil and examine the localization of PIIH at synapses. Synaptotagmins are associated with both synaptic vesicles and dense-core vesicles, including dense-core vesicles of neurohemal structures and synaptic-like microvesicles, which are considered the endocrine equivalent of neural synaptic vesicles (Skiebe and Wollenschlaeger, 2002; Walch-Solimena et al., 1993; Goodall et al., 1997; Marxen et al., 1997; Redecker et al., 1997; review: Marqueze et al., 2000). I found cloudy synaptotagmin labeling in the fine neuropil (Figure 4.13) but also as larger patches in larger neurites. Some processes and boutons exhibited both PIIH and synaptotagmin labeling but these were typically not overlapping in location.

Several explanations could underlie the localization of I_h protein in the synaptic neuropil. I_h might affect the electrical separation of different synaptic and

110

dendritic compartments by altering the membrane resistance at very localized sites, such as branch points. If the input from chemically or electrically coupled neurons were spatially organized within the neuropil region of a neuron, modulation of I_h could provide a powerful mechanism to change the weights of different synaptic inputs in a context dependent manner. To date, there is only limited literature on neuronal branching patterns and their functionality in the STG. There appears to be some cell-type-specific spatial organization, but no prominent segregation of synaptic inputs into different neuropil areas has been found (Bucher et al, 2007, Baldwin and Graubard, 1995, Christie et al., 1997, Wilensky et al., 2003). The close localization of PIIH and synaptotagmin labeling in the branches of the fine neuropil is a strong indication, that I_h can be involved in regulating synaptic events. The staining pattern for PIIH and synaptotagmin only rarely overlapped, suggesting that I_h is not strongly localized at the pre-synaptic terminal itself. However, nearby I_h channels could still affect transmitter release even if not exactly located at the terminal itself. Similarly, modulatory activation of postsynaptic I_h channels close to synaptic inputs could effectively shunt inhibitory and excitatory events. Since there are many reciprocal pyloric synapses with the interacting partners being pre-and postsynaptic at the same time (King, 1976), activation of I_h channels in close vicinity to the synapse could affect synaptic strength of both synapses simultaneously. This could result either in a reduction of both pre-and postsynaptic events through shunting, or in a strengthening in one direction through increased transmitter release by one of the mechanism described above, combined with a weakened synaptic strength in the other direction through postsynaptic shunting. Independent of the mechanism, the intense labeling of PIIH in the fine neuropil and near synaptic sites suggests a role in the regulation or integration of synaptic events. The relative paucity of double-labeling for PIIH and synaptotagmin, despite the large occurrence of synaptotagmin-labeled structures, suggests a primarily postsynaptic distribution of PIIH. I will further address the functional implications of this localization on synaptic strength in Chapter 5.

Pre-synaptically, it has been suggested that modulation of I_h increases transmitter release from the pre-synaptic cell (Kaupp, Seifert 2003, Yu et al 2004, Chevaleyre and Castillo, 2002, Beaumont and Zucker, 2002). At the Crustacean neuromuscular junction, serotonin-induced increase of cAMP can lead to I_h-dependent enhancement of synaptic strength by increasing transmitter release through its depolarizing effects {{122; }}. In inhibitory GABAergic interneurons of the dentate gyrus, I_h reduces the threshold for action potentials and increases the rate of vesicle release (Aponte et al., 2006). I_h channels might also play the role of a bifunctional protein and increase transmitter release in a depolarization-independent way: Traditionally, increased frequency of mEPSCs after raising the intracellular concentration of cAMP in cultured hippocampal neurons is attributed to a protein kinase A dependent increase of glutamate release (Nguyen PV, Woo NH. 2003). However, Genlain et al. described a mechanism in which I_h activation through cAMP depolarized the resting potential, but also lead to an increased rate of vesicle release in a depolarization-independent way in a low K^+ solution that compensated for changes of the membrane potential (Genlain et al., 2007). The underlying mechanism for this role of I_h could be Ca^+ entry through I_h channels, triggering Ca^+ release from stores in axonal terminals (Zhong et al., 2004; Yu et al., 2004). Alternatively, I_h channels could be directly coupled to the transmitter release and regulate intracellular signaling pathways, similar to the ether-a`-go-go (EAG) channel (Beaumont, Zucker, 2000; Hegle et al., 2006). Interestingly, presynaptic I_h can also attenuate NMDA-evoked transmitter release (Klar et al., 2003). Shunting effects of I_h activation through reduced input resistance after I_h activation could weaken synaptic transmission on either side of a synapse. A gradient of I_h channel density in hippocampal neurons appears to be involved in synaptic integration and normalization of synaptic input from different locations.

All these mechanism require a distinct spatial distribution of I_h channels, which made it particularly interesting to examine the distribution of PIIH protein in the STG within regions that do or do not contain synaptic sites. Essentially all the synaptic interactions in the STG occur at the level of the fine neuropil (King,

1976a,b; Cabirol-Pol et al., 2000, 2002), There is some evidence for very few synaptic contacts in the coarse neuropil, however, it is not well documented (Bucher et al., 2007, Eve Marder, personal communication). The fine neuropil partially surrounds the coarse neuropil and often forms concentrated areas of extensive fine branching on the dorsal and ventral surface below the ganglion sheath or even between the STG somata. (Bucher et al., 2007, King 1976). Anatomical studies include electron microscopic characterization of the neuropil and synaptic contacts (Maynard, 1971; King,1976a,b; Kilman and Marder, 1996), the cellular localization of ion channels and receptors (Mizrahi et al., 2001; French et al., 2002; Clark et al., 2004; French et al., 2004), and the spatial organization of the neuronal branching pattern, modulatory input and calcium influx (Wilensky et al., 2003, Graubard and Ross, 1985; Ross and Graubard, 1989; Kloppenburg et al., 2000, Baldwin and Graubard, 1995, Christie et al., 1997). The spike initiation zones are thought to be located in the posterior regions of the coarse neuropil, near where the axons leave the ganglion (Raper, 1979; Miller, 1980).

The homeostatic interaction of I_h and I_A described in Chapter 1 could in theory be mediated by their participation in multi-protein complex as has been described for other G-protein coupled receptor channels, like calcium dependent cation channels, NMDA receptors and Kir2 channels (Giamarchi et al., 2006, Delmas, 2005,). These complexes consist of one or more receptor/channel proteins, a protein scaffold in which the signaling molecules are localized and membrane-to-cytoskeleton interactions to stabilize the complex. Neuronal multi-protein complexes often use a PDZ-domain based protein scaffold. Interestingly, the amino acid sequences of the A-channel protein Shal and the H-channel protein PIIH, as well as the stomatogastric dopamine and serotonin receptors, contain one or several PDZ-binding motifs, as determined by a Eukaryotic Linear Motif resource search for functional protein interaction sites. If both Shal and PIIH channels interacted physically in a multi-protein complex, one would expect to find similar patterns of PIIH and Shal immunoreactivity with at least a reasonable

113

amount of co-localization of overlapping signals. However, the evidence in this study is not strong enough to rule out the possibility of co-localization of a smaller subset of channels, which would lead to some overlap and some differential staining.

Double labeling of PIIH and Shal in a single preparation revealed similarities and differences in their expression patterns. At a coarse level of detail, both proteins exhibited intense staining of the fine neuropil (Figure 4.17, Figure 4.20). At a fine level of detail, however, the distribution was different. In the cell body, intense Shal labeling occurred particularly in the membranes of the soma and primary neurites, and showed a high ratio of membrane bound versus cytosolic Shal protein. This caused the appearance of ring-like staining in cross-sections of the soma and parallel "highways" of intense labeling along primary neurites (Figure 4.16). There was less specific I_h immunoreactivity in the soma and little or none in the primary dendrite. The fine neuropil exhibited equally strong labeling of PIIH and Shal protein. However, at high magnifications, the sites of the most intense staining in the fine neuropil often showed Shal- and PIIH immunoreactivity adjacent to each other, but more rarely overlapping (Figure 4.18, Figure 4.19). Triple labeling in neurobiotin-injected neurons revealed that these adjacent stainings were likely on processes from different neurons. Frequently, I observed Shal labeling in fine branches of Neurobiotin-injected and identified neurons, while the areas of the strongest PIIH signal were often localized on small processes of adjacent, unidentified neurons or non-neuronal structures (Figure 4.20, Figure 4.21, Figure 4.22). Occasionally, PIIH was also on small, fingerlike endings of thin branches, or on bulbous varicosities within a thin process (Figure 4.9) found in identified neurons (PD, LP neurons).   The lack of overlap with Shal was surprising, given how well I_h upregulation appeared to maintain stable firing patterns in the presence of increased I_A (Chapter 1). This lack of membrane-bound PIIH labeling makes direct interactions of the channels in a multi-protein complex a less attractive hypothesis to explain the homeostatic response. It appears that this compensation can occur even though the proteins are physically separate, though

114

both are highly enriched in the synaptic neuropil. Overall, my experiments suggest that a significant fraction of I_h channels are expressed in the fine neuropil in close vicinity to synapses and may therefore be involved in the regulation of synaptic transmission. This is further explored with electrophysiological experiments in Chapter 5.

5 Activation of I_h channels Can Shunt Synaptic Transmission

The dendritic localization of I_h protein in pyloric neurons implied a possible role of I_h in the regulation of synaptic processing. To investigate if and how I_h could affect synaptic events, the graded glutamatergic LP-PD synapse was studied with and without block of I_h channels. LP-evoked IPSPs were recorded in the PD during injection of a range of hyperpolarizing steps in PD neurons that activated I_h to differing extents. The amplitudes of IPSPs were measured with and without I_h activation. For this purpose, I took advantage of the very slow activation rate of I_h channels. At the beginning of PD hyperpolarization, I_h channels have only just begun to open, so I_h is low. I compared IPSP amplitudes at this point to ones recorded after 8 sec of PD hyperpolarization, when I_h channels were maximally activated for each voltage step. Action potentials and transient potassium currents were blocked by application of 0.1 μM TTX, and 4 mM 4-AP. The PD and LP cells were each impaled with two electrodes to allow independent current injection and voltage recording in each cell. The Clampex computer software drove current injections to both cells. The PD membrane potential was changed by a series of current injecting steps of eight sec in 0.5-2 nA increments, with one step each minute to allow recovery of I_h between steps. If necessary, a bias current was injected into the PD cell to hold the resting potential at -58 mV. This is a relatively hyperpolarized potential compared to typical cycling PD neurons under control conditions with trough potentials between -50 and -55mV. However, it reflects the more hyperpolarized membrane potentials of PD neurons after blocker application and allowed me to include the majority of my initial recordings, when bias current injection was not applied. IPSPs were elicited by 200ms depolarizing current injections to -30 mV in the LP cell at the beginning (after 200 ms) or at the end (after 8sec) of the PD polarization (Figure 5.3). The LP cell was held at -58 to -

116

60mV between steps. Relatively high resistance (20 MΩ or higher) electrodes were used for current injection and voltage recording.

To avoid changes in V_{rev} of the IPSP as a consequence of loading the cell with Cl⁻ anions during the long hyperpolarizing steps, I used 0.6M KSO4 + 20mM KCl in the current or both electrodes. Complete elimination of chloride-induced drift and changes of the IPSP reversal potential could only be achieved by the use of 0.6M KSO4 + 20mM KCl in both electrodes, although noise from the higher resistance affected the quality of the recordings. Care was taken to adjust the bias current in the pre-synaptic LP cell to consistently elicit LP depolarizations from a resting potential of -58mV to a peak of -28 (± 2) mV. To let the PD cell recover from the long hyperpolarizing steps, and to avoid rapid synaptic plasticity, the time between individual current pulses was set to 60 seconds. The order of current injections into the PD cell (from more to less hyperpolarized potentials or vice versa) was kept constant for both protocols. Since I_h is the major low-voltage-activated current in pyloric neurons, the I_h independent components of the PD cell's input resistance should not change during hyperpolarized steps, as long as the cell was not damaged. The depolarizations were mostly below the range at which major outward and calcium currents are activated, and these only affected the measurements with the most depolarized current steps. Data sets in which the PD cell's input resistance changed noticeably in between steps were discarded.

Figure **5.2** and Figure 5.3 show typical recordings of IPSPs in the PD cell at the beginning and at the end of PD membrane polarizations, respectively. A direct comparison showed that the amplitude of the IPSPs was remarkably smaller at the end of the hyperpolarizing step, when I_h was fully activated, than at the beginning, when only a fraction of I_h channels was open (Figure 5.4, A and B). This effect could be significantly decreased by application of the I_h blockers ZD7288 and CsCl (Figure 5.7 and Figure 5.8). Finally, in order to separate the effects of current activation from changes in the driving force at different membrane potentials,

experimental data were compared with predictions based on the current-Goldman-Hodgkin-Katz (GHK) equation for single ionic species (Figure 5.13).

early IPSP − I_h only weakly activated   late IPSP − I_h activated
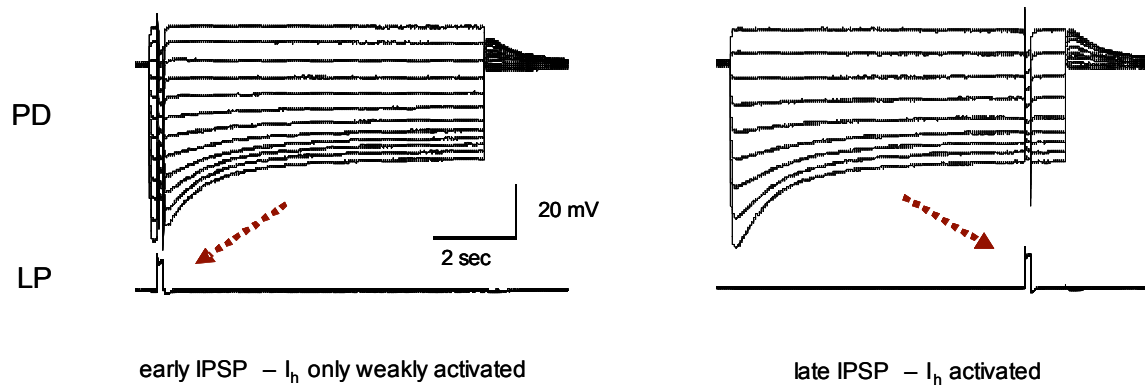
Figure 5.1 Protocol to elicit IPSPs from the LP to the PD neuron with and without activation of I_h.

5.1 Effects of I_h Activation under Control Conditions

I consistently found the amplitude of IPSPs at the same voltage at the end of PD hyperpolarization to be smaller than that at the end, but only when the neuron was hyperpolarized below -70 mV (

Figure 5.4, Figure 5.5). At low voltages, when I_h was maximally activated at the end of the current injection step and, I observed a large reduction in amplitude from the initial IPSP amplitude. For example, when the PD neuron was hyperpolarized to -115 mV at the beginning of the step, the IPSP amplitude was 14.5 ± 3.5 mV, while the IPSP amplitude when the PD was at -115 mV at the end of the step was only 5.5±0.5 mV (62% decrease; n=11, p< 0.01). On the other hand, measurements of IPSP amplitude at the beginning and end of long depolarizations or modest hyperpolarizations of the PD cell did not differ

118

significantly (Figure 5.5). Overall, the difference between IPSPs before and after activation of I_h was statistically significant at all PD membrane potentials of -80mV and below (Figure 5.5). The IPSP reversal potential measured from the soma was -72 ± 1.3 mV for the early IPSP and -75 ± 2.2 mV for the late IPSP, when I_h was maximally activated. Although small, this difference was statistically significant (p = 0.029). At the most depolarized membrane potentials between -40 and -30 mV, the IPSPs began to reduce in amplitude overall, most likely due to activation of voltage sensitive currents. In addition, the IPSPs at the beginning of the PD polarization tended to be smaller than at the end in this depolarized voltage range. This could be a consequence of slow inactivation of voltage dependent currents (including K^+ and Ca^{2+} channels) or even deactivation of resting I_h itself. The IPSP amplitudes at depolarized membrane potentials varied more between different experiments than at hyperpolarized potentials. Within an individual experiment, the difference between beginning and end IPSPs during depolarization was usually small (Figure 5.5A).
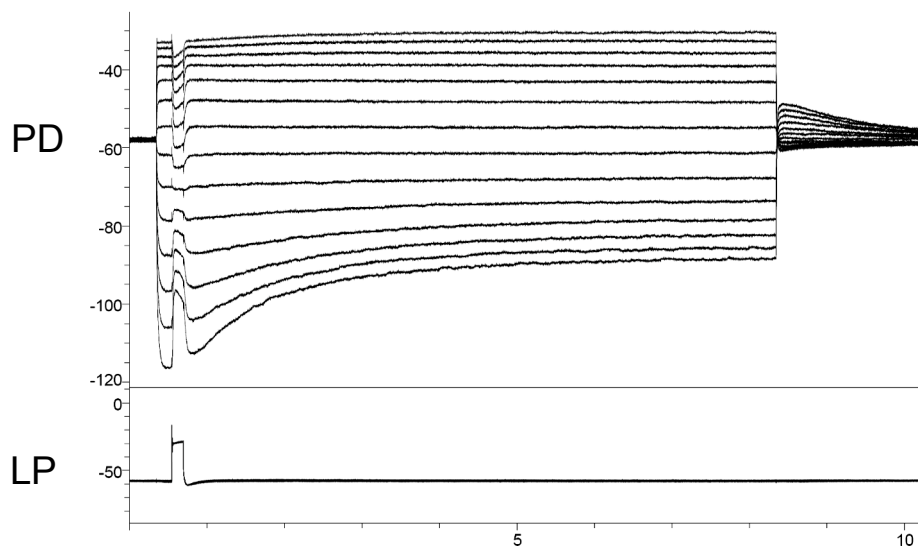
Figure 5.2 IPSPs in the PD cell at the beginning of the PD polarization, when Ih is not activated. The slow sag in the PD cell reflects the opening of Ih channels.

119
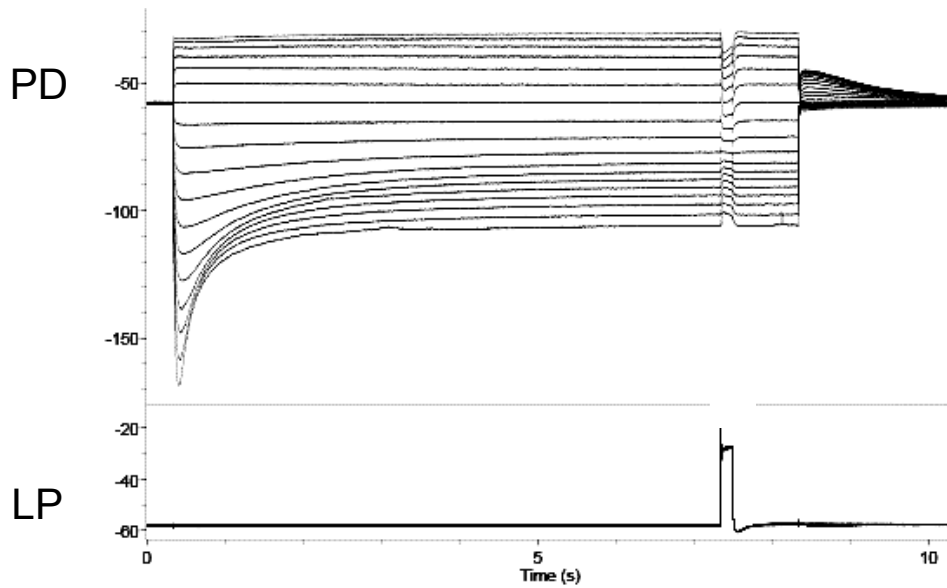
Figure 5.3 IPSPs in the PD cell at the end of PD polarization, when Ih is maximally activated. The slow sag reflects the opening of Ih channels in the PD cell. To compensate for the depolarizing effect of Ih, the PD cell had to be hyperpolarized much more to reach comparable potentials at the time of the IPSP than during the previous protocol.
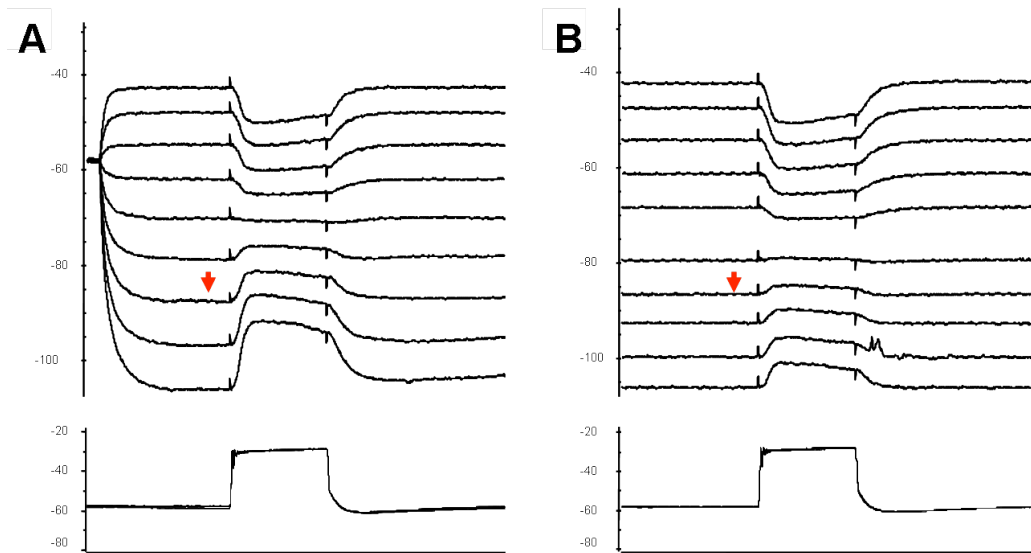
Figure 5.4 Comparison of IPSP amplitudes at A) beginning of polarization of the PD cell, when very little I_h has been activated and B) at the end of the PD polarization, when I_h is

maximally activated. The red arrows point to traces at equal membrane potential of the PD cell (-86mV).
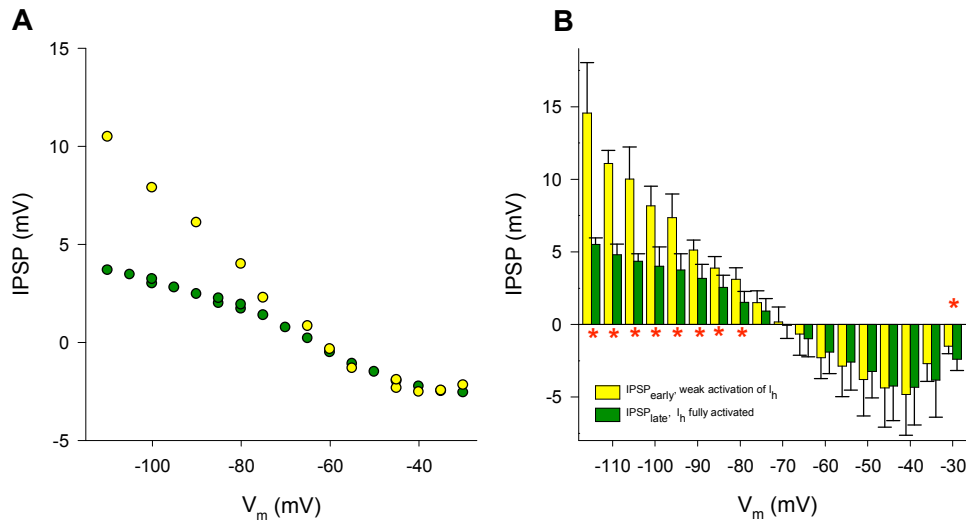
Figure 5.5 IPSP amplitude at different membrane potentials of the PD cell at the beginning (yellow) or at the end (green) of PD polarizing current injection. A. Data from one individual cell.   B. Data from 11 experiments. Stars indicate statistically significant differences (p<0.05).

5.2 IPSP Amplitude during Block of I_h Channels

If activation of I_h channels were shunting synaptic input, then I_h blockers should reduce or eliminate the difference between the IPSP amplitudes at the beginning and at the end of the PD current injection. Furthermore, if a fraction of I_h channels are open at resting potential, their blockade should change the resting potential and perhaps alter the IPSP amplitude at the beginning of the PD polarization. For these experiments, I_h was blocked by bath application of 100 μM ZD7288 or 5 mM CsCl for 20 minutes or longer (see Chapter 3 and Peck et al., 2006).

ZD7288 bath application had a tendency to hyperpolarize the resting potential of the cells by 3 ±2.3 mV, although the effect was not statistically significant with our small sample size (n =5, p = 0.09). This hyperpolarization is consistent with the block of an inward conductance and suggests that a small fraction of I_h channels is open at -58 mV. During I_h blockade by ZD7288, the IPSP reversal potential did not change significantly (Figure 5.6). Block of I_h dramatically changed the IPSP amplitudes in the PD neuron (Figure 5.7, Figure 5.8, Figure 5.9). In the presence of 100 μM ZD7288 (Figure 5.7) and 5mM CsCl (Figure 5.9) the IPSP elicited at the end of the PD polarization was significantly increased in amplitude at all membrane potentials below -80mV. There also appeared to be a trend to larger IPSP amplitudes at more depolarized potentials between -70mV and -45 mV, approaching significance at -60 and -65 mV ($p \leq 0.2$).

If the IPSP attenuation after long hyperpolarizing steps under control conditions was entirely due to activation of I_h, the difference between early and late IPSP amplitudes should be eliminated during I_h block. Indeed, after application of ZD7288, IPSPs at the beginning of the PD polarization were not significantly different from those at the end of the pulse (n=5; p>0.05, Figure 5.10). Only at extremely hyperpolarized membrane potentials of -100 mV and below were the IPSPs still attenuated at the end of the PD current injection.

To estimate whether some I_h was active at more depolarized membrane potentials and affected synaptic transmission within the normal voltage range for the PD neurons, IPSPs at the *beginning* of the PD polarization were compared under control conditions and after I_h block with 100 μM ZD7288. The effect of I_h blockade on the early IPSPs was an increase of IPSP amplitude at all membrane potentials, which was more noticeable (up to 2-fold) in the physiological range of -70 to -30mV. This increase was statistically significant during PD current injection to -30, -35, -65, -85 and -110mV (n=5; p<0.05) and approaching significance at -50, -60 and -70 mV (n=5; p≤0.2; Figure 5.11). These data indicate that either a fraction of I_h channels is open at physiological membrane potentials, or that ZD 7288 affects the IPSP amplitude in an unknown, I_h-independent way. This can be tested by comparing ZD7288's actions with another I_h blocker.

Contrary to expectation, application of 5 mM CsCl led to a slight depolarization of the PD resting potential, that was not statistically significant, and the IPSP reversal potential was not reliably changed. However, consistent with a model of I_h blockage, CsCl also caused a significant increase of IPSP amplitudes after long PD hyperpolarizations from -70 to below -110 mV. This effect could be partially reversed after 30-45 minutes of wash (Figure 5.12). CsCl had no significant effect on the IPSP amplitude at more depolarized PD potentials.
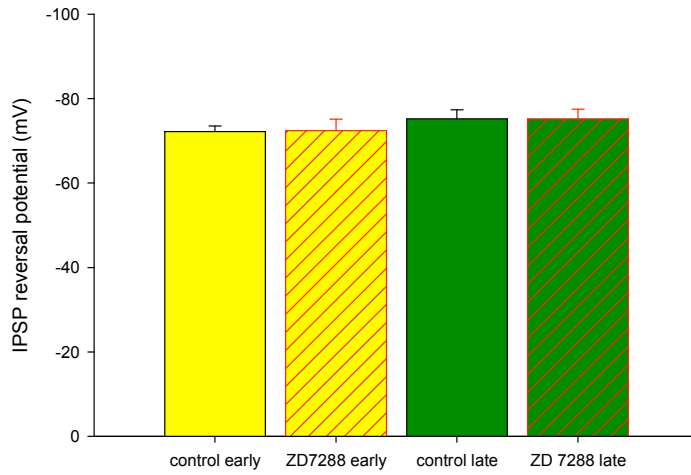
Figure 5.6 Reversal Potential of IPSP at beginning (yellow) and end (green) of PD polarization under control conditions and during I_h block with 100 μM ZD7288 (red diagonal pattern).
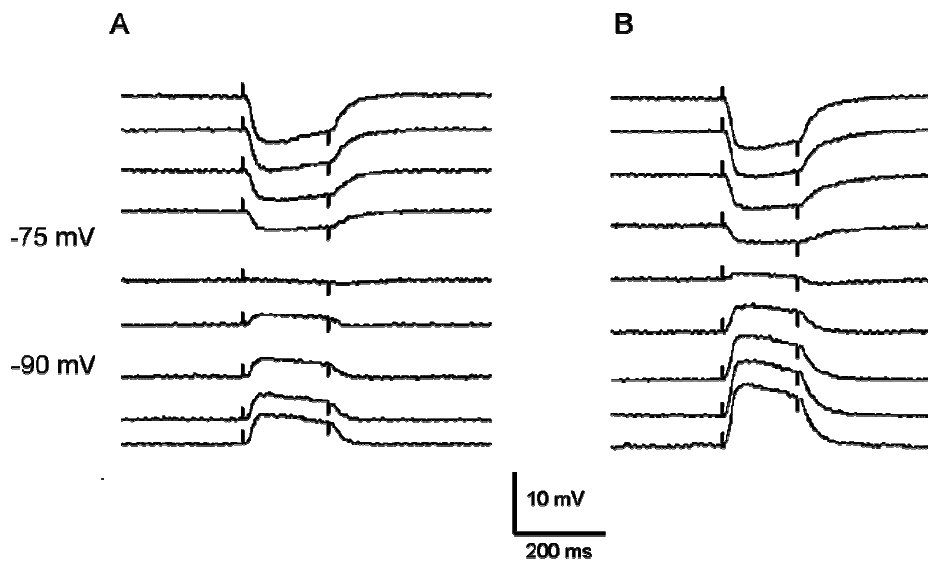
Figure 5.7 IPSP amplitude (A.) at the end of PD polarization under control conditions and (B.) in presence of the I_h blocker ZD7288 (B).
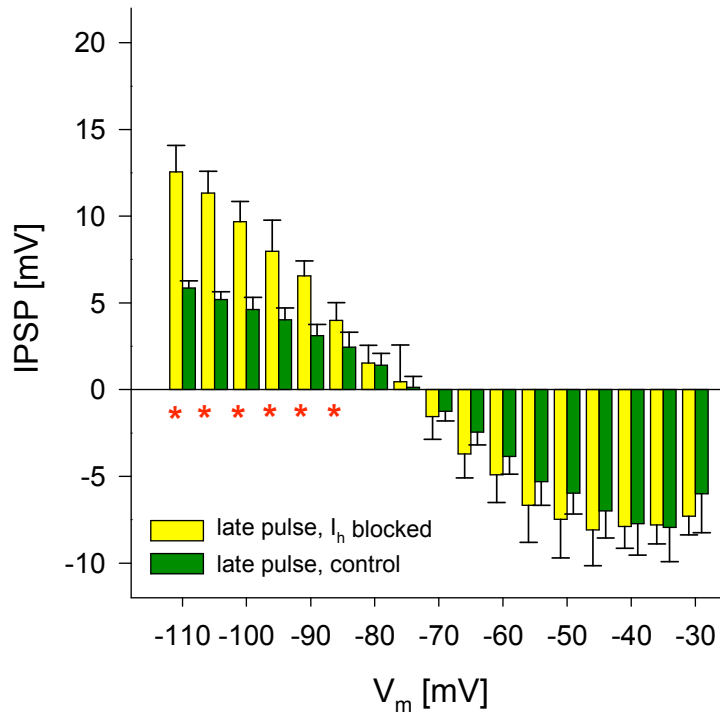
Figure 5.8 Effect of I_h block through ZD7288 on IPSP amplitude in the PD cell. IPSPs were elicited at the end of the PD current injection under control conditions (green) and during I_h blockade (yellow). Stars indicate statistically significant differences ($p < 0.05$) N=5
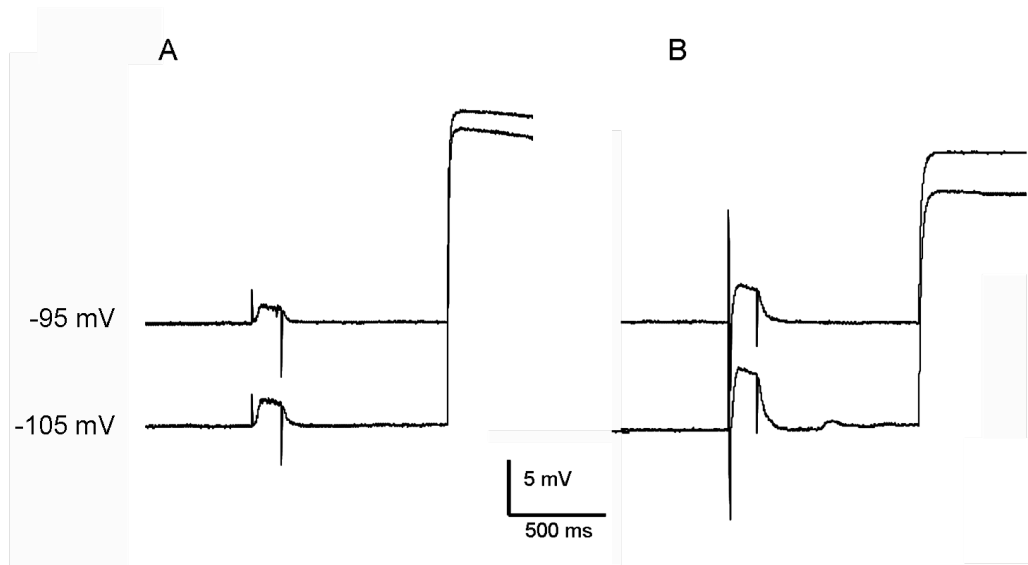
Figure 5.9 IPSP amplitude at the end of PD polarization under control conditions (A) and in presence of I_h blocker CsCl (B).
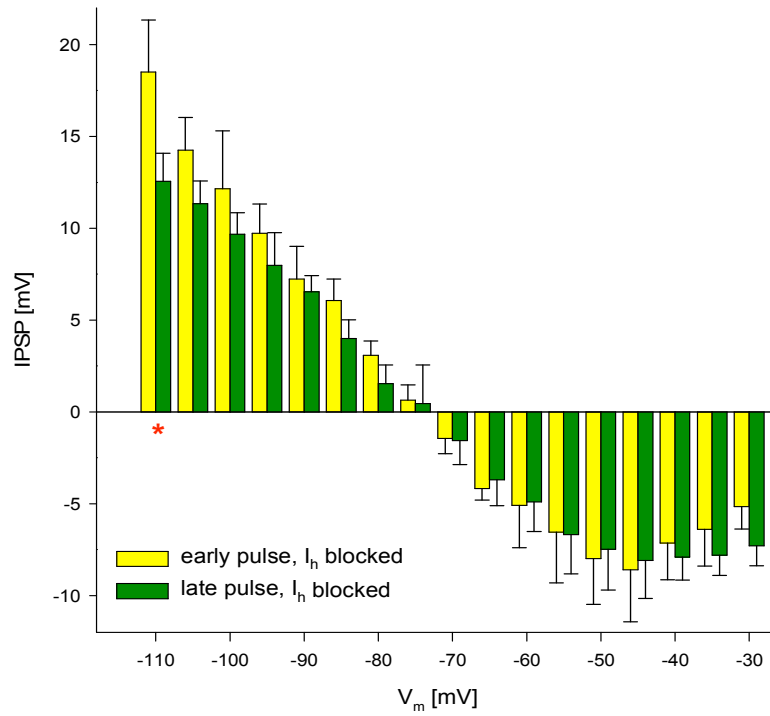
Figure 5.10 Almost no difference between IPSP amplitudes at the beginning (yellow) and at the end (green) of PD cell polarization during block of I_h (100µM ZD7288). Stars indicate statistically significant differences ($p<0.05$); N=5
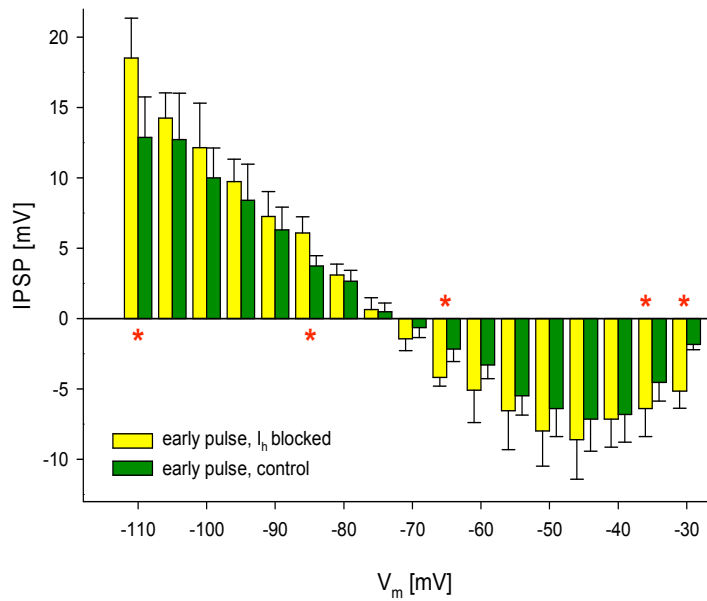
Figure 5.11 I_h blockade caused an overall increase of IPSP amplitudes at beginning of polarizing current injection, when only a small fraction of I_h channels is open. Green bars represent early IPSPs under control condition, yellow bars represent early IPSPs during I_h block by (100 µM ZD7288). Stars indicate statistically significant differences ($p < 0.05$).
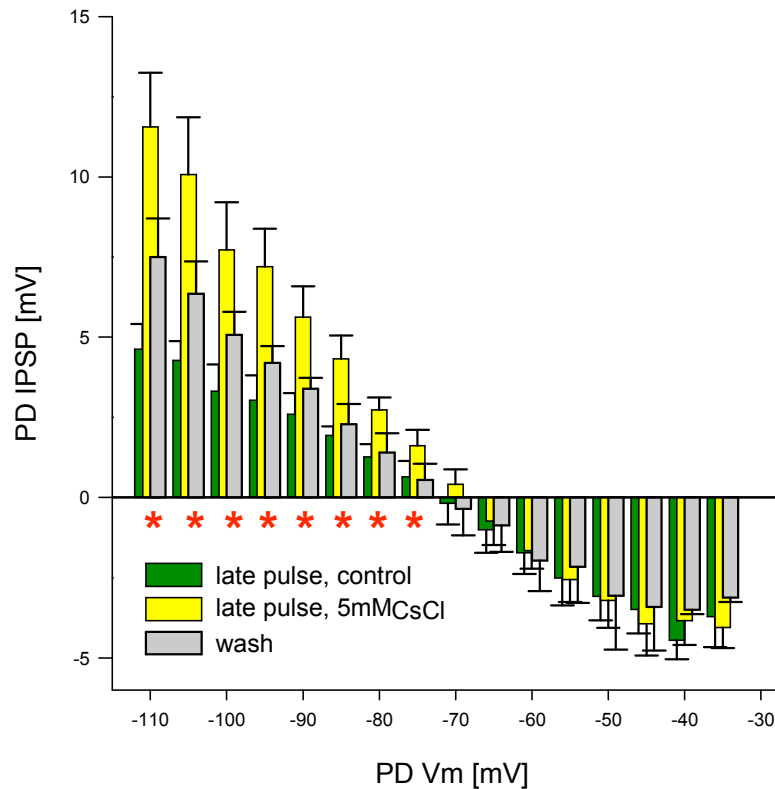
Figure 5.12 I_h block through 5mM CsCl on IPSP amplitude in the PD cell. IPSPs were elicited at the end of the PD current injection under control conditions (green) and during I_h blockade (yellow). Effect was partially reversible through washout (grey). Stars indicate statistically significant differences between control and CsCl data ($p<0.05$).

5.3 Comparison with calculated expectations of IPSP amplitudes

The Goldman Hodgkin Katz equation was used to predict IPSP amplitudes in the absence of I_h activation (see methods for details). The ratio of IPSPs at different membrane potentials can be calculated in a simplified model that takes into account the internal and external chloride and potassium activities and reflects the

changing driving force for the IPSP at different membrane potentials. The experimentally derived IPSP amplitude at -90 mV in the presence of 5mM CsCl was chosen as reference, in order to calculate expected IPSP amplitudes at different membrane potentials. I_h is blocked under these conditions and most likely no other voltage dependent channels are active. Figure 5.13 shows that the experimental IPSP values in the absence of I_h channel activation match the driving-force dependent, predicted changes very well under control conditions (Figure 5.13A) and in the presence of CsCl (Figure 5.13B). However, in the presence of ZD7288, the experimental data at depolarized PD membrane potentials is different from the model data, indicating non-specific effects of this blocker on other currents in addition to I_h (Figure 5.13C).
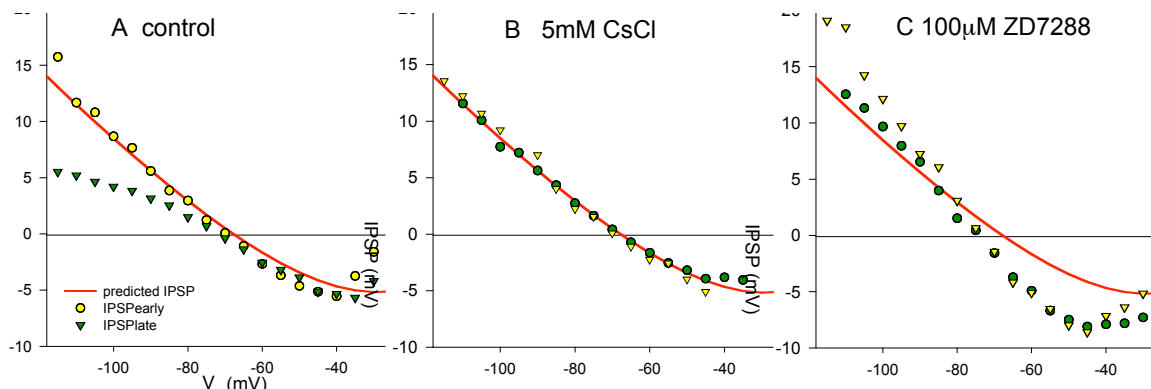
Figure 5.13 Comparison of IPSP amplitudes at different membrane potentials with predicted IPSP amplitudes (red) based on changes in driving force at different membrane potentials. Symbols: mean IPSP at end of PD current injection (control: N=11, CsCl: N=6; ZD7288: N=5);

130

Discussion

In the STG, pyloric constrictor neurons (LP, PYs, IC) and the AB interneuron use glutamate as neurotransmitter for graded inhibition while the dilator neurons (PDs, VD) use acteylcholine. Descending excitation onto the PD and VD neurons might be mediated in part by excitatory glutamate receptors (Ayali, Harris-Warrick 1998, Johnson, Harris-Warrick 1997, Marder, Eisen 1984, Marder, Paupardin-Tritsch 1978). Previous work showed that glutamatergic responses could be elicited in all pyloric neurons by puffing glutamate onto the soma or over the neuropil. Inhibitory acetycholine responses in the VD and PD could only be evoked by acetylcholine injection into the neuropil (Marder, Eisen 1984) or not at all (Johnson, Harris-Warrick 1997). At the LP to PD synapse, depolarization of the LP neuron evokes glutamate release, which leads to the opening of postsynaptic glutamate receptor (GluR or GluCl) chloride channels. A small fraction of the current (21%) appears to be carried by potassium. The reversal potential in isolated cultured neurons was between -50 and -70mV, and 50% external [Cl] reduction shifted the reversal potential by +10-14 mV, versus a calculated shift of +16 mV for a pure chloride electrode. The difference could be due to activity/concentration nonlinearity or other permeability (Cleland, Selverston 1998, Marder, Eisen 1984). It is likely that the shunting effect of Cl currents is a more meaningful effect than the polarizing effect. $[Cl]_i$ likely fluctuates with some lag behind the oscillating membrane potential in the peri-membrane region (Cleland, personal communication).

Although they are found at all locations in pyloric neurons, I_h channels in the STG are concentrated distally from the soma in the fine neuropil of the ganglion (Chapter 4), the site of synaptic contacts and integration. Previous studies in other systems show that I_h channels may be directly linked to the transmitter release machinery (Beaumont, Zucker, 2000; Genlain et al., 2007), but can also affect synaptic transmission indirectly by altering the membrane resistance and therefore affecting the strength of the pre-or postsynaptic signal. These effects can be modulated by changes of the intracellular cAMP concentration, where elevated

cAMP levels enhance I_h by shifting its voltage dependence of activation in the depolarizing direction (Genlain, Godaux and Ris 2007, Ouyang et al, 2007; Peck et al 2006; Johnson et al., 1995). I studied the effects of I_h activation on the size of inhibitory input at the graded glutamatergic LP to PD synapse. I found that activation of I_h decreased the amplitude of synaptic potentials, and pharmacological block of I_h dramatically increased IPSP amplitudes. This result was somewhat surprising, as I_h is best known for its indirect effects on postsynaptical integration. In the hippocampus, postsynaptic I_h potentially shapes temporal summation by spatially normalizing synaptic events from different input locations. (Lupica et al. 2001; Maccaferrie et al. 1993; Magee 1998, 1999; McCormick and Pape 1990). Non-uniform distribution of post-synaptic I_h channels changes the amplitude and kinetics of synaptic events by its influence on the membrane resistance, and therefore on the length constant in both hippocampal and neocortical pyramidal neurons (Magee, 1998, 1999; Williams and Stuart, 2000; Berger et al. 2001). In dendrites of pyramidal CA1 cells in the hippocampus, the density of I_h channels increases dramatically towards more distal regions. Presumably, this gradient of channel expression can normalize for different locations of synaptic input and regulate spatial and temporal summation (Magee, 1988; 1999). Migliore et al. showed that I_h could selectively block temporal summation of unsynchronized input in these cells (Migliore et al., 2004). However, it appears that this spatial normalization depends on the sign of the synaptic input. I_h normalizes EPSPs, so that distant and close synaptic events cause EPSPs of similar amplitude at the soma. However, normalization of inhibitory potentials could not been found. A possible function of the sign-selectivity was proposed by Heckmann et al., based on the hypothetical role of synaptic input in rhythmic networks. Especially in motor systems, excitatory inputs are considered to be important for integration at the spike initiation zone close to the soma, while IPSPs are important for very localized effects through membrane polarization or shunting, and are not required to travel far through the dendritic tree (Heckmann, 2005).

132

However, there is also evidence for I_h channels decreasing synaptic transmitter release in the rat neocortex (Klar et al, 2003). I_h is also known for increasing synaptic transmission by depolarizing the pre-synaptic terminal, activating calcium currents and increasing the frequency of vesicle release as well as increasing facilitation (Genlain et al, 2007; Beaumont and Zucker, 2000; Boyes et al., 2007; Siegelbaum and Robinson, 1990).

The somatic IPSP amplitude depends on the amount of presynaptic transmitter release and postsynaptic properties. These are determined in part by plasticity at the receptor level, the postsynaptic input resistance and the membrane potential (driving force). I chose the experimental conditions to reveal changes of IPSP amplitude that were only caused by the activation of I_h channels. To estimate the effect of I_h on synaptic transmission, the amplitudes of IPSPs were recorded during injection of a range of hyperpolarizing steps in PD neurons that activated I_h to differing extents. IPSP amplitudes at the beginning of the polarizing step, when I_h was only weakly activated, were compared to IPSP amplitude at the end of the PD hyperpolarization, when I_h was maximally activated. In order to measure IPSP amplitudes independent of the driving force, IPSP amplitudes were compared at equal soma potentials. I found that activation of of I_h dramatically decreased the size of synaptic inputs I recorded from the soma (Figure 5.4, Figure 5.5). This effect could be significantly abolished by application of the I_h blockers ZD7288 and CsCl (Figure 5.8, Figure 5.12). These data indicate that an increase in I_h conductance reduces the synaptic amplitude. The simplest interpretation is that this occurs at the post-synaptic neuron, either by reducing the local input resistance at the postsynaptic sites, or by contributing to the overall input resistance of the cell. Given that I_h protein is primarily located in the fine neuropil, and that the somatic input resistance during I_h blockade changes only marginally, the first explanation seems more likely. With more I_h channels open, the neuropil or parts of it become leakier, and synaptic transmission and integration would be dramatically reduced through shunting of IPSPs. The effects were only seen at hyperpolarized membrane potentials of -80 mV and below, reflecting the fact that

the pyloric I_h current is a relatively small current with very hyperpolarized voltage dependence of activation. Data from two-electrode voltage-clamp experiments show $V_{1/2\ max}$ at -79 mV (Chapter 3). It could be argued that this might prevent I_h from shaping synaptic strength during pyloric activity where the typical trough of the PD neuron is at -55 mV. However, activation kinetics are significantly affected by cAMP binding, which can be changed by neuromodulatory inputs. For example, in the AB cell, dopamine can shift the activation curve of I_h by 10 to 15 mV in the depolarizing direction (Peck et al, 2006). Thus, modulation of the voltage dependence of I_h could potentially be a very powerful way to regulate synaptic strength in a cell specific manner (Johnson et al, 87; Johnson et al., 1995; Peck et al., 2006). Furthermore, the membrane potential in distal parts of the neuron might be more hyperpolarized than the soma, which would enhance the activation of I_h and thus its role in regulating synaptic strength.

The IPSP reversal potential measured from the soma was -72 ± 1.3 mV for the early IPSP, and -75 ± 2.2 mV for the late IPSP, when I_h was maximally activated (Figure 5.6). Although small, this difference was statistically significant (p = 0.029). It could be explained by a small leak of charged ions from the electrode into the cell during the long step. I_h block by ZD7288 resulted in a subtle hyperpolarization by 3 ±2.3 mV, although the effect was not statistically significant with our small sample size. This hyperpolarization is consistent with the block of an inward conductance and also suggests that a small fraction of I_h channels was open at resting potential. The effect may have been more obvious under the experimental conditions used in this study, where the PD neuron was held at a relatively hyperpolarized membrane potential of -58mV, compared to -50 to -55.mV during ongoing pyloric activity in a cycling preparation.

The difference of IPSP amplitudes at the beginning and at the end of the hyperpolarizing PD steps were almost entirely eliminated during pharmacological block of I_h (Figure 5.10), suggesting that activation of I_h alone is responsible for the shunting of synaptic input at these voltages. Only at extremely hyperpolarized membrane potentials of -100 mV and below were IPSPs still attenuated at the end

of the PD current injection. This indicates that the block by 100 μM ZD7288 or 5mM CsCl is incomplete. Supporting the idea of an incomplete block, I observed small residual sag potentials at very hyperpolarized potentials (data not shown). These results could also be explained by the presence of a low-threshold, non-I_h component, like a hyperpolarization-activated chloride conductance. In addition to the pronounced effects of I_h activation at hyperpolarized membrane potentials, I often observed a smaller change in IPSP amplitude at the beginning and at the end of depolarizing steps, and a slight reduction of IPSP amplitudes elicited at the beginning of some PD depolarizations relative to the end of the step (Figure 5.5). This effect was statistically significant only at -30 mV and might have been due to voltage-dependent inactivation of K and Ca currents, since only TTX-sensitive sodium currents and transient potassium currents were blocked; alternatively, it could reflect the closing of I_h channels that are open at rest (see below). Early IPSPs were elicited 200ms after start of PD current injection, at which time a fraction of depolarization-activated channels is not yet completely inactivated completely, shunting and reducing the IPSP amplitude compared with IPSPs after 8 sec of depolarization when these channels have inactivated. This mechanism would explain the difference between the early and late IPSPs at depolarized PD membrane potentials of -40mV and -35mV. Smaller IPSP amplitudes at the beginning of the PD depolarization could also be explained by the presence of a hyperpolarization-activated background conductance like I_h, which slowly deactivates upon depolarization. Similar to the inactivation of I_{CA}, the even slower deactivation kinetics of I_h, with τ in the range of several seconds could explain the difference between early and late IPSP amplitudes.

To estimate whether some I_h was is active at more depolarized membrane potentials and thus could synaptic transmission within the normal voltage range for the PD neurons, IPSPs at the beginning of the PD polarization were compared under control conditions and after I_h block with 100 μM ZD7288. Consistent with the presence of a background activation of I_h, I observed an increase of IPSP

amplitude at all membrane potentials, which was more noticeable (up to 2-fold) in the physiological range of -70 to -30mV (Figure 5.11). These data indicate that either a fraction of I_h channels are open at physiological membrane potentials, or that ZD 7288 affects the IPSP amplitude in an I_h-independent way, for example by blocking other depolarization-activated ion channels. Although ZD7288 is generally considered a very specific blocker for I_h in vertebrates, it has recently been shown to have unspecific effects on synaptic transmission (Gonzalez-Iglesias, 2006). Therefore, the experiments were repeated with low concentrations of CsCl, a specific blocker of I_h in the STG. The results confirmed the observed trends under ZD7288 block (Figure 5.12). Block with 5 mM CsCl also showed a small increase of the early IPSPs at depolarized potentials, consistent with an inward current that is active at physiological relevant resting potential, but the effect was not statistically significant (data not shown). Since calcium currents could not be blocked in these experiments, the significance of I_h at these membrane potentials needs to be further tested. These data show, however, that at hyperpolarized membrane potentials, activation of I_h can effectively shunt synaptic input. The data of I_h block by CsCl suggests that most of the effects on IPSP amplitude by ZD7288 were in fact due to block of I_h.

Lastly, I compared the experimental data with a model based on properties of the GluR receptor and passive cable analysis. A prediction of the absolute IPSP size is not possible, as it depends on unknown variables like the number and single channel conductance of the GluR receptors at the postsynaptic site, the membrane conductance g_m in the intervening membrane between the synapse and the somatic recording site, and the cell geometry. However, for a simplified cable model, it is possible to predict the ratio of IPSP amplitudes recorded in the soma at different membrane potentials, based on the driving force for chloride through synaptic GluR receptors, and using an experimentally derived value for an IPSP in the absence of I_h activation as a starting value. Comparison of data derived from this model with experimental data helps to distinguish between driving-force-dependent changes of the IPSP amplitudes and those arising from

136

hyperpolarization-activated I_h (Figure 5.14). The model shows that in the absence of I_h, changes in IPSP amplitude could be perfectly described by the cable model (Figure 5.14). It is thus more clear that activation of I_h shunts the IPSP dramatically (Figure 5.14 A).

Thus, enhancement of I_h can significantly reduce the effects of synaptic inputs in the pyloric network by effectively shunting them. While this study only examined the effects of I_h activation on graded synaptic inhibition, it is likely that the same mechanisms contribute to the regulation of excitatory synaptic inputs as well. My results show that I_h plays a major role in shunting IPSPs only when it is activated, which under non-modulated conditions is at non-physiological hyperpolarized voltages. However, the voltage dependence of I_h can be modulated, for example by modulatory control of cAMP levels, and the voltage dependence of I_h is significantly affected in some pyloric neurons by dopamine (Peck et al 2006). This modulation provides a potentially important and powerful mechanism in the STG to regulate the strength of synaptic input that could modulate the rhythmic activity of the entire circuit in a context dependent manner.

Bibliography

An WF, Bowlby MR, Betty M, Cao J, Ling HP, Mendoza G, Hinson JW, Mattsson KI, Strassle BW, Trimmer JS, Rhodes KJ., 2000, "Modulation of A-type potassium channels by a family of calcium sensors.", *Nature*; 403(6769):553-6.

Angstadt JD, Calabrese RL., 1989, "A hyperpolarization-activated inward current in heart interneurons of the medicinal leech.", *J Neurosci.* (8):2846-57.

Ayali, A. and Harris-Warrick, R.M. 1999, "Monoamine control of the pacemaker kernel and cycle frequency in the lobster pyloric network", *The Journal of neuroscience: the official journal of the Society for Neuroscience,* vol. 19, no. 15, pp. 6712-6722.

Ayali, A. and Harris-Warrick, R.M. 1998, "Interaction of dopamine and cardiac sac modulatory inputs on the pyloric network in the lobster stomatogastric ganglion", *Brain research,* vol. 794, no. 1, pp. 155-161.

Ayali, A., Johnson, B.R. and Harris-Warrick, R.M. 1998, "Dopamine modulates graded and spike-evoked synaptic inhibition independently at single synapses in pyloric network of lobster", *Journal of neurophysiology,* vol. 79, no. 4, pp. 2063-2069.

Baro DJ, Cole CL, and Harris-Warrick RM., 1996a, "RT-PCR analysis of shaker, shab, shaw, and shal gene expression in single neurons and glial cells." *Receptors Channels* 4: 149–159,

Baro DJ, Coniglio LM, Cole CL, Rodriguez HE, Lubell JK, Kim MT, and Harris-Warrick RM., 1996b, "Lobster shal: comparison with Drosophila shal and native potassium currents in identified neurons". *J Neurosci* 16: 1689–1701.

Baro DJ, Levini RM, Kim MT, Willms AR, Lanning CC, Rodriguez HE, and Harris-Warrick RM., 1997, "Quantitative single-cell-reverse transcription-PCR demonstrates that A-current magnitude varies as a linear function of shal gene expression in identified stomatogastric neurons." *J Neurosci* 17: 6597–6610.

Baro, D.J., Ayali, A., French, L., Scholz, N.L., Labenia, J., Lanning, C.C., Graubard, K. and Harris-Warrick, R.M. 2000, "Molecular underpinnings of

motor pattern generation: differential targeting of shal and shaker in the pyloric motor system", *The Journal of neuroscience : the official journal of the Society for Neuroscience,* vol. 20, no. 17, pp. 6619-6630.

Baro DJ and Harris-Warrick RM., 1998, "Differential expression and targeting of K-channel genes in the lobster pyloric central pattern generator." *Ann NY Acad Sci* 860: 281–295.

Baruscotti, M. and Difrancesco, D. 2004, "Pacemaker channels", *Annals of the New York Academy of Sciences,* vol. 1015, pp. 111-121.

Beaumont, V. and Zucker, R.S. 2000, "Enhancement of synaptic transmission by cyclic AMP modulation of presynaptic Ih channels", *Nature neuroscience,* vol. 3, no. 2, pp. 133-141.

Beenhakker MP, Nusbaum MP., 2004, "Mechanosensory activation of a motor circuit by coactivation of two projection neurons." *J Neurosci.*;24(30):6741-50

Beenhakker MP, Blitz DM, Nusbaum MP., 2005, "Long-lasting activation of rhythmic neuronal activity by a novel mechanosensory system in the crustacean stomatogastric nervous system." *J Neurophysiol*;91(1):78-91.

Beenhakker MP, DeLong ND, Saideman SR, Nadim F, Nusbaum MP., 2005, "Proprioceptor regulation of motor circuit activity by presynaptic inhibition of a modulatory projection neuron." *J Neurosci.*;25(38):8794-806.

Berger T, Senn W, Lüscher HR., 2003, "Hyperpolarization-activated current Ih disconnects somatic and dendritic spike initiation zones in layer V pyramidal neurons.", *J Neurophysiol.*, 90(4):2428-37.

Blitz DM, Beenhakker MP, Nusbaum MP., 2004, "Different sensory systems share projection neurons but elicit distinct motor patterns.", *J Neurosci.*24(50):11381-90.

Beurrier C, Bioulac B, Hammond C., "Slowly inactivating sodium current (I(NaP)) underlies single-spike activity in rat subthalamic neurons. ", J Neurophysiol. 2000 Apr;83(4):1951-7.

Büschges A, Manira AE. "Sensory pathways and their modulation in the control of locomotion." *Curr Opin Neurobiol.* 1998 Dec;8(6):733-9. Review

Butt, S.J., Harris-Warrick, R.M. and Kiehn, O. 2002, "Firing properties of identified interneuron populations in the mammalian hindlimb central pattern generator", *The Journal of neuroscience : the official journal of the Society for Neuroscience,* vol. 22, no. 22, pp. 9961-9971.

Chen, C. 2004, "ZD7288 inhibits postsynaptic glutamate receptor-mediated responses at hippocampal perforant path-granule cell synapses", *The European journal of neuroscience,* vol. 19, no. 3, pp. 643-649.

Chevaleyre, V. and Castillo, P.E. 2002, "Assessing the role of Ih channels in synaptic transmission and mossy fiber LTP", *Proceedings of the National Academy of Sciences of the United States of America,* vol. 99, no. 14, pp. 9538-9543.

Chevallier, S., Nagy, F. and Cabelguen, J.M. 2006, "Cholinergic control of excitability of spinal motoneurones in the salamander", *The Journal of physiology,* vol. 570, no. Pt 3, pp. 525-540.

Clarac F, Cattaert D. "Invertebrate presynaptic inhibition and motor control." *Exp Brain Research* 1996 Nov;112(2):163-80. Review

Clarac F, Cattaert D, Le Ray D. "Central control components of a 'simple' stretch reflex." *Trends Neurosciene.* 2000 May;23(5):199-208. Review

Cleland, T.A. and Selverston, A.I. 1998, "Inhibitory glutamate receptor channels in cultured lobster stomatogastric neurons", *Journal of neurophysiology,* vol. 79, no. 6, pp. 3189-3196.

Clemens, S., Massabuau, J.C., Legeay, A., Meyrand, P. and Simmers, J. 1998, "In vivo modulation of interacting central pattern generators in lobster stomatogastric ganglion: influence of feeding and partial pressure of oxygen", *The Journal of neuroscience : the official journal of the Society for Neuroscience,* vol. 18, no. 7, pp. 2788-2799.

Decher N, Bundis F, Vajna R, Steinmeyer K., 2003, "KCNE2 modulates current amplitudes and activation kinetics of HCN4: influence of KCNE family members on HCN4 currents.", *Pflugers Arch.*; 446(6):633-40.

Delcomyn F. "Neural basis of rhythmic behavior in animals.", *Science*, 1980 Oct 31;210(4469):492-8.

Dickinson, P.S. 2006, "Neuromodulation of central pattern generators in invertebrates and vertebrates", *Current opinion in neurobiology,* vol. 16, no. 6, pp. 604-614.

DiFrancesco, D. 2006, "Funny channels in the control of cardiac rhythm and mode of action of selective blockers", *Pharmacological research : the official journal of the Italian Pharmacological Society,* vol. 53, no. 5, pp. 399-406.

140

DiFrancesco, D. 1986, "Characterization of single pacemaker channels in cardiac sino-atrial node cells", *Nature,* vol. 324, no. 6096, pp. 470-473.

DiFrancesco, D. and Ojeda, C. 1980, "Properties of the current if in the sino-atrial node of the rabbit compared with those of the current iK, in Purkinje fibres", *The Journal of physiology,* vol. 308, pp. 353-367.

Duysens J. "Human gait as a step in evolution." *Brain.* 2002 Dec;125(Pt 12):2589-90.

Eisen, J.S. and Marder, E. 1982, "Mechanisms underlying pattern generation in lobster stomatogastric ganglion as determined by selective inactivation of identified neurons. III. Synaptic connections of electrically coupled pyloric neurons", *Journal of neurophysiology,* vol. 48, no. 6, pp. 1392-1415.

Flamm RE and Harris-Warrick RM., 1986a, "Aminergic modulation in lobster stomatogastric ganglion. I. Effects on motor pattern and activity of neurons within the pyloric circuit. J Neurophysiol 55: 847–865.

Flamm RE and Harris-Warrick RM., 1986b, "Aminergic modulation in lobster stomatogastric ganglion. II. Target neurons of dopamine, octopamine, and serotonin within the pyloric circuit.", *J Neurophysiol* 55: 866–881.

Freel RW., 1978, "Osmotic Regulation in Animals." Science., 202(4374):1276.

French, L.B., Lanning, C.C. and Harris-Warrick, R.M. 2002, "The localization of two voltage-gated calcium channels in the pyloric network of the lobster stomatogastric ganglion", *Neuroscience,* vol. 112, no. 1, pp. 217-232.

Genlain, M., Godaux, E. and Ris, L. 2007, "Involvement of hyperpolarization-activated cation channels in synaptic modulation", *Neuroreport,* vol. 18, no. 12, pp. 1231-1235.

Gill, C.H., Brown, J.T., Shivji, N., Lappin, S.C., Farmer, C., Randall, A., McNaughton, N.C., Cobb, S.R. and Davies, C.H. 2006, "Inhibition of Ih reduces epileptiform activity in rodent hippocampal slices", *Synapse (New York, N.Y.),* vol. 59, no. 5, pp. 308-316.

Goldman MS, Golowasch J, Marder E, Abbott LF., 2001, "Global structure, robustness, and modulation of neuronal models.", *J Neurosci.*;21(14):5229-38.

Golowasch J, Buchholtz F, Epstein IR, and Marder E., 1992, "Contribution of individual ionic currents to activity of a model stomatogastric ganglion neuron.", *J Neurophysiol* 67: 341–349.

Golowasch J and Marder E., 1992, "Ionic currents of the lateral pyloric neuron of the stomatogastric ganglion of the crab." *J Neurophysiol* 67: 318–331.

Graubard K and Hartline DK., 1991, "Voltage clamp analysis of intact stomatogastric neurons" *Brain Res* 557: 241–254.

Gruhn, M., Guckenheimer, J., Land, B. and Harris-Warrick, R.M. 2005, "Dopamine modulation of two delayed rectifier potassium currents in a small neural network", *Journal of neurophysiology,* vol. 94, no. 4, pp. 2888-2900.

Hashemzadeh-Gargari and Freschi, 1992

Hartline DK, 1979, "Pattern generation in the lobster (Panulirus) stomatogastric ganglion. II. Pyloric network simulation", *Biol Cybern* 33: 223–236.

Hartline DK and Graubard K, 1992, "Cellular and synaptic properties in the stomatogastric nervous system*.", Dynamic Biological Networks: The Stomatogastric Nervous System*, edited by Harris-Warrick RM, Marder E, Selverston AI, and Moulins M. Cambridge, MA: MIT Press, p. 1–30.

Harris-Warrick, R.M. 2002, "Voltage-sensitive ion channels in rhythmic motor systems", *Current opinion in neurobiology,* vol. 12, no. 6, pp. 646-651.

Harris-Warrick, R.M. 1993, "Pattern generation", *Current opinion in neurobiology,* vol. 3, no. 6, pp. 982-988.

Harris-Warrick, R.M., Coniglio, L.M., Levini, R.M., Gueron, S. and Guckenheimer, J. 1995a, "Dopamine modulation of two subthreshold currents produces phase shifts in activity of an identified motoneuron", *Journal of neurophysiology,* vol. 74, no. 4, pp. 1404-1420.

Harris-Warrick RM., 2002, Voltage-sensitive ion channels in rhythmic motor systems.", *Curr Opin Neurobiol* 12: 646–651.

Harris-Warrick RM, Coniglio LM, Barazangi N, Guckenheimer J, and Gueron S., 1995, "Dopamine modulation of transient potassium current evokes phase shifts in a central pattern generator network." *J Neurosci* 15: 342–358.

Harris-Warrick RM, Johnson BR, Peck JH, Kloppenburg P, Ayali A, and Skarbinski J., 1998, "Distributed effects of dopamine modulation in the crustacean pyloric network." *Ann NY Acad Sci* 860: 155–167.

Harris-Warrick R, Marder E, Selverston A. and Moulins M., 1992, "Dynamic Biological Networks: The Stomatogastric Nervous System", Cambridge, MA: MIT Press.

Harris-Warrick RM, Marder E., 1991, "Modulation of neural networks for behavior.", *Annu Rev Neurosci.*; 14:39-57.

Heckmann, C.J., Gorassini, M.A. and Bennett, D.J. 2005, "Persistent inward currents in motoneuron dendrites: implications for motor output", *Muscle and nerve,* vol. 31, no. 2, pp. 135-156.

Heinzel, H.G., Weimann, J.M. and Marder, E. 1993, "The behavioral repertoire of the gastric mill in the crab, Cancer pagurus: an in situ endoscopic and electrophysiological examination", *The Journal of neuroscience : the official journal of the Society for Neuroscience,* vol. 13, no. 4, pp. 1793-1803.

Hille, B., 2001, "Ion Channels of Excitable Membranes", Third Edition, University of Washington

Hooper, S.L. and DiCaprio, R.A. 2004, "Crustacean motor pattern generator networks", *Neuro-Signals,* vol. 13, no. 1-2, pp. 50-69.

Jerng Jerng HH, Pfaffinger PJ, Covarrubias M., "Molecular physiology and modulation of somatodendritic A-type potassium channels." *Mol Cell Neuroscience* 2004 Dec;27(4):343-69. Review

Johnson, B.R. and Harris-Warrick, R.M. 1997, "Amine modulation of glutamate responses from pyloric motor neurons in lobster stomatogastric ganglion", *Journal of neurophysiology,* vol. 78, no. 6, pp. 3210-3221.

Johnson, B.R., Kloppenburg, P. and Harris-Warrick, R.M. 2003, "Dopamine modulation of calcium currents in pyloric neurons of the lobster stomatogastric ganglion", *Journal of neurophysiology,* vol. 90, no. 2, pp. 631-643.

Johnson, B.R., Peck, J.H. and Harris-Warrick, R.M. 1995, "Distributed amine modulation of graded chemical transmission in the pyloric network of the lobster stomatogastric ganglion", *Journal of neurophysiology,* vol. 74, no. 1, pp. 437-452.

Johnston D, Hoffman DA, Magee JC, Poolos NP, Watanabe S, Colbert CM, Migliore M. "Dendritic potassium channels in hippocampal pyramidal neurons." *The Journal of physiology*, 2000 May 15;525 Pt 1:75-81. Review.

Kaupp UB, Seifert R., 2002, "Cyclic nucleotide-gated ion channels." *Physiol Rev.*; 82(3):769-824

Katz PS, Harris-Warrick RM., 1990, "Actions of identified neuromodulatory neurons in a simple motor system.", *Trends Neurosci.*; 13(9):367-73

Kiehn, O. 2006a, "Locomotor circuits in the mammalian spinal cord", *Annual Review of Neuroscience,* vol. 29, pp. 279-306.

Kiehn, O. and Harris-Warrick, R.M. 1992, "5-HT modulation of hyperpolarization-activated inward current and calcium-dependent outward current in a crustacean motor neuron", *Journal of neurophysiology,* vol. 68, no. 2, pp. 496-508.

Kiehn, O. and Kjaerulff, O. 1998, "Distribution of central pattern generators for rhythmic motor outputs in the spinal cord of limbed vertebrates", *Annals of the New York Academy of Sciences,* vol. 860, pp. 110-129.

Kiehn, O., Kjaerulff, O., Tresch, M.C. and Harris-Warrick, R.M. 2000, "Contributions of intrinsic motor neuron properties to the production of rhythmic motor output in the mammalian spinal cord", *Brain research bulletin,* vol. 53, no. 5, pp. 649-659.

King, D.G. 1976a, "Organization of crustacean neuropil. I. Patterns of synaptic connections in lobster stomatogastric ganglion", *Journal of neurocytology,* vol. 5, no. 2, pp. 207-237.

King, D.G. 1976b, "Organization of crustacean neuropil. II. Distribution of synaptic contacts on identified motor neurons in lobster stomatogastric ganglion", *Journal of neurocytology,* vol. 5, no. 2, pp. 239-266.

Klar, M., Surges, R. and Feuerstein, T.J. 2003, "Ih channels as modulators of presynaptic terminal function: ZD7288 increases NMDA-evoked [3H]-noradrenaline release in rat neocortex slices", *Naunyn-Schmiedeberg's archives of pharmacology,* vol. 367, no. 4, pp. 422-425.

Kloppenburg, P., Levini, R.M. and Harris-Warrick, R.M. 1999, "Dopamine modulates two potassium currents and inhibits the intrinsic firing properties of an identified motor neuron in a central pattern generator network", *Journal of neurophysiology,* vol. 81, no. 1, pp. 29-38.

Kocsis B, Li S., 2004, "In vivo contribution of h-channels in the septal pacemaker to theta rhythm generation." *Eur J Neurosci.* 2004 Oct;20(8):2149-58.

Kuruma A, Hirayama Y, Hartzell HC., 2000, "A hyperpolarization- and acid-activated nonselective cation current in Xenopus oocytes.", *Am J Physiol Cell Physiol.*, 279(5):C1401-13.

Liu Z, Bunney EB, Appel SB, Brodie MS., 2003, "Serotonin reduces the hyperpolarization-activated current (Ih) in ventral tegmental area dopamine

neurons: involvement of 5-HT2 receptors and protein kinase C*.", Journal of Neurophysiology*; 90(5):3201-12.

Lund, J.P. and Kolta, A. 2006, "Brainstem circuits that control mastication: do they have anything to say during speech?", *Journal of communication disorders,* vol. 39, no. 5, pp. 381-390.

Lüthi A, McCormick DA., 1999, "Ca(2+)-mediated up-regulation of Ih in the thalamus. How cell-intrinsic ionic currents may shape network activity.", *Ann N Y Acad Sci*.; 868:765-9

MacLean, J.N., Zhang, Y., Goeritz, M.L., Casey, R., Oliva, R., Guckenheimer, J. and Harris-Warrick, R.M. 2005, "Activity-independent coregulation of IA and Ih in rhythmically active neurons", *Journal of neurophysiology,* vol. 94, no. 5, pp. 3601-3617.

MacLean, J.N., Zhang, Y., Johnson, B.R. and Harris-Warrick, R.M. 2003, "Activity-independent homeostasis in rhythmically active neurons", *Neuron,* vol. 37, no. 1, pp. 109-120.

Magee JC, Carruth M. "Dendritic voltage-gated ion channels regulate the action potential firing mode of hippocampal CA1 pyramidal neurons." *Journal of neurophysiology,* 1999 Oct;82(4):1895-901.

Magee JC., 1998, "Dendritic hyperpolarization-activated currents modify the integrative properties of hippocampal CA1 pyramidal neurons.", *J Neurosci*.; 18(19):7613-24.

Marder, E. and Bucher, D. 2007, "Understanding circuit dynamics using the stomatogastric nervous system of lobsters and crabs", *Annual Review of Physiology,* vol. 69, pp. 291-316.

Marder E, Bucher D.,2001, "Central pattern generators and the control of rhythmic movements.", Curr Biol. 2001 Nov 27;11(23):R986-96.

Marder E, Thirumalai V., 2002, "Cellular, synaptic and network effects of neuromodulation.", *Neural Netw*; 15(4-6):479-93;

Marder E., 1976, "Cholinergic motor neurones in the stomatogastric system of the lobster.", *J Physiol*.; 257(1):63-86.

Marder E, Paupardin-Tritsch D., 1980, "Picrotoxin block of a depolarizing ACh response.", *Brain Res*.; 181(1):223-7.

Marder E, Calabrese RL., 1996, "Principles of rhythmic motor pattern generation." *Physiol Rev.*; 76(3):687-717.

Marder, E. and Eisen, J.S. 1984, "Transmitter identification of pyloric neurons: electrically coupled neurons use different transmitters", *Journal of neurophysiology,* vol. 51, no. 6, pp. 1345-1361.

Marder, E. and Paupardin-Tritsch, D. 1978, "The pharmacological properties of some crustacean neuronal acetylcholine, gamma-aminobutyric acid, and L-glutamate responses", *The Journal of physiology,* vol. 280, pp. 213-236.

Marquèze B, Berton F, Seagar M., 2000 "Synaptotagmins in membrane traffic: which vesicles do the tagmins tag?", *Biochimie*; 82(5):409-20.

Maynard DM., 1972, "Simpler networks.", *Ann N Y Acad Sci.*, 193:59-72

MacLean JN, Zhang Y, Johnson BR, Harris-Warrick RM., 2003, "Activity-independent homeostasis in rhythmically active neurons.", *Neuron*, 37(1):109-20.

MacLean JN, Zhang Y, Goeritz ML, Casey R, Oliva R, Guckenheimer J, Harris-Warrick RM., 2005, "Activity-independent coregulation of IA and Ih in rhythmically active neurons.", *J Neurophysiol.*, 94(5):3601-17

McCormick, D.A. and Contreras, D. 2001, "On the cellular and network bases of epileptic seizures", *Annual Review of Physiology,* vol. 63, pp. 815-846.

McLarnon, J.G. 1995, "Potassium currents in motoneurones", *Progress in neurobiology,* vol. 47, no. 6, pp. 513-531.

Migliore M, Ferrante M, Ascoli GA., 2005, "Signal propagation in oblique dendrites of CA1 pyramidal cells.", *J Neurophysiol.*, 94(6):4145-55.

Miller JP, Selverston AI., 1980, "Mechanisms underlying pattern generation in lobster stomatogastric ganglion as determined by selective inactivation of identified neurons. II. Oscillatory properties of pyloric neurons.", *J Neurophysiol*; 48(6):1378-91

Mulloney B, Selverston A., 1972, "Antidromic action potentials fail to demonstrate known interactions between neurons.", *Science.*, (43):69-72

Nistri, A., Ostroumov, K., Sharifullina, E. and Taccola, G. 2006a, "Tuning and playing a motor rhythm: how metabotropic glutamate receptors orchestrate generation of motor patterns in the mammalian central nervous system", *The Journal of physiology,* vol. 572, no. Pt 2, pp. 323-334.

146

Nistri, A., Ostroumov, K., Sharifullina, E. and Taccola, G. 2006b, "Tuning and playing a motor rhythm: how metabotropic glutamate receptors orchestrate generation of motor patterns in the mammalian central nervous system", *The Journal of physiology,* vol. 572, no. Pt 2, pp. 323-334.

Nowotny T, Szücs A, Levi R, Selverston AI., 2007 "Models wagging the dog: are circuits constructed with disparate parameters?" *Neural Comput.* 19(8):1985-2003.

Nusbaum MP, Blitz DM, Swensen AM, Wood D, Marder E., 2001, "The roles of co-transmission in neural network modulation.", *Trends Neurosci.*, (3):146-54.

Ouyang, Q., Goeritz, M. and Harris-Warrick, R.M. 2007a, "Panulirus interruptus Ih-channel gene PIIH: modification of channel properties by alternative splicing and role in rhythmic activity", *Journal of neurophysiology,* vol. 97, no. 6, pp. 3880-3892.

Ouyang, Q., Goeritz, M. and Harris-Warrick, R.M. 2007b, "Panulirus interruptus Ih-channel gene PIIH: modification of channel properties by alternative splicing and role in rhythmic activity", *Journal of neurophysiology,* vol. 97, no. 6, pp. 3880-3892.

Pape, H.C. 1996, "Queer current and pacemaker: the hyperpolarization-activated cation current in neurons", *Annual Review of Physiology,* vol. 58, pp. 299-327.

Peck, J.H., Gaier, E., Stevens, E., Repicky, S. and Harris-Warrick, R.M. 2006, "Amine modulation of Ih in a small neural network", *Journal of neurophysiology,* vol. 96, no. 6, pp. 2931-2940.

Peck, J.H., Nakanishi, S.T., Yaple, R. and Harris-Warrick, R.M. 2001b, "Amine modulation of the transient potassium current in identified cells of the lobster stomatogastric ganglion", *Journal of neurophysiology,* vol. 86, no. 6, pp. 2957-2965.

Pinsker, H.M. 1982, "Integration of reflex activity and central pattern generation in intact Aplysia", *Journal de physiologie,* vol. 78, no. 8, pp. 775-785.

Poolos NP, Migliore M, Johnston D., 2002, "Pharmacological upregulation of h-channels reduces the excitability of pyramidal neuron dendrites.", *Nat Neurosci.* (8):767-74.

Prinz AA, Bucher D, Marder E., 2004, "Similar network activity from disparate circuit parameters.", *Nat Neurosci.*, (12):1345-52.

Prinz AA., 2004, "Neural networks: models and neurons show hybrid vigor in real time.", *Curr Biol.*, 14(16):R661-2.

Raper JA., 1979, "Nonimpulse-mediated synaptic transmission during the generation of a cyclic motor program.", *Science.*; 205(4403):304-6.

Ramirez, J.M. and Richter, D.W. 1996, "The neuronal mechanisms of respiratory rhythm generation", *Current opinion in neurobiology,* vol. 6, no. 6, pp. 817-825.

Rateau, Y. and Ropert, N. 2006, "Expression of a functional hyperpolarization-activated current (Ih) in the mouse nucleus reticularis thalami", *Journal of neurophysiology,* vol. 95, no. 5, pp. 3073-3085.

Robinson, R.B. and Siegelbaum, S.A. 2003, "Hyperpolarization-activated cation currents: from molecules to physiological function", *Annual Review of Physiology,* vol. 65, pp. 453-480.

Rosenkranz, J.A. and Johnston, D. 2006, "Dopaminergic regulation of neuronal excitability through modulation of Ih in layer V entorhinal cortex", *The Journal of neuroscience : the official journal of the Society for Neuroscience,* vol. 26, no. 12, pp. 3229-3244.

Santoro, B. and Baram, T.Z. 2003, "The multiple personalities of h-channels", *Trends in neurosciences,* vol. 26, no. 10, pp. 550-554.

Schneider, H., Baro, D.J., Bailey, D., Ganter, G., Harris-Warrick, R.M. and Kravitz, E.A. 2000, "Patterns of shaker family gene expression in single identified neurons of the American lobster, Homarus americanus", *Receptors and channels,* vol. 7, no. 1, pp. 53-64.

Schulz, D.J., Goaillard, J.M. and Marder, E. 2006, "Variable channel expression in identified single and electrically coupled neurons in different animals", *Nature neuroscience,* vol. 9, no. 3, pp. 356-362.

Schulz DJ, Baines RA, Hempel CM, Li L, Liss B, Misonou H., 2006, "Cellular excitability and the regulation of functional neuronal identity: from gene expression to neuromodulation.", *J Neurosci.*; 26(41):10362-7.

Schulz, D.J., Goaillard, J.M. and Marder, E.E. 2007, "Quantitative expression profiling of identified neurons reveals cell-specific constraints on highly variable levels of gene expression", *Proceedings of the National Academy of Sciences of the United States of America,* vol. 104, no. 32, pp. 13187-13191.

Selverston, A.I. and Moulins, M. 1985, "Oscillatory neural networks", *Annual Review of Physiology,* vol. 47, pp. 29-48.

Selverston AI, Ayers J., 2006, "Oscillations and oscillatory behavior in small neural circuits." *Biol Cybern*; 95(6):537-54.

Skiebe P, Wollenschläger T., 2002, "Putative neurohemal release zones in the stomatogastric nervous system of decapod crustaceans." *J Comp Neurol.*; 453(3):280-91.

Sosa MA, Spitzer N, Edwards DH, Baro DJ., 2004, "A crustacean serotonin receptor: cloning and distribution in the thoracic ganglia of crayfish and freshwater prawn.", *J Comp Neurol*; 473(4):526-37.

Stein, P.S. 2007a, "Motor pattern deletions and modular organization of turtle spinal cord", *Brain Research Reviews,* .

Stein, P.S. 2007b, "Motor pattern deletions and modular organization of turtle spinal cord", *Brain Research Reviews,* .

Straub VA, Benjamin PR., 2001, "Extrinsic modulation and motor pattern generation in a feeding network: a cellular study.", *J Neurosci.*; 21(5):1767-78

Surges R, Freiman TM, Feuerstein TJ., 2003, "K(+)-induced changes in the properties of the hyperpolarization-activated cation current I(h) in rat CA1 pyramidal cells." *Neurosci Lett.*; 332(2):136-40.

Svoboda, K.R. and Lupica, C.R. 1998, "Opioid inhibition of hippocampal interneurons via modulation of potassium and hyperpolarization-activated cation (Ih) currents", *The Journal of neuroscience : the official journal of the Society for Neuroscience,* vol. 18, no. 18, pp. 7084-7098.

Thirumalai, V., Prinz, A.A., Johnson, C.D. and Marder, E. 2006, "Red pigment concentrating hormone strongly enhances the strength of the feedback to the pyloric rhythm oscillator but has little effect on pyloric rhythm period", *Journal of neurophysiology,* vol. 95, no. 3, pp. 1762-1770.

Tierney, A.J. and Harris-Warrick, R.M. 1992, "Physiological role of the transient potassium current in the pyloric circuit of the lobster stomatogastric ganglion", *Journal of neurophysiology,* vol. 67, no. 3, pp. 599-609.

Theander S, Edman A, Fåhraeus C, Akoev GN, Grampp W., 1999, "Cl- transport in the lobster stretch receptor neurone." *Acta Physiol Scand*; 167(4):285-98.

Thoby-Brisson M, Simmers J., 2002, "Long-term neuromodulatory regulation of a motor pattern-generating network: maintenance of synaptic efficacy and oscillatory properties.", *J Neurophysiol*; 88(6):2942-53.

Turrigiano, G.G. and Marder, E. 1993, "Modulation of identified stomatogastric ganglion neurons in primary cell culture", *Journal of neurophysiology,* vol. 69, no. 6, pp. 1993-2002.

Turrigiano GG, Marder E, Abbott LF., 1998, "Cellular short-term memory from a slow potassium conductance." *J Neurophysiol.*;75(2):963-6.

Turrigiano GG, Nelson SB., 1998, "Thinking globally, acting locally: AMPA receptor turnover and synaptic strength." *Neuron*; 21(5):933-5.

Turrigiano GG, Van Wormhoudt A, Ogden L, Selverston AI., 1998 , "Partial purification, tissue distribution and modulatory activity of a crustacean cholecystokinin-like peptide." *J Exp Biol.*, 187:181-200.

Weaver, A.L., 2002, "The functional roles of the Lateral Pyloric and Ventricular Dilator neurons in the pyloric network of the lobster, Panulirus interruptus ", Dissertation

van Welie, I., Remme, M.W., van Hooft, J.A. and Wadman, W.J. 2006, "Different levels of Ih determine distinct temporal integration in bursting and regular-spiking neurons in rat subiculum", *The Journal of physiology,* vol. 576, no. Pt 1, pp. 203-214.

van Welie, I., van Hooft, J.A. and Wadman, W.J. 2004, "Homeostatic scaling of neuronal excitability by synaptic modulation of somatic hyperpolarization-activated Ih channels", *Proceedings of the National Academy of Sciences of the United States of America,* vol. 101, no. 14, pp. 5123-5128.

von Euler, C. 1981, "The contribution of sensory inputs to the pattern generation of breathing", *Canadian journal of physiology and pharmacology,* vol. 59, no. 7, pp. 700-706.

Wiersma C.A, Hughes G.M., "On the functional anatomy of neuronal units in the abdominal cord of the crayfish, Procambarus clarkii (Girard)*J Comp Neurol.* 1961 Apr;116:209-28.

Williams SR, Stuart GJ., 2000, "Backpropagation of physiological spike trains in neocortical pyramidal neurons: implications for temporal coding in dendrites.", *J Neurosci.*; 20(22):8238-46

150

Wyman, R.J. 1976, "Neurophysiology of the motor output pattern generator for breathing", *Federation proceedings,* vol. 35, no. 9, pp. 2013-2023.

Yamaguchi, T. 2004, "The central pattern generator for forelimb locomotion in the cat", *Progress in brain research,* vol. 143, pp. 115-122.

Yu H, Wu J, Potapova I, Wymore RT, Holmes B, Zuckerman J, Pan Z, Wang H, Shi W, Robinson RB, El-Maghrabi MR, Benjamin W, Dixon J, McKinnon D, Cohen IS, Wymore R., 2001, "MinK-related peptide 1: A beta subunit for the HCN ion channel subunit family enhances expression and speeds activation.", *Circ Res.* 88(12):E84-7.

Yu X, Duan KL, Shang CF, Yu HG, Zhou Z., 2004, "Calcium influx through hyperpolarization-activated cation channels (I(h) channels) contributes to activity-evoked neuronal secretion." *Proc Natl Acad Sci* U S A,. 27;101(4):1051-6.

Zhang, B., Wootton, J.F. and Harris-Warrick, R.M. 1995, "Calcium-dependent plateau potentials in a crab stomatogastric ganglion motor neuron. II. Calcium-activated slow inward current ", *J Neurophysiol,* vol. 74, pp. 1938-1946.

Zhang, K., Peng, B.W. and Sanchez, R.M. 2006, "Decreased IH in hippocampal area CA1 pyramidal neurons after perinatal seizure-inducing hypoxia", *Epilepsia,* vol. 47, no. 6, pp. 1023-1028.

Zhang, Y., MacLean, J.N., An, W.F., Lanning, C.C. and Harris-Warrick, R.M. 2003, "KChIP1 and frequenin modify shal-evoked potassium currents in pyloric neurons in the lobster stomatogastric ganglion", *Journal of neurophysiology,* vol. 89, no. 4, pp. 1902-1909.

Zhang, Y., Oliva, R., Gisselmann, G., Hatt, H., Guckenheimer, J. and Harris-Warrick, R.M. 2003b, "Overexpression of a hyperpolarization-activated cation current (Ih) channel gene modifies the firing activity of identified motor neurons in a small neural network", *The Journal of neuroscience : the official journal of the Society for Neuroscience,* vol. 23, no. 27, pp. 9059-9067.

Acknowledgements

Erklaerung

Ich versichere, daß ich die von mir vorgelegte Dissertation selbständig angefertigt, die benutzten Quellen und Hilfsmittel vollständig angegeben und die Stellen der Arbeit - einschließlich Tabellen, Karten und Abbildungen -, die anderen Werken im Wortlaut oder dem Sinn nach entnommen sind, in jedem Einzelfall als Entlehnung kenntlich gemacht habe; daß diese Dissertation noch keiner anderen Fakultät oder Universität zur Prüfung vorgelegen hat; daß sie - abgesehen von unten angegebenen Teilpublikationen - noch nicht veröffentlicht worden ist sowie, daß ich eine solche Veröffentlichung vor Abschluß des Promotionsverfahrens nicht vornehmen werde. Die Bestimmungen dieser Promotionsordnung sind mir bekannt. Die von mir vorgelegte Dissertation ist von Prof. Dr.Peter Kloppenburg betreut worden.

Ithaca, NY, den 20. 9. 2007

Marie-Luise Göritz
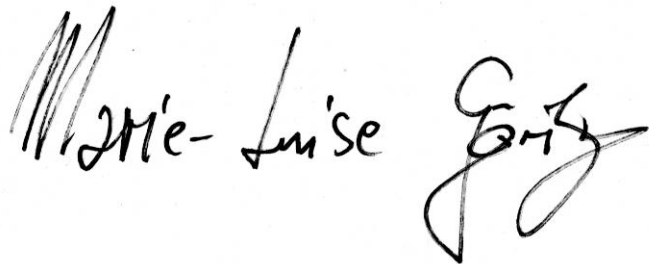
Teilpublikationen

Journal Publications

I_h channel distribution and function in rhythmically active neurons
Goeritz M, Ouyang Q, Harris-Warrick RM, (in preparation)

The *Panulirus interruptus* I_h-channel gene PIIH: modification of channel properties by alternative splicing and role in rhythmic activity.
Ouyang Q, Goeritz M, Harris-Warrick RM. (2007): J Neurophysiol. 2007 Apr 4;

Segment Specificity of Load Signal Processing Depends on Walking Direction in the Stick Insect Leg Muscle Control System.
Akay T, Ludwar BCh, Göritz ML, Schmitz J and Büschges A. (2007): J Neurosci 27: 3285-3294.

Activity-independent co-regulation of I_A and I_h in rhythmically active neurons.
MacLean, JN, Zhang Y, Goeritz ML, Casey R, Oliva R, Guckenheimer J, and Harris-Warrick RM. (2005): J. Neurophysiol., 94: 3601-3617.

Intersegmental coordination of walking movements in stick insects.
Ludwar BCh, Göritz ML, and Schmidt J (2005): J. Neurophysiol. 93(3): 1255-65.

Abstracts/ Conference Talks

M.-L. Goeritz, Q. Ouyang, R. M. Harris-Warrick (2007): Distribution of Ih channels and their role in synaptic integration in the stomatogastric ganglion of Panulirus Interruptus. Society for Neuroscience 37th Annual Meeting, San Diego

T. Akay, B. C. Ludwar, M. Goeritz, A. Bueschges, J. Schmitz (2006): Segment specificity of load signal processing depends on walking direction in the stick insect leg muscle control system. Society for Neuroscience 36th Annual Meeting, Atlanta

Q.Ouyang*; M.Goeritz; R.M.Harris-Warrick (2005): Cloning, Characterization, and Channel Localization of I_h in the stomatogastric ganglion of Panulirus interruptus (poster and talk). Society for Neuroscience 35th Annual Meeting, Washington D.C.

M.Goeritz, J. Schmidt (2003): Intersegmental effects of the femoral chordotonal organ on motoneuron activity in the stick insect. Society for Neuroscience 33th Annual Meeting, New Orleans

M.Goeritz, J. Schmidt (2003): Intersegmental effects of a joint receptor on leg motoneurons in the stick insect. Proceedings of the 28th Göttingen Neurobiology Conference

M. Goeritz (2002): Die Rolle des femoralen Chordotonalorgans auf Motoneuronaktivitaet in der Stabheuschrecke *Carausius morosus*. (talk), Arthropodentreffen Blaubeuren

Ludwar, B. C.; Göritz, M. L.; Schmidt, J. (2002) Intersegmental coordination in walking stick insects. Zoology 105, Supplement V (05.1), Abstracts of the 95th Annual Meeting of the Deutsche Zoologische Gesellschaft Halle (Saale)

Lebenslauf:

Marie-Luise Goeritz

Geburtsdatum: 05.04.1975
Familienstand: verheiratet
Staatsangehoerigkeit: Deutsch
Wohnsitz: Hinter der Vest 25, D-93077 Bad Abbach

                         Tel.: 09405/2792

                         Email: marie.goeritz@gmail.com

Schulausbildung

1985 – 1994:   Von Müller Gymnasium Regensburg, Deutschland
                Abschluss: Abitur (mit der Note 2)
1988:   Martin-Murphy Middle School, USA

Hochschulausbildung

1994 – 2002:   Universität zu Köln, Deutschland
                Studium der Biowissenschaften
                Schwerpunkt: Biologie
                Abschluss: Diplom (mit der Note 1)

Diplomarbeit: "Einflüsse des femoralen Chordotonalorgans auf die Aktivitaet von Motoneuronen eines ipsilateral benachbarten Beines", betreut von Prof. Dr. A. Bueschges

seit 2003:   Promotionsstudium an der Universität zu Köln unter der Anleitung von Prof. Dr. P. Kloppenburg (Universität zu Köln) und Prof. Dr. R. M. Harris-Warrick (Cornell University, Ithaca NY)

Lehr-und Praktikumsassistent in den Kursen:

        1.Neurobiology/Electrophysiology" (Prof. Dr. B. Johnson, Cornell University)

        2.Physiologie neuronaler Netze (Prof. Dr. A. Büschges u.a., UniversitätKöln)

        3.Tierphysiologie für Fortgeschrittene (Prof. Dr. W.Kleinow u.a., Universität zu Köln)